LAND AND WATER
www.csiro.au

CSG Water Injection Impacts: Modelling, Uncertainty and Risk Analysis

Groundwater flow and transport modelling and uncertainty analysis to quantify the water quantity and quality impacts of a coal seam gas produced water injection scheme in the Surat Basin, Queensland.

J Sreekanth and Catherine Moore

March, 2015

ISBN PRINT: 978-1-4863-0522-3

ISBN WEB: 978-1-4863-0523-0

Citation

J Sreekanth, Catherine Moore (2015) CSG water injection impacts: Modelling, uncertainty and risk analysis; Groundwater flow and transport modelling and uncertainty analysis to quantify the water quantity and quality impacts of a coal seam gas produced water injection scheme in the Surat Basin, Queensland. CSIRO, Australia.

Copyright and disclaimer

Important disclaimer

Contents

Figures

Tables

Acknowledgement

This research was supported by the Gas Industry Social and Environmental Research Alliance (GISERA). GISERA is a collaborative vehicle established to undertake publicly-reported independent research addressing the socio-economic and environmental impacts of Australia's natural gas industries. For more details about GISERA visit www.gisera.org.au.

Executive summary

This study developed and applied an integrated multi-scale groundwater modelling methodology to assess the risks of water quantity and quality changes resulting from a large scale injection scheme proposed by Australia Pacific LNG (APLNG) in the Surat Basin, Queensland. The proposed scheme, in the full scale operation phase, would inject 30 – 40 ML/day of reverse osmosis-treated coal seam gas (CSG) produced water into the Precipice sandstone at the Reedy Creek site in Surat Basin. Similar injection schemes are planned at other APLNG CSG production sites including Spring Gully, Condabri and Talinga. The quantification of groundwater quantity and quality changes resulting from such large scale injection schemes is challenged by a number of factors. Simulating the impacts of operational scale injection scenarios required upscaling of the information from injection trial and tracer tests data to larger spatial and temporal scales in the numerical groundwater models used to assess cumulative impacts. Prediction of the risk of impacts using a stochastic modelling framework necessitated development of the models with least possible computational burden. Specifically this study;

- Developed a multi-scale integrated groundwater modelling approach and used it to predict groundwater head and quality changes in the Precipice sandstone and other neighbouring aquifers resulting from the injection of CSG produced water at the operational scale.
- Developed an inversion based upscaling approach, to efficiently upscale information from the well-scale injection trials, pump tests and tracer tests conducted by APLNG at the Reedy Creek site and use this information to constrain regional scale groundwater models.
- Applied state-of-the-art uncertainty analysis techniques to quantify the prediction uncertainty in the simulated groundwater quality and head changes.
- Explored the potential impacts of the presence of faults in the injection well field on the predicted groundwater quality changes.
- Explored a hypothesis testing framework to test whether the occurrence of an undesirable level of water quality could be rejected with high confidence at a risk receptor.
- Investigated the relative worth of different data types and their spatial and temporal disposition to optimise injection trial design for the Spring Gully site as well as for the long-term monitoring of groundwater quality at the Reedy Creek site.
- Employed stochastic particle track analysis to determine the probability distribution of groundwater age in different formations in the study area.
- Developed a novel simulation-optimisation modelling approach for the stochastic optimisation of injection well field design and tested it using a proof-of-concept case study.

The groundwater models used in this study were developed based on the USGS modelling codes MODFLOW and MT3D. Model calibration and uncertainty analysis were based on PEST and its utility software. Also, new utilities were built for specific purposes as required.

The integrated modelling approach developed in this study built and applied groundwater flow and transport models for four different but overlapping spatial and temporal domains. Each model was used to simulate the groundwater flow and transport process that was best represented in one spatio-temporal scale. For example, the coarse scale regional groundwater model developed by the Office of groundwater impact assessment, Queensland (OGIA model) for the Surat Basin was used to characterise the regional flow system and was informed by the regional groundwater monitoring data. Similarly a very fine scale 2-dimensional radial transport model was built and calibrated to the APLNG injection tracer test data and was used to simulate near-well break through curve. The models simulating groundwater flow and transport processes in different scales were then used in an integrated modelling framework using inversion based upscaling. The integrated models were then

used to predict the local and regional scale groundwater head and dilution changes resulting from the proposed operational scale injection scheme.

The stochastic simulation using these models indicated that a groundwater head increase of up to 140 m could occur in the monitoring bores within the injection field. The simulated maximum groundwater head increase in the nearest domestic bore, which is at around 15 km from the well field, was 4.3 m. The stochastic simulation also indicated that the propagation of the groundwater head into the overlying Hutton sandstone aquifer is unlikely.

Potential groundwater quality changes were simulated, to identify the distances and times where injectate would be sufficiently diluted. These water quality simulations were carried out using a flow and transport model built specifically for the Reedy Creek well field and the areas surrounding it within a square block of 16 km. Transport simulations were performed for the proposed injection scenario. A continuous stream of injectate, at a uniform concentration over the entire injection period of 22 years was considered. While no such injectate is planned for the APLNG injection scheme, the purpose of this scenario was to simulate the dilutions and travel times for a worst case contamination scenario. The simulation results indicated that the injectate would dilute to very low concentrations ($1/100^{th}$) over a distance of 5 km from the well field. Simulations based on this worst case scenario indicated that water quality changes are very unlikely in the existing domestic bores, as they are at least 15 km away from the well field in this location. An hypothesis testing approach was used to explore whether the occurrence of an undesirably high concentration at a location 5 km from the closest well could be rejected with high confidence, in spite of the large uncertainty in the predictions. This was assessed by exploring the likelihood of the model parameter distribution that is required for simulating the hypothesised extreme prediction. The results indicated that a dilution of less than half the initial concentration at the location 5 km away from the well field was extremely unlikely and could not be simulated with reasonable values of hydraulic properties for the Precipice sandstone.

The uncertainty in the dilution and travel time estimates were computed using Null-space Monte Carlo analysis. Null-space Monte Carlo analysis quantifies the model prediction uncertainty by exploring the uncertainty in the parameter estimates of the model and propagating it to the predictions. Conceptual model uncertainties resulting from the incomplete knowledge of the boundary conditions and possible presence of faults were also explored. Uncertainty in the boundary condition was addressed by stochastic simulation of the model boundary fluxes and constrained by regional head observations. A new PEST utility FAULTSIM was used to simulate the presence of faults in the numerical models. Using this approach the faults were simulated by modifying the horizontal and vertical conductivity properties of the models cells which are impacted by the fault(s). The uncertainty in the fault properties were then incorporated in the stochastic simulations by varying the fault parameters within a pre-specified range in the Null-space Monte Carlo analysis.

Relative worth of groundwater monitoring data types and their spatial and temporal disposition were explored in a data-worth analysis using linear uncertainty analysis principles. One application of this analysis explored the relative data-worth of the injection tracer tests, pump tests and regional groundwater monitoring data in informing the dilution predictions made using the well field water quality model. The analysis indicated that the tracer test data was most useful in informing the porosity of the Precipice formation and thus reducing the uncertainty in the dilution predictions. Data-worth analysis was also applied for the optimal injection tracer test design for the Spring Gully site. The results of this application indicated that bromide tracers had relatively highest data-worth compared to other tracers and head measurements. The spatial and temporal sampling strategy was also optimised using the approach. In a third application data-worth of long-term monitoring of concentration measurements during the operational phase for the Reedy Creek site was computed.

Particle tracking analysis was undertaken using the stochastic modelling framework to estimate the probability distribution of groundwater age in different aquifer formations within the study area. The results indicated that the groundwater ages varied between 50,000 years to over a million years in different aquifers.

The utility of a simulation-optimisation approach for optimising the design of injection well field to maximise the operational benefits while meeting the regulatory constraints was illustrated using a proof-of-concept study. The results indicated that for given level of information about properties of the aquifer and specified maximum number of injection wells, optimal well locations and injection rates which maximise the total injection rate and simultaneously satisfies the regulatory constraints could be identified.

1 Introduction

1.1 Overview

The Gas Industry Social and Environmental Research Alliance (GISERA) is undertaking research on social and environmental impacts of Coal Seam Gas (CSG) activity in the Bowen and Surat Basins in Queensland. Four related projects under this research alliance focussed on the surface and groundwater impacts of coal seam gas activity in the Surat Basin. In one of these projects (project 3), groundwater modelling and uncertainty analysis was undertaken to study the impacts of coal seam gas produced water injection into beneficial aquifers in Surat Basin. This report compiles the research methods and outcomes of this groundwater modelling study.

APLNG is expanding their coal seam gas exploration and production from the Walloon Coal Measures in the Surat and Bowen Basins in Queensland. Unlike conventional gas, production of coal seam gas requires depressurization of the surrounding coal seams. Thus, CSG production in the Surat and Bowen Basins is accompanied by the extraction of large volumes of groundwater in order to depressurize the coal seams. Injection of the water produced from the coal seams into surrounding aquifers after reverse osmosis treatment is one of the most viable measures for its management. A key advantage of this approach compared with other management options is that a local benefit can be created for the Great Artesian Basin groundwater users. APLNG has proposed a scheme for injecting approximately 30-40 GL/y of water into aquifers with drinking water quality. The injection will occur over a CSG development area of large spatial extent, potentially via a large number of wells. The extent of the scheme combined with the large numbers of users and existing wells in the target aquifers necessitated a comprehensive assessment of the risks of the injection scheme on a variety of potential risk receptors.

APLNG conducted a set of injection trials to deliver detailed measurements on local impacts. The groundwater modelling exercise reported here provided a methodology for the necessary upscaling of the injection trial findings and used state of the art modelling techniques to investigate risks perceived by communities, regulators and scientists. An inversion based upscaling methodology was developed and applied for predicting regional scale groundwater level and dilution impacts resulting from the proposed injection scheme. A stochastic modelling framework was used to quantify the uncertainty in the groundwater models and quantify the probability of hypothesised impacts.

In addition to this final report, a number of workshops and ongoing discussions were undertaken and memos on individual tasks were delivered to APLNG during the course of the project.

1.2 Objective

The main purpose of the groundwater modelling undertaken in this project was to quantify the environmental impacts of large scale injection schemes. The impacts of such large scale injection may be felt over a large area in terms of groundwater pressure changes, yet near-well conditions and dilution processes cannot be ignored when considering water quality impacts. Modelling of such large scale groundwater injection schemes necessitated integration of groundwater monitoring information available in different spatial and temporal scales. This included upscaling of information from the well-scale injection trial and tracer tests to predict the regional impacts of operational scale injection. The primary objective of this project was development of an integrated modelling framework which is capable of doing this.

Given the public debate over the potential impacts of coal seam gas industry in Queensland on the environment, it has become inevitable to perform comprehensive assessment of the environmental impacts of any planned activity for coal seam gas development. Such assessments inform the potential impacts of the planned CSG activities on the environment which are of direct or indirect relevance to all stakeholders including the community, regulatory decision makers and CSG Company. Given the complexity of the problem and lack of sufficient information for subsurface characterization, it is obvious that

deterministic predictions of these potential impacts are not feasible. Predicting these impacts using a stochastic modelling framework has the advantage that the impacts can be quantified probabilistically. Using such a probabilistic modelling framework enables the identification of impacts which are unlikely to occur and can be rejected with high confidence. Those impacts which cannot be rejected would then require continued monitoring and early intervention with mitigation and other management activities. The second objective of this project was to develop a stochastic groundwater modelling framework for probabilistic quantification of the groundwater impacts of the large scale injection scheme. Two types of impacts resulting from the injection were dealt with in this study. They are

1) Changes in the groundwater flow and head distribution.
2) Changes in the groundwater quality.

In addition to these main objectives of quantifying the impacts of injection and the associated uncertainty, the project also explored stochastic modelling approaches for simulating the groundwater ages for different formations in the Surat Basin. Additionally, the utility of modelling based approaches for the monitoring and management of injection impacts were also explored. This included development of methods to analyse the worth of future data collection to inform these predictions and optimise the injection well field designs.

1.3 Injection sites and target aquifers

Four target sites were identified by APLNG for injection well fields in the Surat Basin. These are at the CSG development sites named Spring Gully, Reedy Creek, Condabri and Talinga. The spatial location of these injection sites are shown in Figure 1. APLNG conducted injection trials targeting three aquifer formations *viz.*, Gubberamunda sandstone, Hutton sandstone and Precipice sandstone at each of the three identified sites - Spring Gully, Reedy Creek and Condabri. During the course of this project, APLNG chose Reedy Creek as the pilot site for conducting injection trials. Comprehensive pump tests and injection trials including tracer tests were conducted in the Precipice sandstone at the Reedy Creek site in 2012 -13. For this reason, Reedy Creek site was chosen for the detailed modelling and analysis in this project. The Precipice sandstone formation is nearly 1300 m deep at this location.

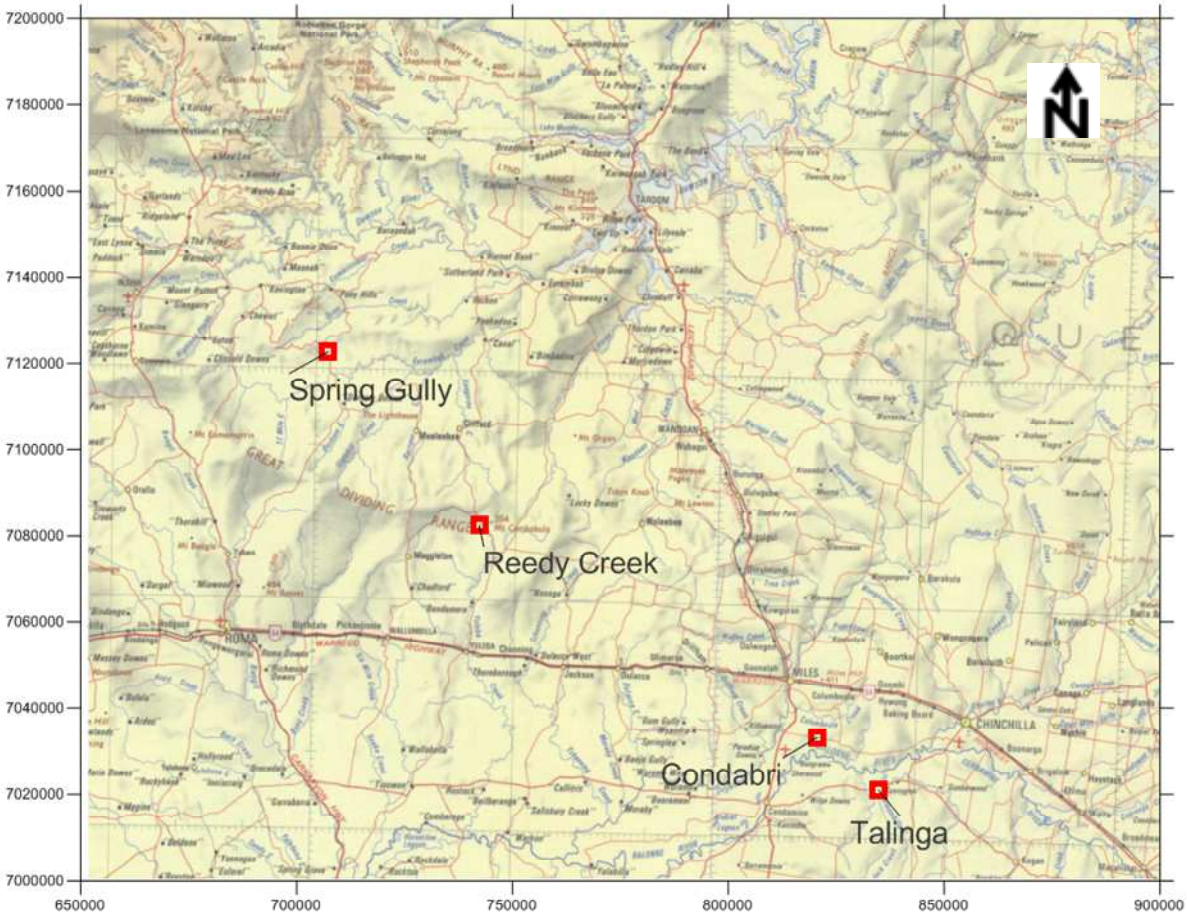

Figure 1: Proposed APLNG CSG production and injection sites in the Surat Basin

1.4 Modelling basis selection

The regional scale groundwater model developed by the Office of Groundwater Impact Assessment (OGIA) for assessing the impacts of CSG development in the Surat Basin was used as the basis for all the models developed in this project. This model is henceforth referred to as the OGIA model in this report. The OGIA model was built using the USGS groundwater modelling code MODFLOW. For the ease of extracting information from this model and compatibility of the newly built models to interact with this model, all the groundwater models built in this project were based on the USGS codes MODFLOW and MT3D. The parameter estimation code PEST, and its suite of utility softwares was used as the major tool for model calibration and uncertainty analysis.

1.5 Structure of the report

The study commenced by mapping all the potential risk receptors in the vicinity of the proposed injection site. A preliminary analysis of the impacts at these risk receptors was conducted by simulating an idealised injection scenario using the OGIA model. Section 2 of this report describes the potential risk receptors and the preliminary modelling results. Approximate spatial and temporal extents of the groundwater quantity and quality changes resulting from the injection scenario were obtained from the preliminary modelling analysis. Based on this, sub-domains were identified for detailed flow and transport modelling. Section 3 describes the flow and transport models for different spatial and temporal sub-domains and the integration of these models into a single integrated modelling framework for upscaling the information from the injection trials and predicting the groundwater level changes and water quality impacts.

These models were then used in a stochastic modelling framework for the probabilistic quantification of the potential impacts. Section 4 describes the Null-space Monte Carlo analysis, which used flow and transport models at two different scales for predicting the groundwater head change and dilution impacts. Further, hypothesis testing was conducted using the stochastic modelling framework to test the influence of the presence of faults in the well field, on the groundwater head change and dilution impacts. The details of this analysis and results are presented in section 5. The stochastic modelling framework was also used to assess the relative worth of the groundwater data in informing the predictions. Data-worth analysis performed to assess the relative worth of concentration measurements at different monitoring locations is described in section 6. Particle tracking analysis was carried out in a stochastic modelling framework to determine the groundwater age distribution of different aquifers in the Surat Basin. A brief description of this analysis is presented in section 7. A simulation-optimisation methodology was developed by coupling the MODFLOW-based simulation model with a multi-objective optimisation algorithm to optimise the injection well field design considering a number of budgetary and regulatory constraints. The methodology was tested using a synthetic aquifer case-study. A brief description of the methodology and the case-study is presented in section 8. The summary of the project, key conclusions and the scope of potential future work in this area is identified in section 9.

2 Data and Preliminary Model Analysis

2.1 Overview

One of the key tasks in quantifying the impacts of injection was to identify all potential risk receptors in the region and shortlist the ones which could be impacted, for detailed analysis. This section describes the process of identifying potential risk receptors associated with the large scale injection into Precipice sandstone at the Reedy Creek injection site. Preliminary modelling of an idealised injection scenario was conducted using the OGIA model to identify the areal and temporal extents over which the impacts could be expected to occur. The relevant details of this analysis and preliminary estimates of groundwater level changes and advective travel times and distances are also presented in this section.

2.2 Risk Receptors

Considering the keen community interest in the coal seam gas environmental impacts, we defined risk resulting from the proposed injection scheme as “any change in the existing groundwater quantity or quality” and risk receptors as “any water dependent asset that may be measurably impacted by a change in water quantity or quality” (Barrett et al., 2013). Thus, an increase or decrease in the groundwater level or quality in a bore or change in the discharge of a spring connected to the target aquifer system, change in the flow pattern of a water course spring etc., could all be considered as risk.

A typical cross section of the Surat basin indicating different geologic formations and their depths from the surface is shown in Figure 2. Considering that the target aquifer is the Precipice sandstone which is over 1000 m below the ground surface at Reedy Creek, the major risk receptors for this study comprised of the domestic and stock bores in Precipice sandstone and other overlying formations in the region. However, for a comprehensive analysis, other risk receptors comprising land surface features including groundwater dependent ecosystems (GDE), springs, water course springs were all considered as potential risk receptors.

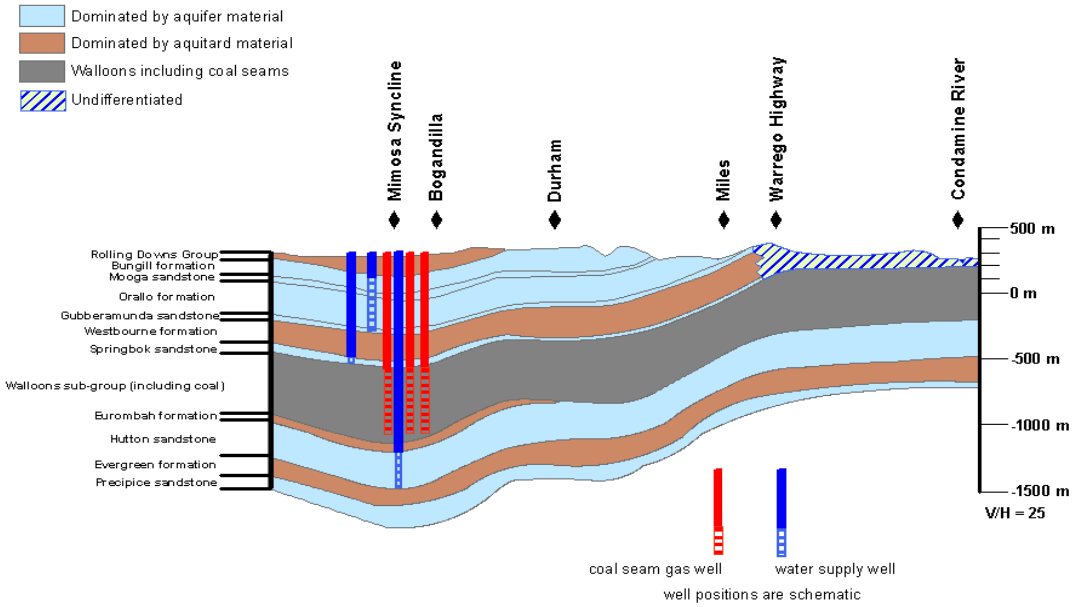

Figure 2: Cross-section of the Surat Basin indicating the depths of formations from the surface.

There is a high density of stock and domestic bores around the CSG tenements in the Surat Basin. Figure 3 shows a distribution of stock and domestic bores tapping aquifers and aquitards in different geologic formations in and around the APLNG tenements. The blue circle includes the Reedy Creek injection well field. It can be seen that there is a high density of stock and domestic bores within this area. Figure 4

indicates the domestic and stock bores in Precipice, springs, GDEs and water course springs within a distance of 80 km from the Reedy Creek injection site.

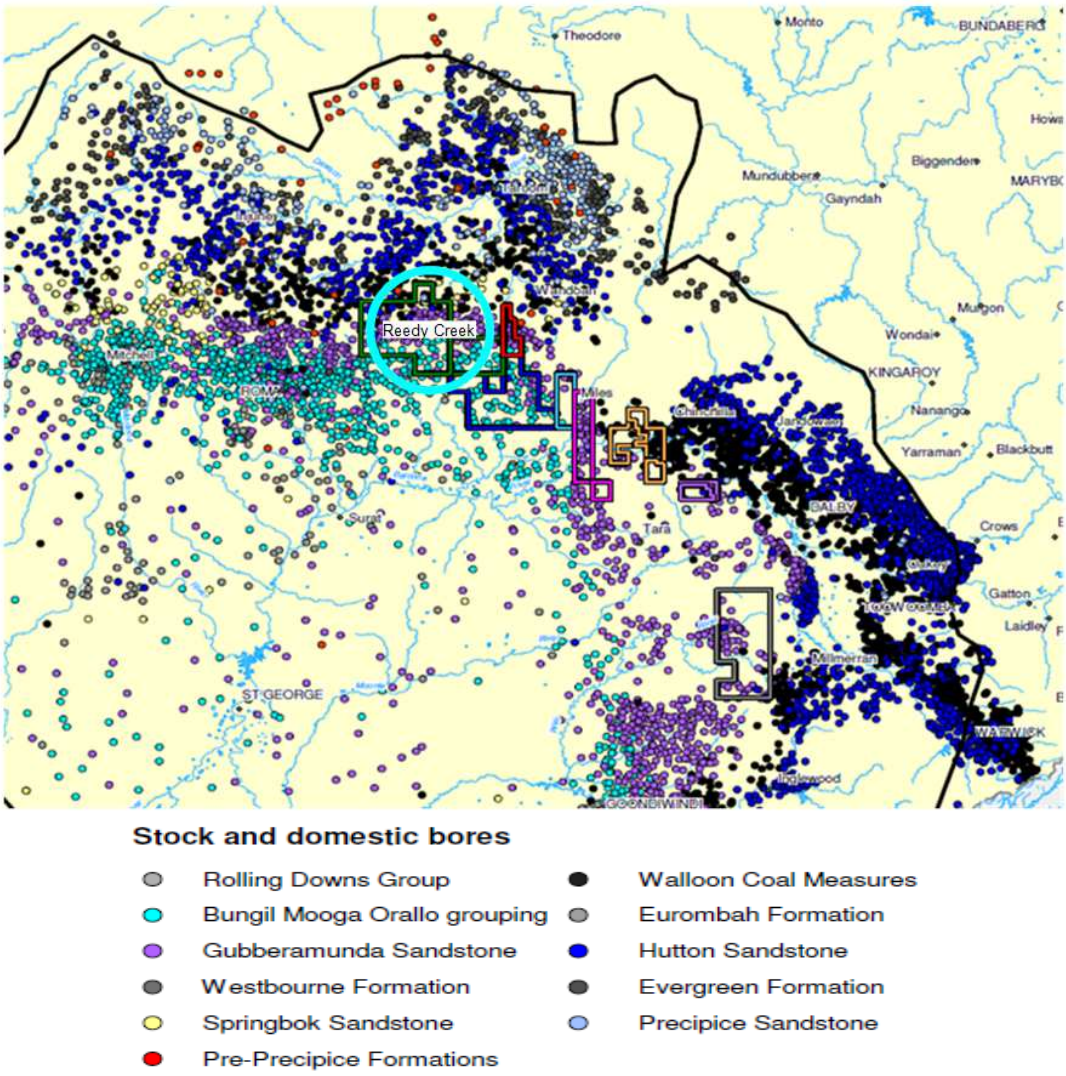

Figure 3 Domestic and stock bores in and around APLNG tenements in the Surat Basin (APLNG EIS, 2010).

2.3 OGIA Model

A very brief overview of OGIA model and relevant information for the injection scenario analysis are presented in this section. For comprehensive information regarding the OGIA model, readers are referred to the OGIA Underground Water Impacts Assessment Report (QWC, 2012). In this study, the OGIA model was used for the preliminary modelling of the impacts from an approximate injection scenario to assist in the identification of risk receptors.

The OGIA model covers a regional extent of 661.5 km × 547.5 km and is comprised of 19 model layers representing different formations in the Surat and Bowen Basin. The Precipice sandstone which is the target aquifer for injection at the Reedy Creek site, was represented by layer 14 of the OGIA model. The formations overlying and underlying Precipice sandstone, the Evergreen and Moolayember formations were represented by Layers 13 and Layer 15 respectively in the model. Groundwater head data from the Queensland regional bore dataset were used as calibration constraints for this model. This included data from 44 monitoring bores in the Precipice formation. The total licensed volumetric groundwater entitlements for the Precipice sandstone in 1995 and 2010 are 7.702 and 29.673 ML/d respectively (QWC, 2012). The estimated total stock and domestic extraction in 1995 and 2010 are 7.441 and 9.123 ML/d

respectively (GHD, 2011). Calibrated recharge from the OGIA model for the Precipice is 20.7 mm/yr. Calibrated average horizontal and vertical conductivities are 3.38×10^{-1} m/d and 2.55×10^{-2} m/d.

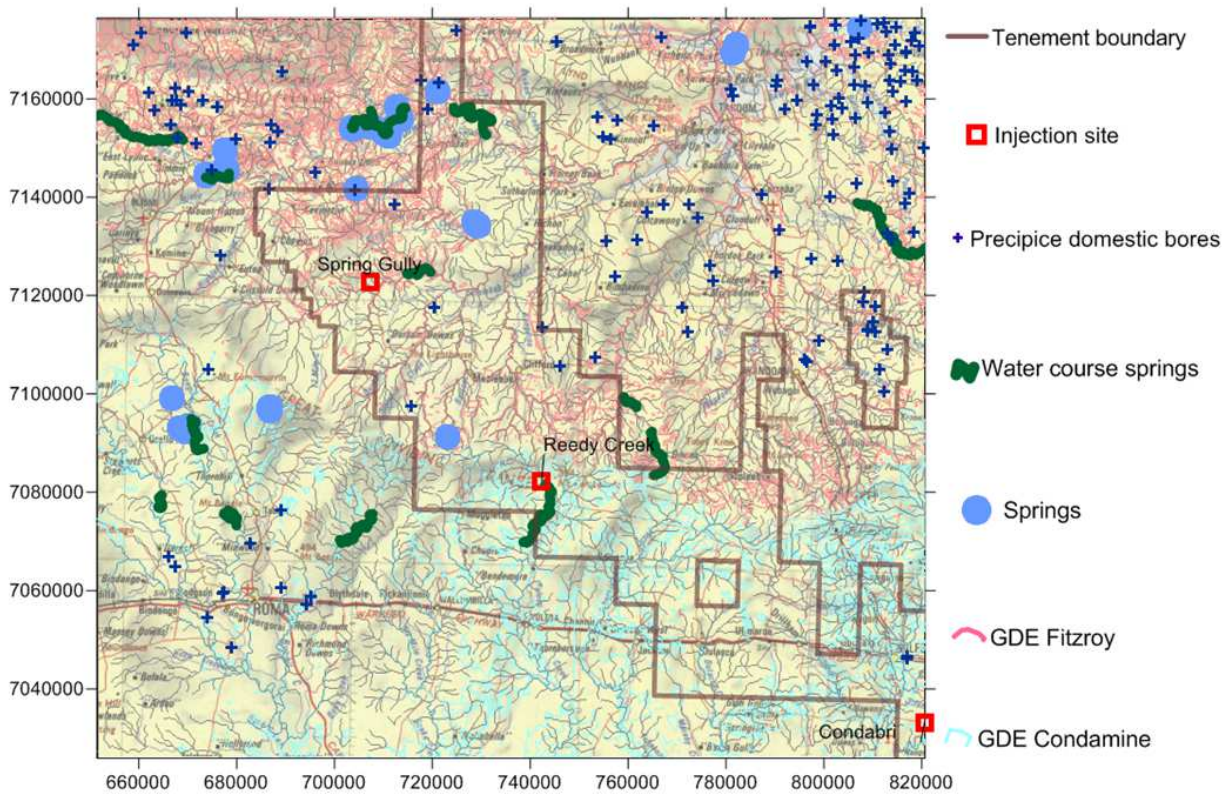

Figure 4: Map indicating the Precipice bores and land surface risk receptors for the Reedy Creek injection site

2.4 Injection scenario analysis

A scenario of injecting 30 ML/d of treated CSG produced water into Precipice sandstone aquifer at Reedy Creek was simulated using the OGIA model. It is noteworthy that the OGIA model was calibrated to the steady state long-term groundwater head observations in different aquifer systems in the Great Artesian Basin. In the injection scenario analysis, subsequent to an initial steady state stress period representing the long-term average groundwater stresses, a transient simulation period of 1000 years was considered. For the transient stress periods, all the groundwater stresses as represented in the transient CSG impact prediction runs of the OGIA model (QWC, 2012) were considered. While the CSG groundwater extraction was represented by the evapo-transpiration (EVT) package in the CSG impact prediction runs of OGIA model, the injection into Precipice sandstone for a period of 30 years was represented by means of the MODFLOW well package. The total injection rate of 30 ML/d was distributed across 20 well locations identified by APLNG at the Reedy Creek injection site, thus accounting for 1500 m^3/d per well. The well locations and rates are given in Table 1.

Table 1: Injection well locations and rates

Easting	Northing	Well ID	Rate (m^3/d)
738002.9	7081942	RCK180	1500
737966.6	7083174	RCK121	1500
739519.6	7082688	RCK156	1500
741501.9	7082163	RCK007	1500
739248.5	7084020	RCK088	1500
736910.6	7084577	RCK062	1500
739733.3	7085130	RCK059	1500
741075.3	7084822	RCK066	1500
740367.4	7086423	RCK047	1500
740804.6	7087354	RCK030	1500
743168	7088313	COM330	1500
742625.6	7085161	COM416	1500
742317.2	7083571	RCK127	1500
743066.5	7081966	RCK185	1500
740546.7	7083447	RCK125	1500
740501	7089195	COM300	1500
741169	7085746	RCK050	1500
743354	7084514	RCK067	1500
742434	7086788	COM373	1500
740492	7091347	COM257	1500

By running the model twice, with and without considering the injection wells respectively and computing the difference in the groundwater level between these two simulations for each model layer, groundwater head increase resulting from the injection scenario was computed.

2.5 Null-space Monte-Carlo analysis

Insufficient information on the subsurface formations and lack of enough groundwater monitoring information almost always results in uncertainty of estimated parameter fields used in groundwater models. By identifying different parameter fields which minimize the calibration objective function equally well, it is possible to explore the uncertainty in the model predictions. During the OGIA model development 200 sets of hydraulic parameters were identified using Null-space Monte Carlo analysis technique (Tonkin and Doherty, 2009). Each parameter set identified using this approach represents a plausible realization of the unknown parameter values in that they minimise the calibration objective function below a pre-specified acceptable value. We used 50 representative sets of parameters from this suite of 200 to make predictive simulations of the impacts of the injection scenario over a 1000-year period. This exercise helped to explore the predictive uncertainty in the groundwater level increase resulting from the injection scenario.

The predicted groundwater head increase for different formations was obtained from these simulations. Contours of the groundwater head increase corresponding to different snapshots in time were plotted. Contours of head rise in the Precipice sandstone at the end of 30 years, 50 years and 400 years are shown in Figure 5, Figure 6 and Figure 7. The hydrographs of groundwater head increase at a number of locations were also analysed. The predicted groundwater head increase in the nearest domestic bore in Precipice (RN123030) is shown in Figure 8.

Analysis of the groundwater head changes in the model layers above and below Precipice (Evergreen and Moolayember formations) indicated considerable increase in the groundwater level in these aquitard layers. A careful evaluation of the stratigraphic representation of the Precipice formation in OGIA model indicated considerable thinning of the Precipice layer close to the Reedy Creek injection location which may

have resulted in the simulation of such large head increases in the Evergreen and Moolayember formations.

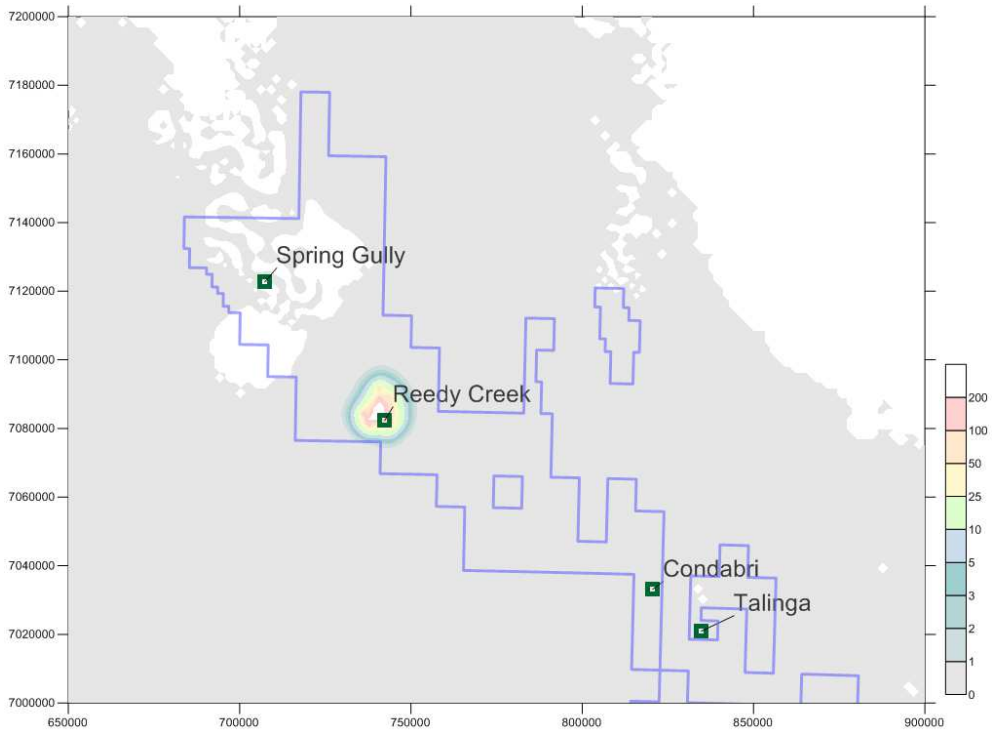

Figure 5: Contours of groundwater mounding (m) at 30 years. Injection stopped after 30 years

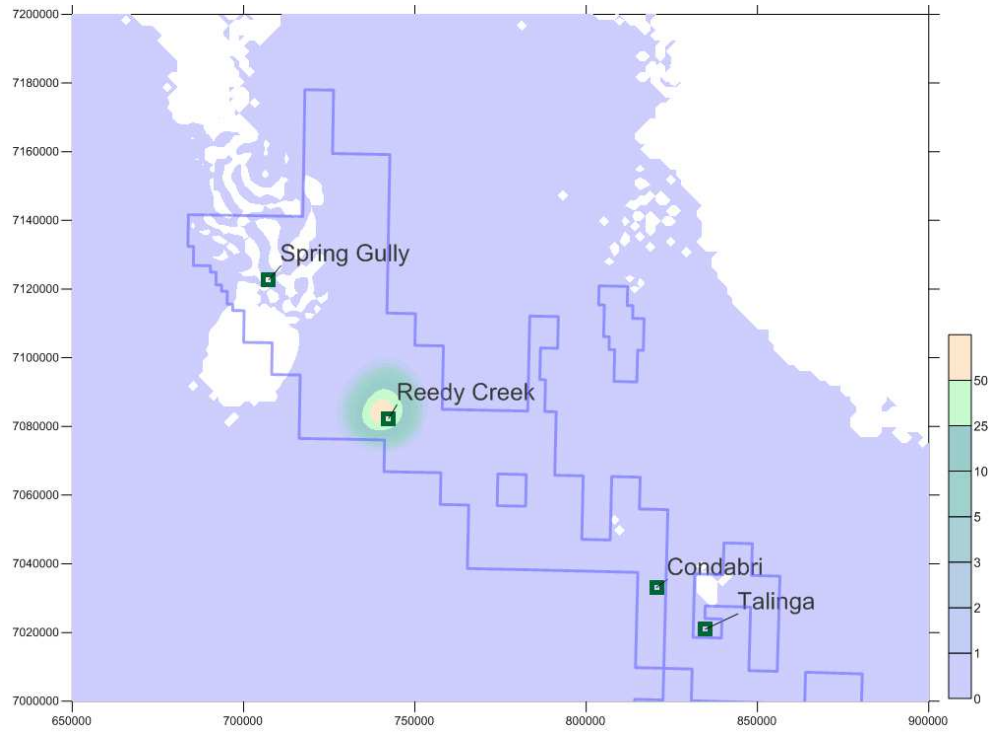

Figure 6: Contours of groundwater mounding (m) after 50 years.

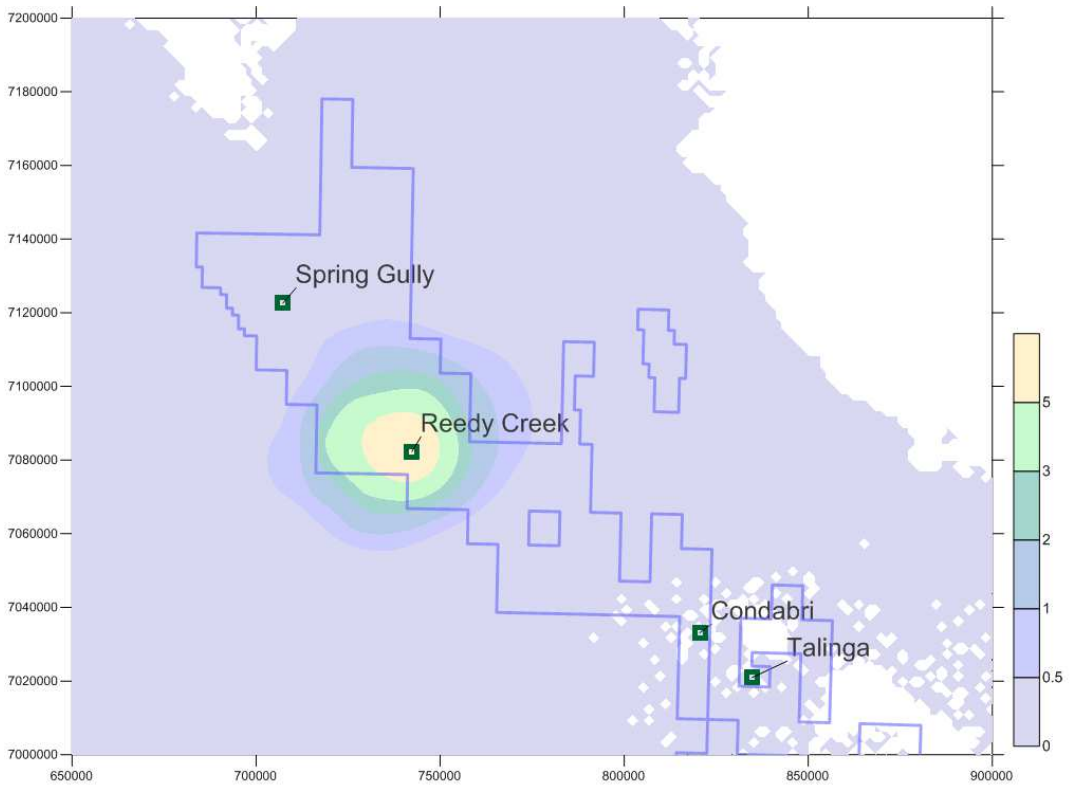

Figure 7: Contours of groundwater mounding (m) after 400 years.

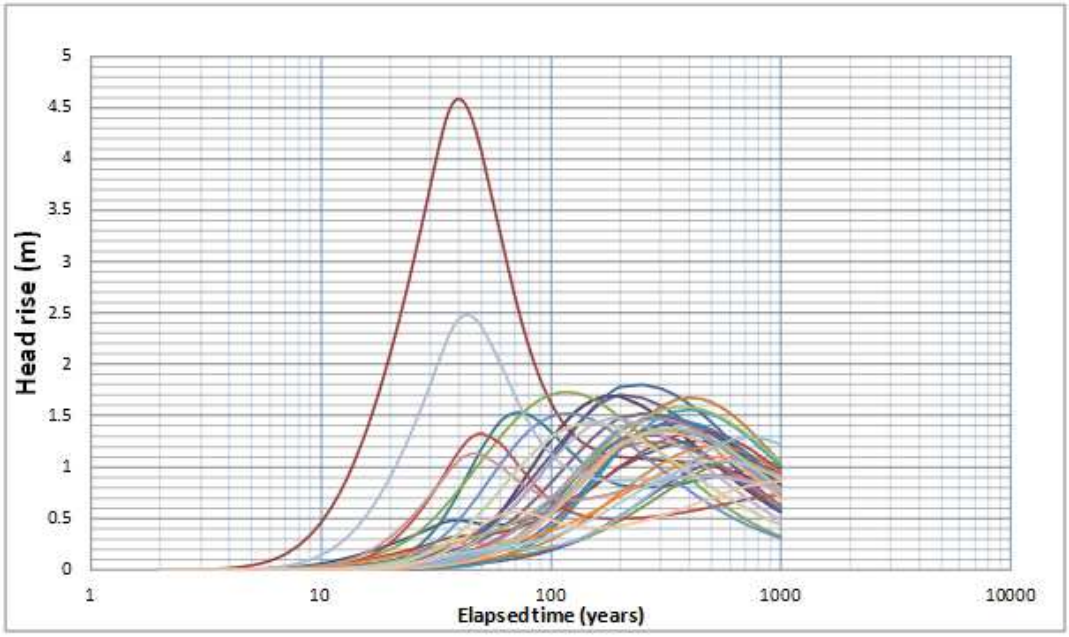

Figure 8: OGIA model predicted groundwater head mounding in the nearest Precipice bore (RN123030)

2.6 Particle tracking analysis

Particle tracking analysis was also undertaken using the OGIA model to simulate the travel times and distances resulting from the advective transport of particles from the injection wells. The advection transport observation package (ADV2) for MODFLOW was used to simulate the particle tracks. Using this approach, the groundwater head gradient resulting from injection is simulated by the solution of the

groundwater flow equation and the resulting groundwater velocities are obtained from these gradients and the porosity of the aquifer material. Using these velocities, the particle displacement is simulated by tracking successive Cartesian components through the groundwater model grid over time.

The particle tracks were simulated in a stochastic modelling framework using the 200 sets of hydraulic parameters obtained from the Null-space Monte Carlo analysis. Porosity values required for the transport simulation were obtained from the porosity and permeability data supplied by APLNG (pers. comm.). In addition a linear functional relationship between the porosity and hydraulic conductivity was obtained from the porosity-permeability relationship also supplied by APLNG and this was used to generate the porosity values corresponding to different hydraulic conductivity sets used in the Null-space Monte Carlo analysis. The relationship between porosity and log hydraulic conductivity values obtained is shown in Figure 9.

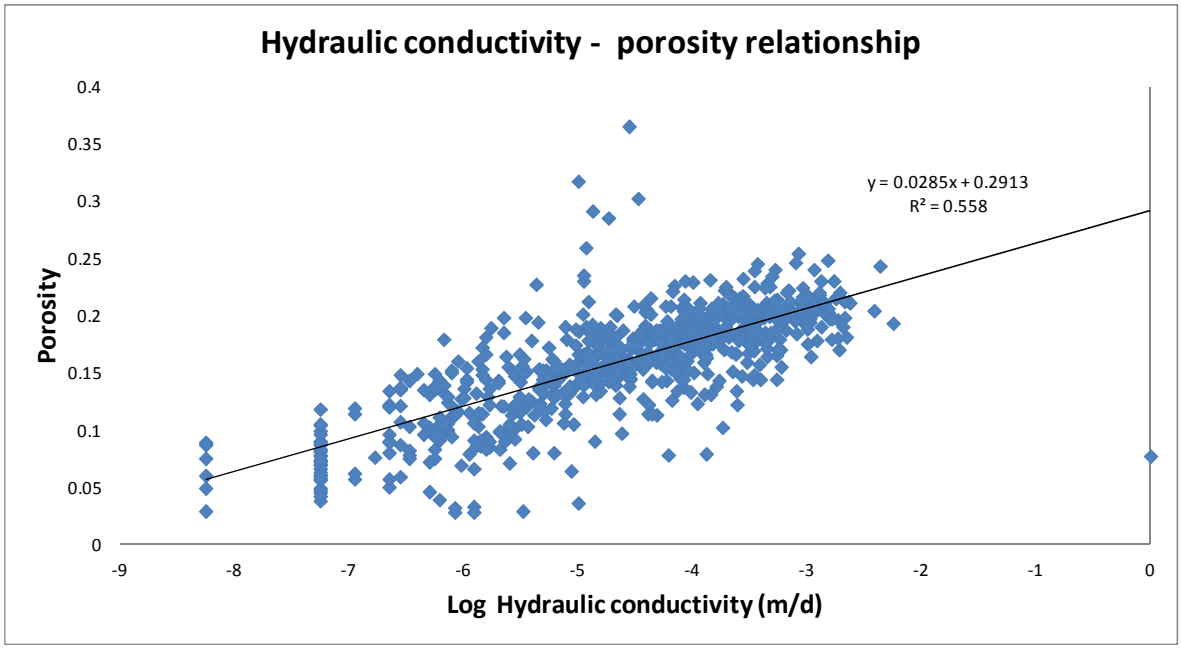

Figure 9: Hydraulic conductivity-porosity relationship for the Precipice sandstone aquifer.

Particle tracks over time were simulated, with starting positions in four model cells, located in the East, West, South and North of the injection well field. A simulation period of 1000 years was considered with the injection lasting for 30 years. The plan view of the simulated particle tracks is depicted in Figure 10. It was observed that the main driving force on the particle movement was the head gradient caused by the injection, whereas the background flow was found to have lesser influence on the particle tracks. This caused the particles to move in a radial direction outwards from the well field. However, it was noteworthy that the particle movement was least in the southwest direction which is attributed to the pinching out of the Precipice sandstone due to the presence of the Great Dividing Range in this direction. The distributions of particle travel distances over the simulation period towards the East of the well field are shown in Figure 11(identified with the ellipse) and the distribution of the corresponding velocities is shown in Figure 12.

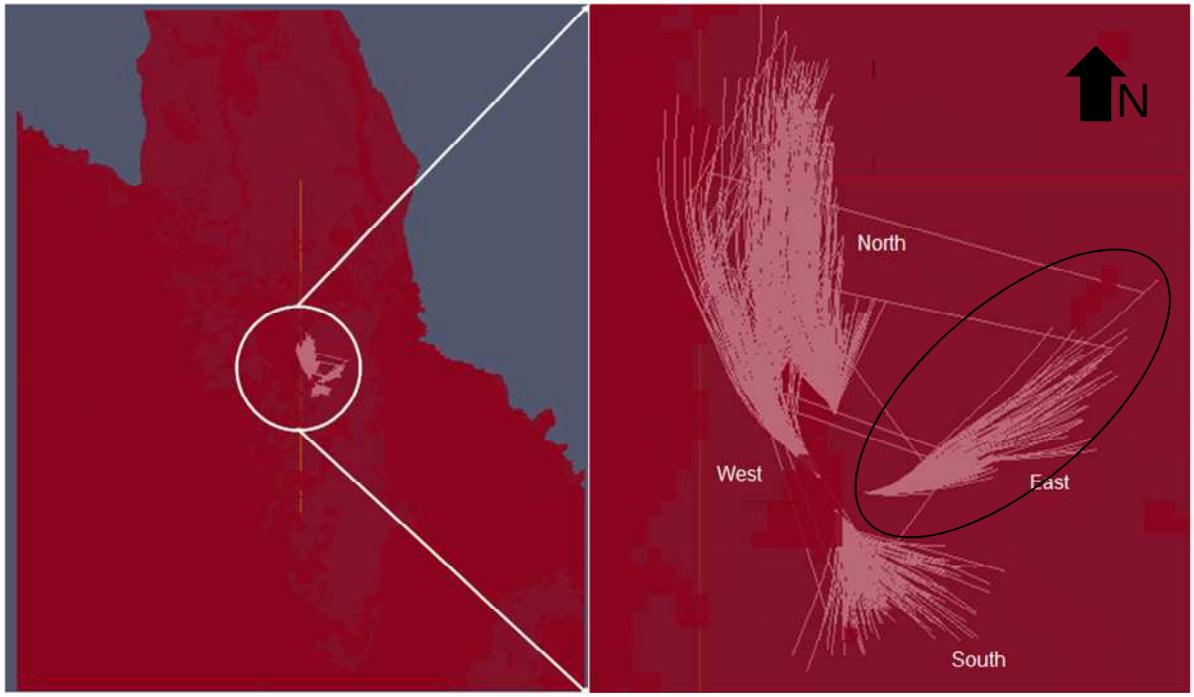

Figure 10: Plan view of the advection based particle tracks in four directions from the well field.

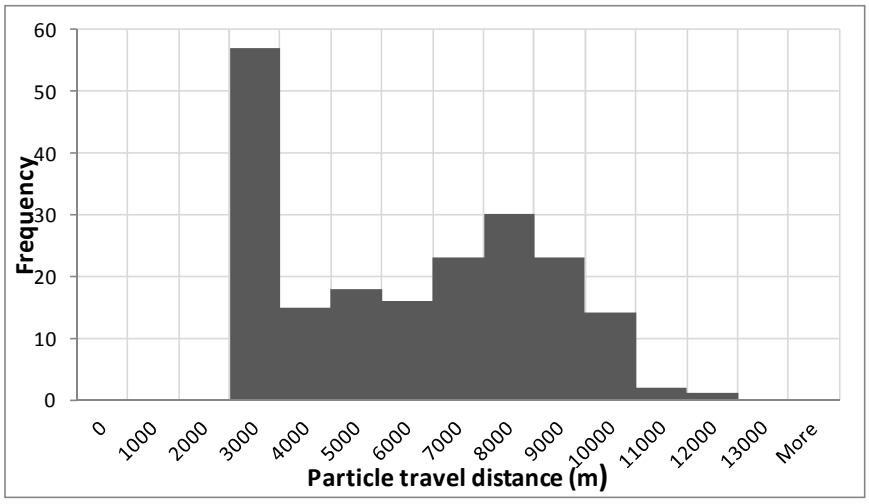

Figure 11: Distribution of particle travel distances in the northeast direction of the well field

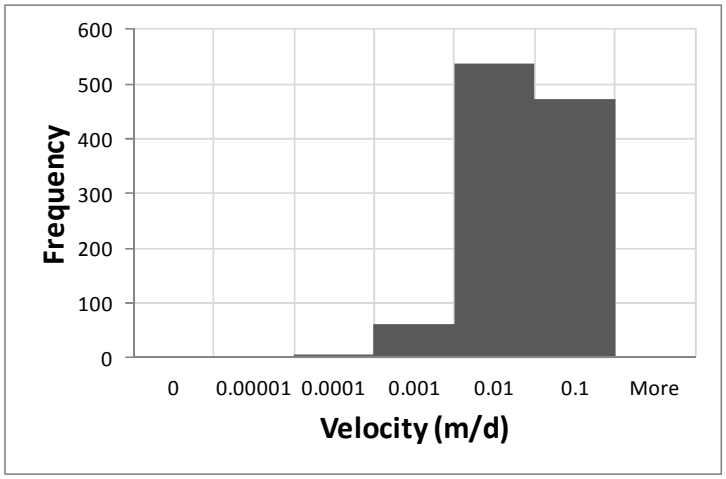

Figure 12: Distribution of particle velocities in the northeast direction of the well field

2.7 Inferences

The preliminary modelling analysis using the OGIA model provided insights into the potential groundwater flow and transport changes resulting from the proposed large scale injection into Precipice sandstone at Reedy Creek. The groundwater head increase simulated using the OGIA model indicated that injection could result in groundwater head changes in the Precipice sandstone over tens of kilometres which may last for hundreds of years. Because, Precipice was represented as a single layer in the OGIA model, it was unable to effectively simulate the vertical fluxes and resulting head changes using the OGIA model. Also, recent Origin bore logs from Reedy Creek show the presence of a less conductive upper part and a highly permeable Braided Stream Facies (BSF) in the lower part of the Precipice. Because of these features, it was decided to represent the Precipice sandstone as two layers corresponding to these two different fractions in the detailed analysis of the injection impacts.

The preliminary modelling indicated that injection impacts are unlikely to propagate to the outcrop or to cause any risk to potential receptors close to the land surface, such as the water course springs or groundwater dependent ecosystems. However, since preliminary simulation did indicate some groundwater flux and head changes in the adjacent layers, it was decided to include the aquifer formations above Precipice sandstone up to the Bungil Mooga and Orallo formations for detailed modelling analysis. In order to conduct a detailed analysis of the groundwater head changes resulting from the injection it was decided to build a subregional model extending over 169 × 151 km with the Reedy Creek injection site at the centre.

The simulation of particle tracks indicated very slow transport velocities resulting in particle displacement of 3 to 12 kilometres over hundreds of years. These calculated velocities were used when designing the dimensions of the contaminant transport model that was necessary for simulating the water quality impacts, which used a finer spatial and temporal scale and lesser spatial extent than the subregional model so as to ensure numerical stability and computational feasibility. This contaminant transport model was calibrated to the injection trials and makes predictions in the finer spatial and temporal scales, as discussed in section 3 of this report.

2.8 Summary

Risk receptors that could potentially be impacted by the large scale CSG produced water injection scheme were identified and mapped. While, the comprehensive list of risk receptors included domestic and stock bores, springs, water course springs and groundwater dependent ecosystems on land surface, preliminary modelling analysis indicated that the injection impacts would be more likely to be confined to the Precipice sandstone and adjacent formations at the Reedy Creek injection site. Preliminary simulations of

groundwater level changes and particle tracking indicated the necessity for conducting detailed modelling to inform the regional scale groundwater mounding resulting from the injection as well as finer scale water quality changes.

3 Upscaling injection trial geochemical and hydraulic response

3.1 Overview

As discussed in the preliminary analysis in section 2, large scale injection is expected to impact the groundwater pressures on a regional scale. While instantaneous groundwater head responses may be observed over hundreds of metres within the re-injection field, groundwater mounding could occur over tens or hundreds of kilometres over many decades or centuries. Prediction of these impacts necessitated development of regional scale groundwater flow models with long simulation periods and large spatial domains. Steep head gradients close to the injection field resulting from high pressure injection necessitated fine spatial and temporal discretization of the model close to the well field. Simulation of the transport processes close to the well field also required finer spatial and temporal discretization of the model. The spatial and temporal resolution of the groundwater head and concentration observations used to calibrate the flow and transport models varied over a wide range. The groundwater level and concentration observation from field injection trials had fine temporal resolution, as small as hourly measurements. On the other hand, temporally sparse groundwater monitoring information over large spatial domains was available from the regional groundwater monitoring data. The flow and transport models had to be developed at various appropriately detailed spatial and temporal scales to make maximum use of the available groundwater information, as well as being able to inform predictive simulations over large regional scales. These challenges of disparate scales were met by using an integrated modelling framework with models developed in different spatial and temporal scales and using upscaling based on inverse modelling, and "linking" predictions used to transfer information between these models.

This section describes the development and application of groundwater flow and transport models in four different scales which were calibrated to different sets of data with varying spatio-temporal resolutions. These models were then used in the integrated modelling framework described above to make predictions of injection-induced groundwater head and water quality changes at the Reedy Creek injection site.

3.2 Method

A suite of groundwater flow and transport models in different spatial and temporal scales were built in this study to predict groundwater head and quality changes resulting from injection. In all, we applied groundwater models in four different scales (Figure 14). The first and coarsest scale model in this group is the OGIA model. The second model is called the 'subregional model' which was built and calibrated specifically for making predictions of groundwater head and flow changes over a subregion extending over 150 km. The third model is called the 'well field water quality' model. These three models were three dimensional and the relative spatial extents they cover in the Surat basin is depicted in Figure 13. The elevation of the Precipice Braided Stream Facies (BSF) is contoured in the map depicted in Figure 13. It is noteworthy that within the well field water quality model domain, the Precipice BSF is relatively flat. However, the subregional model covers a spatial domain over which there is a steep gradient in the elevation of Precipice sandstone from the outcrop in the North to around -2000 m in the South. The fourth model is a '2D radial transport model' built to model the flow and transport in the immediate vicinity of the injection trial bore R-INJ2-P (APLNG name).

Although built as independent models for overlapping spatial domains, all these models were linked together by means of the information transfer between each other in terms of the groundwater stress representation, boundary conditions and upscaling "linking" predictions. Linking predictions are simply predictions made with the smaller scale model, which are then used as calibration targets in the larger scale model. The links between these four model scales is indicated in Table 2. The vertical discretization of these four models as well as their respective uses is illustrated in Figure 14: The vertical discretization of

the four groundwater models and their purposes. The red arrows in Figure 14 indicate the direction of information transfer between these models. Based on the purpose for which the models are used they belong to two classes viz., prediction models and input models. The subregional model and well field water quality model were used as prediction models for predicting respectively the groundwater head and water quality impacts resulting from the operational scale injection. The OGIA model and 2D radial transport models were classified as input models because their predictions were used as inputs for calibrating and upscaling the hydraulic properties of the prediction models. The well field water quality model was used both as a prediction model as well as an input model. In its role as an input model the well field water quality model provided upscaling information for the subregional model.

A brief description of the simulation of the injection scenario using the OGIA model is provided in section 2.3. The readers are referred to Underground Water Impact Report (QWC, 2012) for details regarding the development and calibration of the OGIA model. The details of the other three models and their calibration are described in the following sections.

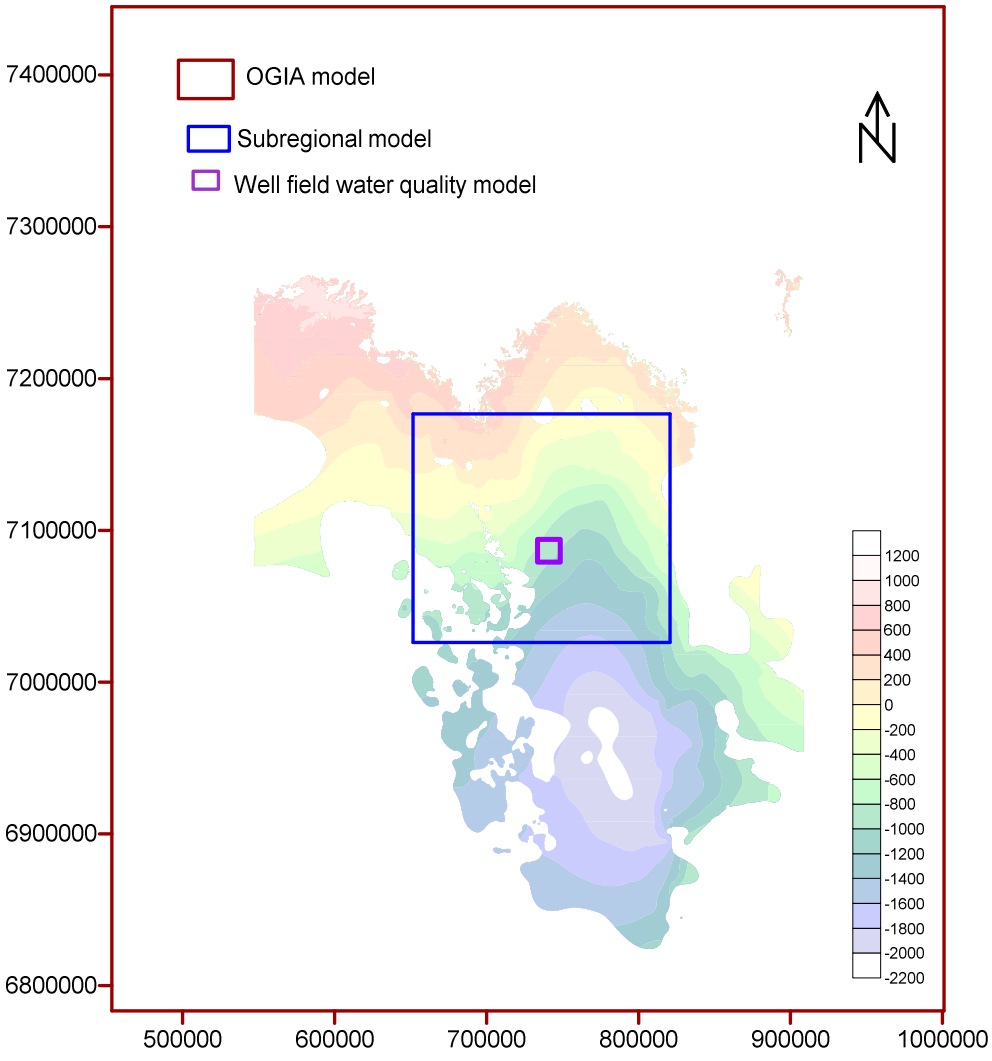

Figure 13: Relative spatial extents of the three 3D models having different spatial and temporal scales. The elevation (m) of Precipice sandstone is shown in the background.

Table 2: Summary of the models in different scales used for injection impact assessment

Model	Prime model purpose	Links between the 4 listed models
1. 2D radial transport model	Analysis of injection trial test for conservative and reactive species	Provides breakthrough curves as calibration targets for well field water quality model (2).
2. Well field water quality model	Making dilution and travel time predictions over the injection well field	Calibrated to predictive breakthrough curve in the radial model (1), regional flows from OGIA model (4), and pump test and injection trials. Upscaling predictions for subregional model (3)
3. Sub regional model	Making groundwater mounding and groundwater flow direction predictions in and beyond the injection field	Calibrated to regional flows from OGIA model (4), and upscaling predictions generated using the well field water quality model (2)
4. OGIA model	Making regional cumulative impact assessments from CSG pumping	Provides background CSG pumping regime, and groundwater flow regime to subregional model (3) and well field water quality model (2).

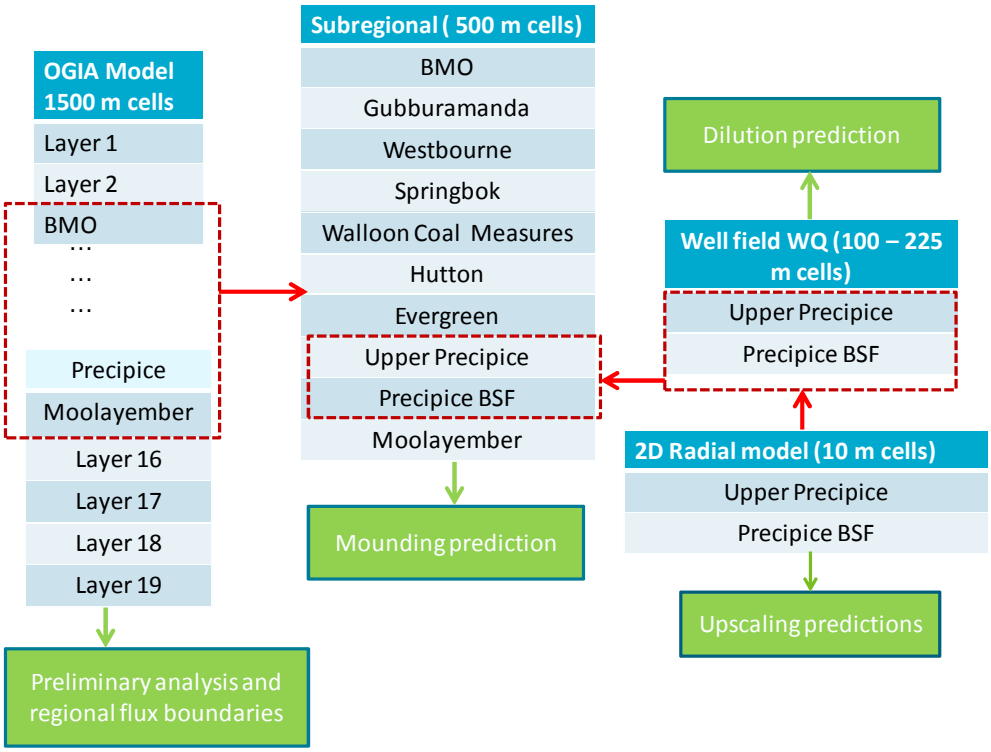

Figure 14: The vertical discretization of the four groundwater models and their purposes

3.2.1 2D RADIAL TRANSPORT MODEL

The 2D radial transport model was used to simulate the flow and transport processes close to the injection wells. This model was calibrated using the tracer data available from the APLNG injection trials. The model

covered a radial distance of 600 m from the injection well R-INJ2-P. Vertically, the model was discretized into 2 layers. Layer 1 represented the upper part of the Precipice sandstone with lower hydraulic conductivity and layer 2 represented the BSF. The injection tracer tests were conducted in the well R-INJ2-P during the injection trials conducted by APLNG between March and September 2013. The model was calibrated to measured bromide and chloride concentrations from the injection trial. The Precipice sandstone was initially represented with a single porosity system but then was replaced with a dual porosity system, which gave a better match to the observed data. Another conceptual model which adopted a vertical discretization of the model domain into 24 layers was also tested; however, the 2-layer representation of the system was sufficient to match to the observed responses from the injection trials.

The calibration parameters for this 2D radial model comprised of the horizontal and vertical hydraulic conductivity, immobile porosity, mobile porosity, mass transfer coefficient, and specific storage and dispersivity values of both the model layers. Spatial variability of these parameter sets, except the mass transfer coefficient, was ensured by using pilot point parameterization. After calibration, the model was used to simulate tracer movement resulting from a "hypothesised" injection scenario, with an injectate concentration of 1 kg/m^3 and a simulation period of 2760 days. This injection scenario was designed such that the injection rates were higher than the rates used for the injection trials, with resulting breakthrough curves extending further into the aquifer, e.g. at distances of 150m and 300m from the injection well. These simulated "hypothesised" break-through curves were then used as calibration targets for upscaling the parameter fields of the well field water quality model, e.g. these break-through curves were the linking predictions.

3.2.2 WELL FIELD WATER QUALITY MODEL

The well field water quality model was built for simulating the flow and advection-dispersion transport processes in the injection well field to predict the travel times and dilutions of any solute present with or mobilised by the injection water. This model represented a block of 16 km × 16 km around the Reedy Creek injection well field. Similar to the 2D radial transport model this model was also discretized vertically into two layers representing the upper Precipice and Precipice BSF. Horizontally the model grid was discretized into cells with size ranging between 100 m to 225 m.

WELL FIELD WATER QUALITY MODEL CALIBRATION

Highly parameterized calibration of the model was achieved using pilot points. Two sets of pilot points were used in the calibration process. One set of pilot points were used to parameterize the hydraulic properties including hydraulic conductivity, storage, porosity and dispersivity. This set comprised of 25 pilot points uniformly distributed across the model grid in all layers. In addition, the spatially varying flux across the four vertical boundaries of the well field water quality model was represented by means of another set of pilot points. This set comprised of 12 pilot points uniformly distributed only along the boundary cells of the model grid in all layers. The general head boundary package (GHB) of MODFLOW was used to define the Neumann boundary condition along the four sides of the model block. The purpose of GHB package is to establish a linear relationship between the flux into (or out of) the model domain and the head in the boundary cell. A reference head is defined in the package and when the head in the boundary cell equals the reference head the flux is zero. If the head in the cell is less than the reference head, water enters the model block through the general-head boundary. If the head in the cell is greater than the reference head, then water leaves the model block. The relationship between the flux and head in the boundary cell is given by

$$Q = -C(H - Href) \qquad (1)$$

where Q is the flux, H is the head in the boundary cell and $Href$ is the reference head and C is the proportionality constant called the conductance. The conductance was considered as the variable parameters during the calibration process. Pilot points distributed at uniform distances were established along the boundary cells to calibrate the GHB conductance. Twelve pilot points were considered for each

model layer. The pilot point conductance values were further interpolated to all the boundary cells using the recently developed pest utility MKGHB (Doherty, 2014). The GHB conductance values were calibrated in a steady state simulation, by matching the positive and negative flux across the well field water quality model block to the corresponding values obtained from the OGIA model.

The calibration objective function of the well field water quality model had four components based on four different calibration target groups, as follows;

(1) Concentration break through curves at 150m and 300 m from the injection trial well simulated using the calibrated 2d radial transport model.
(2) Groundwater fluxes across the well field water quality model domain computed using the OGIA model.
(3) Pump test and injection trial observations.
(4) Steady-state heads within the well field water quality model domain simulated using OGIA model.

Parameter estimation, undertaken to achieve matches to these different sets of calibration targets, was performed in a single calibration exercise using PEST (Doherty, 2010a,b; Doherty et al 2010). To achieve this, the model was run three times in batch processing mode, where each model run corresponded to different stress regimes to simulate the aquifer response corresponding to the different observation groups. For instance, the match to the groundwater boundary fluxes and steady state heads were evaluated by running the model in steady state. The match to the observed heads from injection trials and simulated break through curves were evaluated with a transient simulation of the model with daily stress periods.

After calibration, the well field water quality model was used to simulate dilution and travel time and the groundwater head changes in the Precipice BSF corresponding to the proposed injection scheme with an operation time period of 22 years. In simulating this scenario a temporal discretization of the model with monthly stress periods was adopted and each stress period was discretized into many time-steps. The injection rates for 12 wells considered in this injection scheme are shown in appendix C. This simulation was carried out in a stochastic modelling framework using Null-space Monte Carlo analysis which is described in section 4. The hydrographs of average head increase at three bores were computed from these simulations and were used as calibration targets for the subregional model calibration.

3.2.3 SUBREGIONAL MODEL

The primary purpose of the subregional model was to predict the regional changes in the groundwater head in Precipice and other overlying aquifer systems resulting from the injection scheme. This model has 10 layers and covers a regional extent of 169.5 km ×151 km. The major difference between the subregional model and the OGIA model is that the subregional model has a reduced spatial extent and finer grid cells (500 m × 500 m). Also, the Precipice sandstone is represented with two model layers in the subregional model as compared with a single layer representation in the OGIA model. The first layer in the subregional model represents the Bungil, Mooga and Orallo formations (BMO). Layer 2 to layer 10 in the increasing order represents the Gubberamunda sandstone, Westbourne formation, Springbok sandstone, Walloon coal measures, Hutton sandstone, Evergreen formation, upper Precipice, Precipice BSF and Moolayember formation. The depressurization of the coal seams in Walloon coal measures was represented using the MODFLOW well package in the subregional model based on the extraction rates as represented in the OGIA model . The simulation of groundwater head changes in different model layers thus account for the impacts from both depressurization and injection.

RECHARGE/DISCHARGE REPRESENTATION

The topmost layer represented in this model development comprises the Bungil, Mooga and Orallo formations (BMO). All the 10 layers, including the Precipice layer, outcrop towards the north of the considered model domain. The diffuse recharge occurring over this model domain was obtained from the OGIA model. Thus, there is recharge entering all the model layers at some locations in the subregional

model (Figure 15). Recharge is represented in the model using the MODFLOW recharge package. There are 1857 wells within the subregional model domain extracting water mainly from BMO, Gubberamunda, Springbok, Walloon coal measures, Hutton, Evergreen and Precipice formations. The extraction from these wells and the CSG depressurization estimates from OGIA model, were represented in the subregional model using the MODFLOW well package. The OGIA model used the MODFLOW drain package to define the outflow conditions for different layers within the model. The same boundary condition was defined for relevant layers within the subregional model as well.

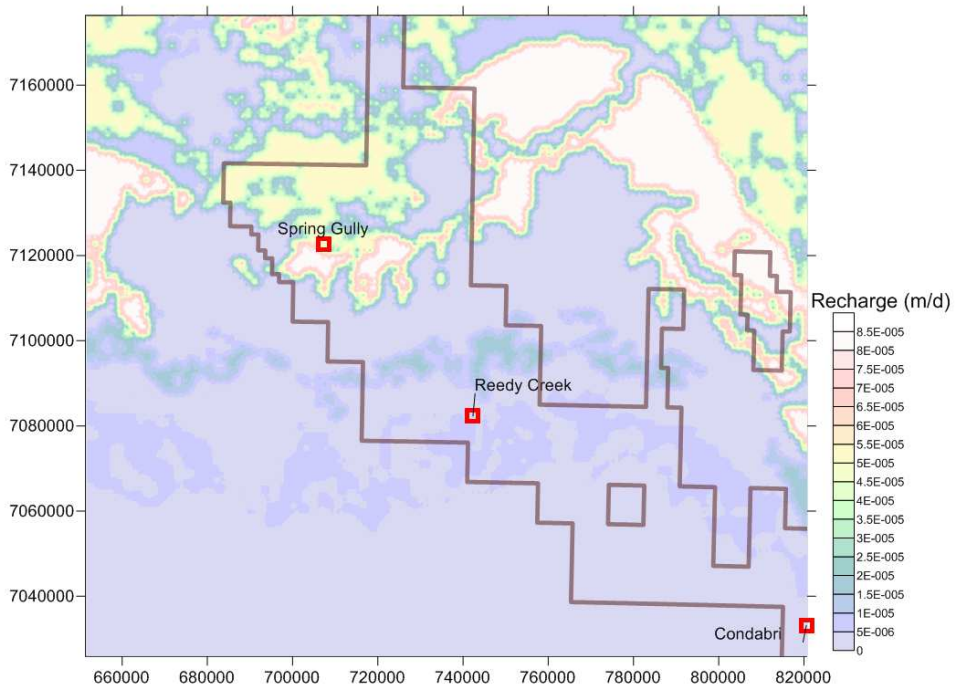

Figure 15: Recharge input represented in the subregional model

SUBREGIONAL MODEL CALIBRATION

A pilot point based parameterization scheme was also implemented for the subregional model to represent the GHB boundary condition and the hydraulic property fields. The locations of pilot points for these two categories in the subregional model are shown in figure 16. There were four calibration target groups for the subregional model. They are;

1) Steady state head observations in the groundwater bores in different formations except the Precipice.
2) Steady state head observations in the Precipice formation.
3) Steady state flux across the subregional model boundaries simulated using the OGIA model.
4) Groundwater head increase at 3 locations within the injection well field simulated using the well field water quality model.

A steady state solution of the flow equation was obtained for the first stress period of the subregional model to simulate the steady state head and flux to match the observation groups 1, 2 and 3. This steady state-stress period represented the pre-CSG groundwater flow system in the Basin. Thus, the CSG depressurization and injection were not included for this stress-period. Subsequently, 264 transient monthly stress periods were considered for simulating the transient groundwater head changes resulting from the proposed injection scheme of CSG produced water injection for 22 years. Calibration targets for this transient simulation period comprised of the groundwater head increase in the monitoring bores close to the well field (R-INJ2-P and R-inj4-P) simulated using the well field water quality model. This was done specifically to upscale the hydraulic parameters near the injection well field in the subregional model. The well field water quality model, with finer spatial discretization, is able to better simulate the steep head

gradient close to the injection well field. An increased level of homogeneity is assumed in the subregional model by choosing a coarser spatial discretization. By matching the groundwater level increase simulated by the subregional model to the better predictions from well field water quality model, equivalent upscaled parameter values are obtained for the area representing the injection well field in the subregional model. Matching to these four calibration targets groups was achieved in two calibration stages. The first stage comprised of the steady state calibration matching to the observation groups 1, 2 and 3. The second stage involved calibrating to the well field water quality model predictions. This ensured that the resulting parameter sets in the subregional model was informed by the regional scale groundwater observations as well as the information from the finer scale water quality model.

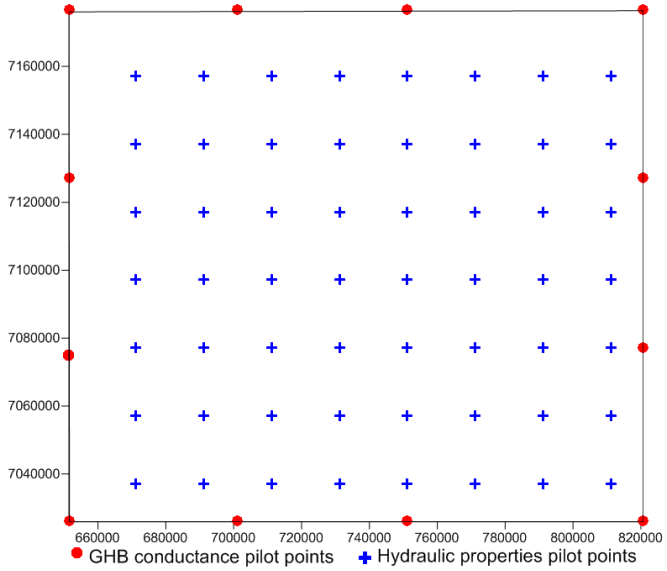

Figure 16: Spatial distribution of the pilot points for the subregional model

Altogether, 991 adjustable parameters were considered in the steady state calibration out of which 91 correspond to the GHB conductance and 900 correspond to the hydraulic properties including horizontal and vertical hydraulic conductivity. Each model layer, except the top and bottom layers, had 56 pilot points for horizontal and vertical hydraulic conductivity. For the transient calibration an additional 450 pilot points were used to represent the adjustable storage values in the model layers. In the transient stage of calibration, only the hydraulic properties in the Precipice BSF (Layer 9) were considered as variable parameters. The hydraulic property values in the other layers were 'tied' to their estimates obtained from the steady state calibration stage. The spatial distribution of the GHB conductance and hydraulic property pilot points for all layers from layer 2 to layer 9 of the subregional model is illustrated in figure 16. In the top and bottom layers of the subregional model representing, respectively the BMO and Moolayember formations, variable but homogenous value of horizontal and vertical hydraulic conductivity was assumed.

3.2.4 INVERSION BASED UPSCALING

As detailed above, each model's specific spatiotemporal scale targets the groundwater monitoring information available in that scale, and then supplies this information to the larger models with its commensurate coarser grid scales. Inversion (calibration) of the coarser scale model to match the simulated characteristics of the fine scale model serves as an upscaling mechanism whereby the model parameters in the relevant regions of the coarse scale model are selected to achieve a match to the model outputs from the fine scale model simulations. Thus, the coarser scale model behaves identically to the fine scale model in the spatial and temporal domains overlapping with that model. For instance, concentration break through simulated by the well field water quality model agrees with the break through obtained using the 2D radial transport model. Similarly the groundwater head increase simulated by the subregional model was similar to that obtained from the well field water quality model. However, for regions outside

the well field water quality model domain in the subregional model, the groundwater head predictions are more informed by the regional groundwater observations.

3.3 Calibration results for the inversion based upscaling

3.3.1 2D RADIAL TRANSPORT MODEL

Calibration of the 2D radial transport model was achieved by matching to the bromide and chloride concentrations observed during the injection trial. The calibration match between the bromide concentrations observed from the injection trial and simulated by the 2D radial transport model is shown in Figure 17.

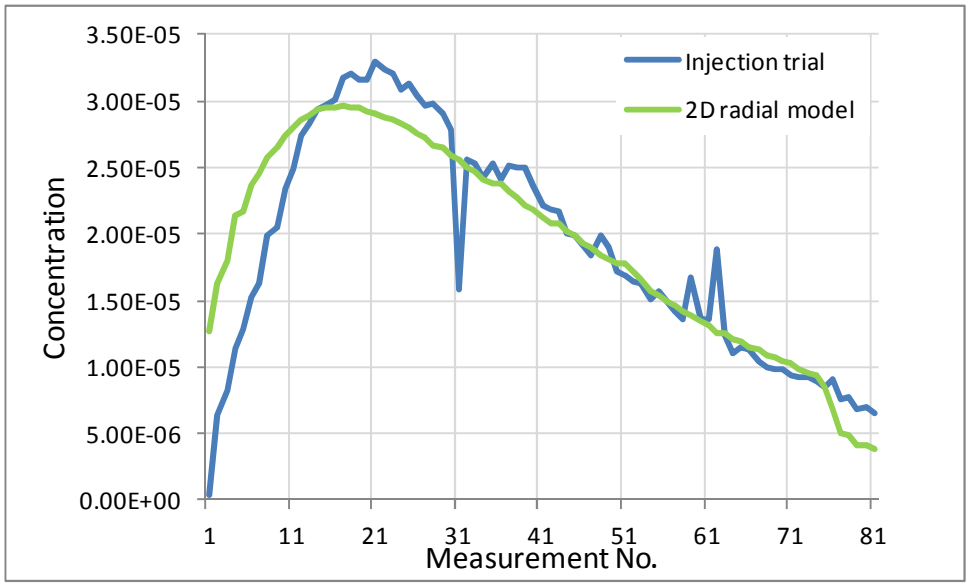

Figure 17: Bromide breakthrough curve simulated by the 2D radial transport model.

3.3.2 WELL FIELD WATER QUALITY MODEL

Calibration of the well field water quality model was completed as described in section 3.2.2. The most sensitive parameters to the different components of the calibration objective function are shown in Table 3. As expected, it was observed that parameters close to the injection well are most sensitive to the calibration target groups (1) and (3) (injection trial head and tracer test data) of the well field water quality model. The determination of parameter values in this region is driven by the head and concentration observations from the injection trial as synthesised via the "linking" prediction at 150m and 300m from the injection well in the 2D radial transport model. The values of other parameters farther from the injection well are informed by the regional calibration targets comprised of the regional flux and steady state heads simulated using the OGIA model.

The four calibration target groups of the well field water quality model had distinct influences on the groundwater flow and transport parameters. The first group contributed to the upscaling of the properties of the well field water quality model in the immediate vicinity of the injection trial well. Mobile and immobile porosities and hydraulic conductivity in the immediate vicinity of the injection well were the most sensitive parameters to this component of the objective function. Calibration to the break-through curve simulated by the 2D radial transport model, resulted in the upscaling of these sensitive parameters. Calibrating to the simulated break-through curve from 2D radial transport model ensures that the flow and transport simulated by the well field water quality model are similar to the more accurate 2D radial transport model simulations near the injection trial well. The match between the break through curves

simulated by the 2D radial transport model and well field water quality model for this injection scenario is shown in Figure 18.

The match between the steady state flux across the well field water quality model domain and the corresponding region of the OGIA model is shown in Figure 19. During the injection trial it was observed that the injection into the well R-INJ2-P did not trigger any groundwater level changes in the well R-INJ4-P. The calibrated well field water quality model reflected this with no change in the head in the monitoring bore over the injection trial period.

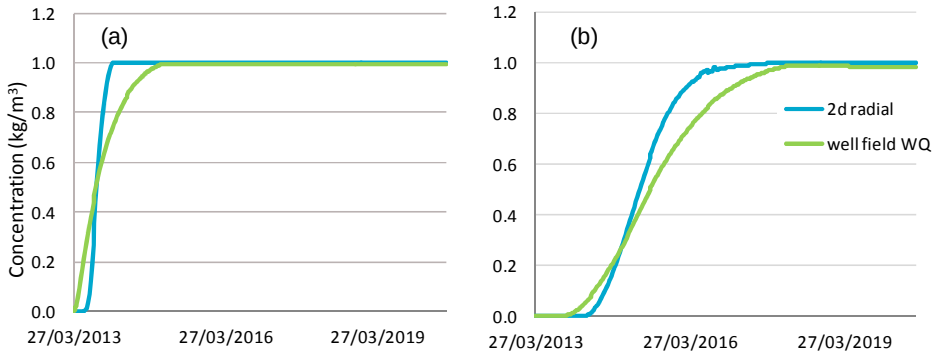

Figure 18: Simulated break through curves for the hypothesized injection scenario using the 2D radial transport model and the well field water quality model at distances (a) 150 m and (b) 300 m

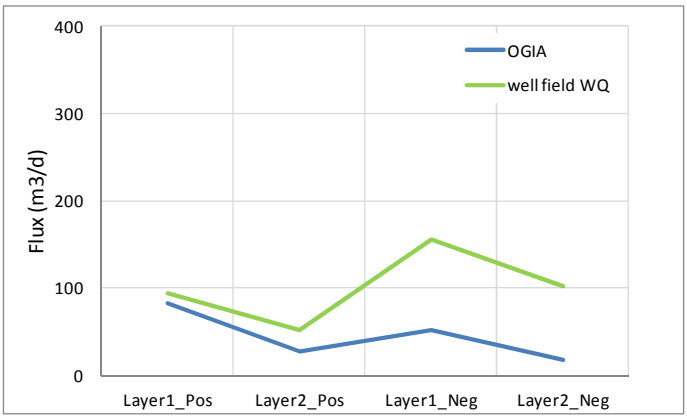

Figure 19: Calibrated steady-state flux across the well field water quality model domain.

Table 3: Components of the calibration objective function of the well field water quality model

Objective function Component number	Objective function component type	Two most sensitive parameter groups	Most sensitive parameter near the injection well?
1	Simulated break through curve	n & K_h	Y
2	Steady state flux	GHB & S	N
3	Injection trial head observations	S & K_h	Y
4	Steady state head	GHB & K_h	N

S = Storage; K_h = Horizontal hydraulic conductivity; GHB= GHB conductance; n = Porosity

3.3.3 SUB REGIONAL MODEL

The subregional model was calibrated as described in section 3.2.3. The match to different calibration target groups is shown below. Figure 20 depicts the match between OGIA and the subregional model boundary fluxes for different model layers. It is apparent that the largest volume of water entering the subregional model domain flows in through the Hutton and the Precipice aquifers. Also, it is clear that more water enters this block than exits it through lateral flow. This indicates that well abstraction is significant in the Hutton and Precipice aquifers. The scatter plot of observed versus modelled steady state heads for bores in all the model layers and in the Precipice layer are shown in Figure 21(a) and 21(b) respectively.

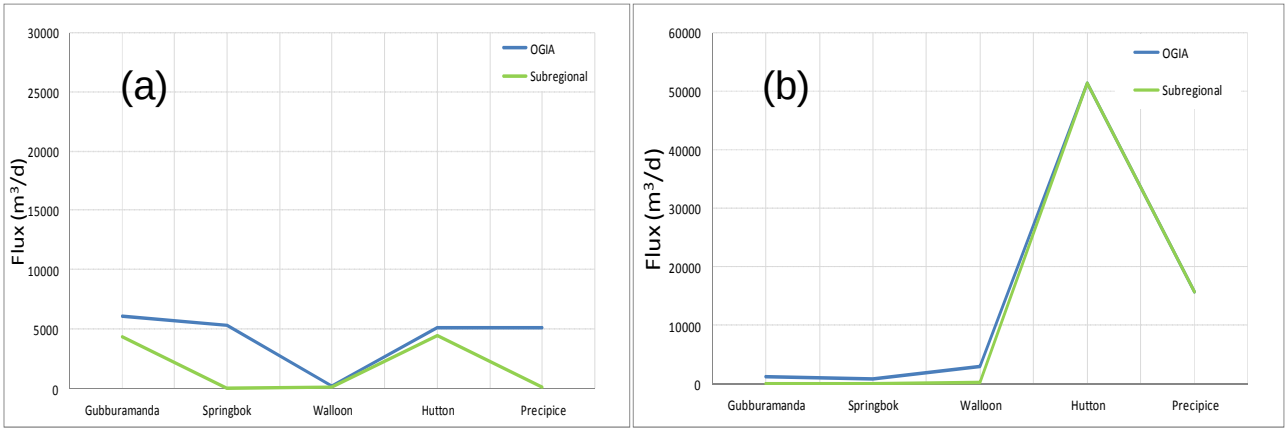

Figure 20: Match between the steady state boundary flux of subregional model and corresponding OGIA values: 19(a) depicts the negative flux (flux out of the model domain) and 19(b) depicts the positive flux (flux into the model domain)

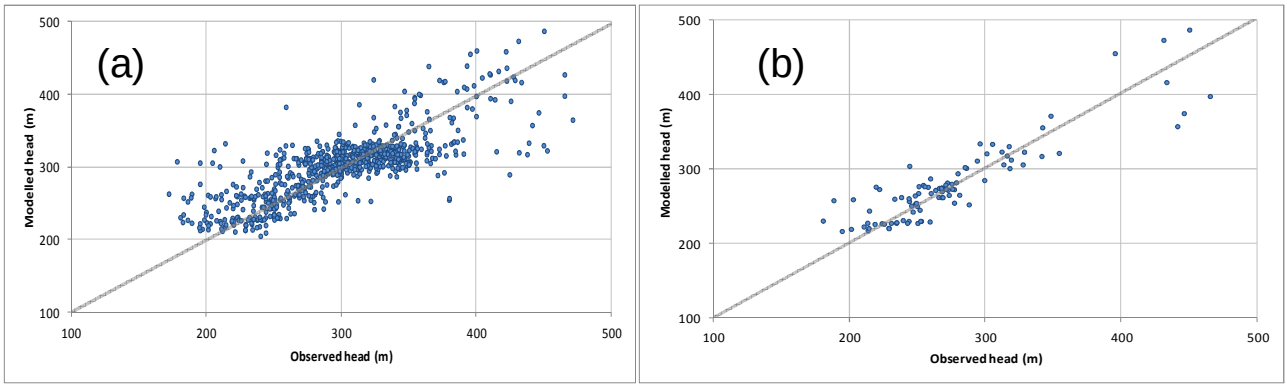

Figure 21: Observed Vs subregional model simulated heads for (a) all bores within the model domain (b) Precipice bores

The match between the observed and modelled heads for different Precipice bores is also illustrated as a line plot in Figure 22. It is notable that the calibration is able to capture the spatial dynamics of flow within the subregional model domain reasonably well where the head values vary over hundreds of metres. The spatial plot of the head residuals for Precipice is shown in Figure 23 indicating lowest errors close to the Reedy Creek injection site.

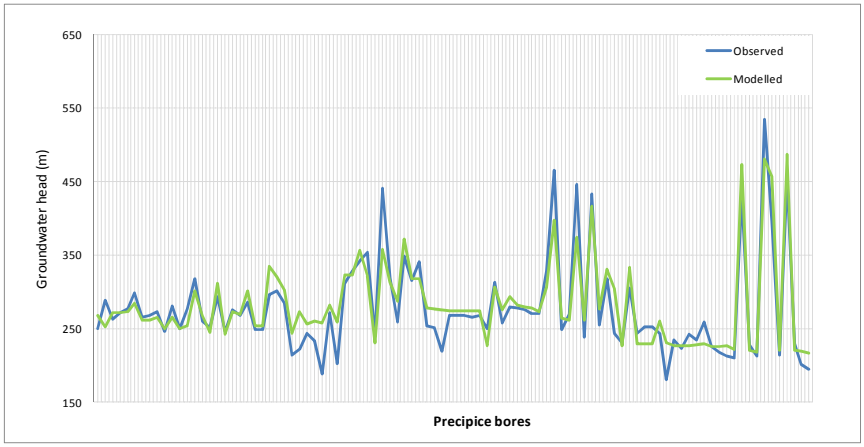

Figure 22: Line plot of the observed and modelled steady state heads for different Precipice bores

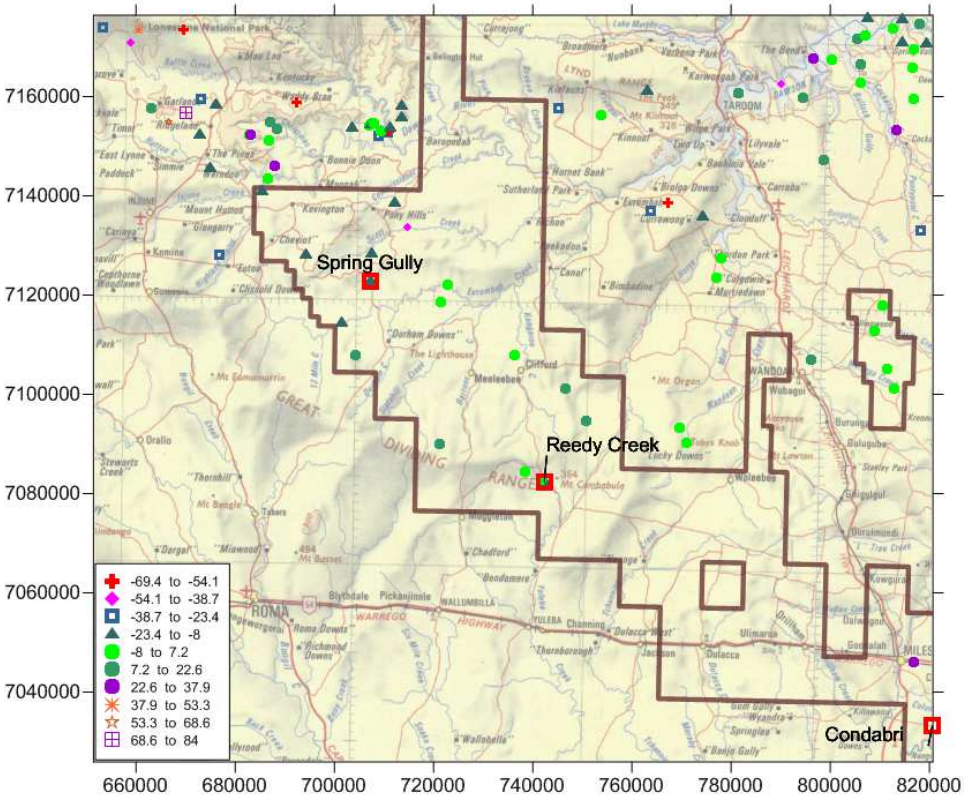

Figure 23: Spatial plot of the steady-state head residuals (m) for Precipice BSF.

The groundwater head contours for Precipice BSF interpolated from the observed head measurements and obtained from the subregional model after steady state calibration are shown in Figure 24.

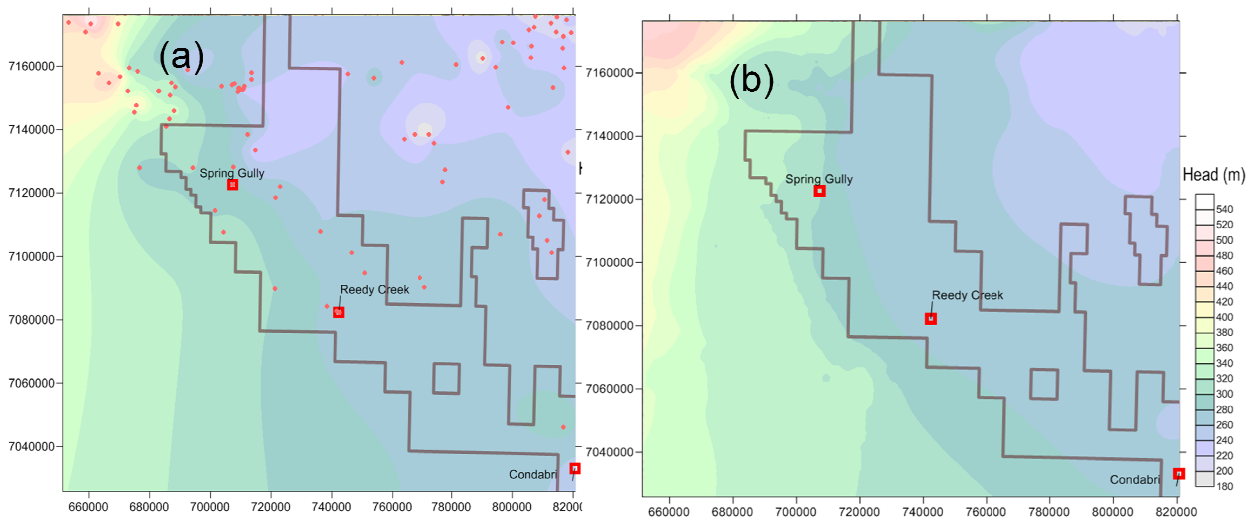

Figure 24: Contours of groundwater heads from: (a) interpolation of bore observations (the dots indicate bore locations) and (b) subregional model simulation

The volumetric steady state budget of the subregional model in comparison with the volumetric budget of the same spatial domain within the OGIA model is shown in Figure 25: Volumetric budget of the subregional model and the OGIA budget for the same area. The budget indicates that the subregional model behaves similar to the OGIA model in terms of the stresses and boundary fluxes.

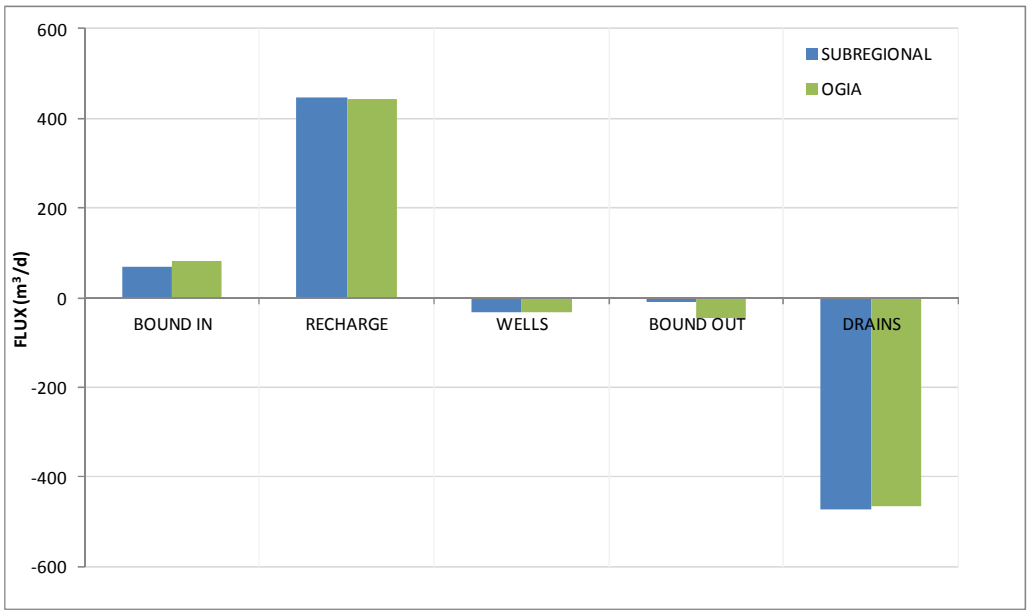

Figure 25: Volumetric budget of the subregional model and the OGIA budget for the same area

In the transient stage of the subregional model calibration, the only adjustable parameters were the hydraulic properties of layer 9 (Precipice BSF) and all other parameters were fixed at their values obtained from the steady state calibration. The transient calibration essentially aimed at upscaling the hydraulic properties near the injection well field so that the subregional model replicate the well field water quality model simulation of flow in this region.

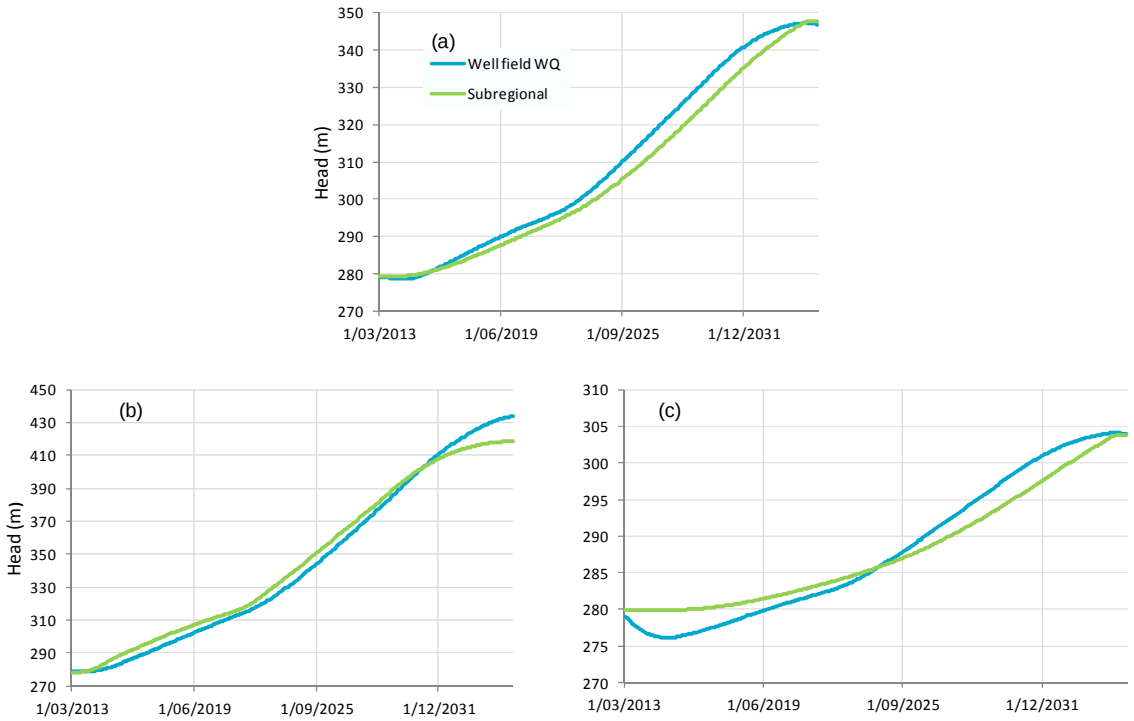

Figure 26: Match between the simulated bore hydrographs obtained using well field water quality model and subregional model for the bores (a) R-INJ2-P (b) R-INJ4-P and (c) pseudo bore

The match in the groundwater heads at three locations simulated by the well field water quality model and subregional model after upscaling is illustrated in Figure 25. It is noteworthy that Figure 26(a) and (b) correspond to the bores R-INJ2-P and R-INJ4-P close to the well field respectively, where as Figure 25(c) correspond to a location (pseudo bore) farther from the well field and is shown in Figure 27.

3.3.4 PREDICTION ANALYSIS

The groundwater head increase resulting from the proposed injection scenario was simulated using both the well field water quality model as well as the subregional model. The groundwater transport processes were simulated using the well field water quality model only. The groundwater head rise and dilution impacts were predicted for an injection scenario proposed by APLNG. The average injection rate for this scenario was 22.1 ML/d over 22 years. As per the proposed scheme, a constant monthly injection rate was simulated to be distributed amongst 12 injection wells in proportion to the estimated transmissivity at these well locations. The injection well locations for this scenario and the APLNG-estimated transmissivity (APLNG, pers. Comm.) contours are shown in Figure 27. The simulation start date of 27/03/2013 was used in plotting the time series of groundwater head increase in different bores. Injection induced groundwater head increase and dilution impacts were simulated in a stochastic framework using Null-space Monte Carlo approach. The Null-space Monte-Carlo simulation of groundwater head increase and dilution impacts is described in section 4.

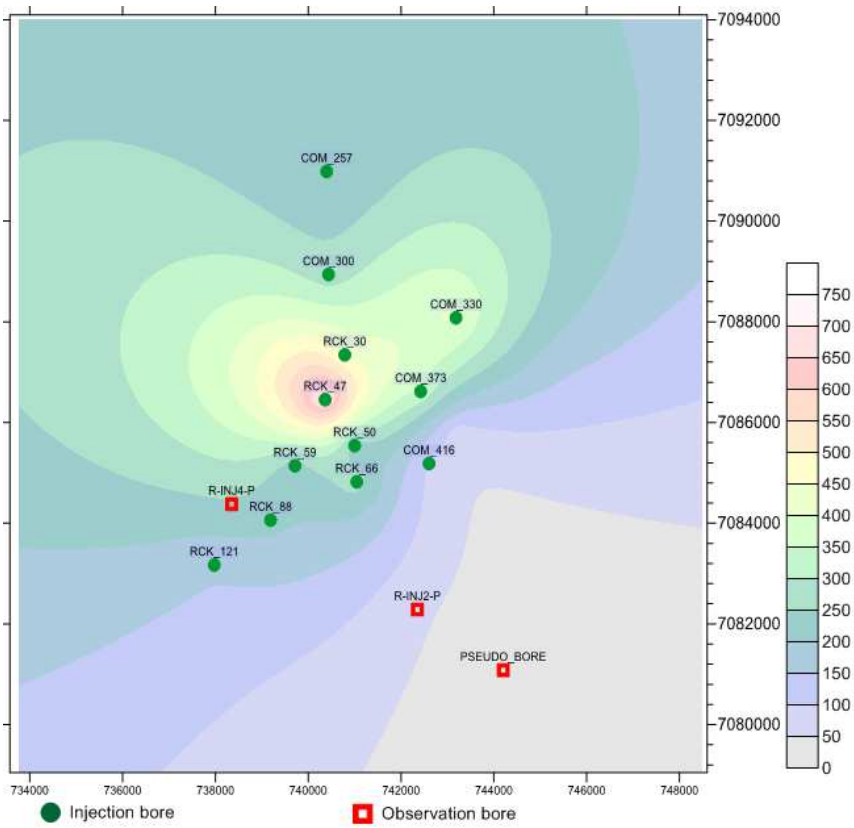

Figure 27: Proposed locations of the injection wells. APLNG estimated transmissivity (m^2/d) at these locations are contoured in the background.

3.4 Summary

An integrated multi-scale modelling approach was developed for simulating the injection induced groundwater quantity and quality changes resulting from the proposed injection scheme at Reedy Creek in Surat Basin. The approach utilized models in different scales ranging from a fine scale model for simulating two dimensional flow and transport near the injection wells to a coarse scale OGIA model for simulating the regional impacts. The models in these different scales were integrated into a single modelling framework for predicting the local and regional impacts of the injection scheme. The local scale models developed in this approach were used to predict the local impacts and provide a basis for estimation of the upscaled parameters required for the models in bigger scales. The regional and subregional scale models were used to predict the regional groundwater head impacts resulting from large scale injection as well as provide flow boundary conditions for the smaller scale models. Predictive simulations using these models were carried out in a stochastic modelling framework using Null-space Monte Carlo simulations and are described in section 4.

4 Uncertainty: Null-space Monte Carlo Analysis

4.1 Overview

Given the small amount of data available from the injection trial and pump tests it is clear that the groundwater flow and transport parameters of the well field water quality model and subregional model cannot be estimated uniquely. Furthermore, even when there is large amount of data available for model calibration, small scale variability of aquifer properties are difficult to represent in models because of computational constraints, resulting in model structural uncertainty. The combined model structural and parameter uncertainty results in model prediction uncertainty.

This uncertainty is reduced by calibration of the models, as described in section 3, which constrains the uncertainty in the parameters to the extent that is possible based on the information available from the groundwater monitoring data. It is also reduced by the use of pilot point parameterisation combined with the multi-scale modelling approach which serves to reduce model structural errors. Despite these strategies, the remaining uncertainty associated with impacts of the proposed injection scheme must be described. This is particularly important for predictions such as dilution, where even a low probability of impact would indicate a risk and mitigation efforts may be necessary.

For this task we used the Null-space Monte Carlo analysis method (Tonkin and Doherty 2009), which provides a useful and efficient approach for the assessment of the uncertainty in the well field water quality model and subregional model predictions. Specifically uncertainties in the peak dilution and travel time were explored by the stochastic simulation of the flow and transport processes using the well field water quality model in the Null-space Monte Carlo analysis framework.

4.2 Methodology

The first step of Null-space Monte Carlo analysis was the generation of stochastic parameter fields using an appropriate parameter covariance matrix, denoted as C(**p**). The covariance matrix was generated using the same description of geostatistical structure (i.e. the variogram) that was used for Kriging the hydraulic properties from the pilot points. The calibrated parameters were then subtracted from the stochastically generated parameter field. The difference between the two was then projected on to calibration null-space (Doherty et al., 2010c). The calibration null-space designates a subset of the model parameter space comprising of combination of parameters that cannot be uniquely estimated based on the calibration data set. In contrast to solution space parameters, any changes to parameter values in the calibration null-space have minimal effects on the state of calibration of the model. Thus, by projecting the difference between the randomly generated parameters and the calibrated parameters onto the null-space enabled the retention of the model in a near-calibration state, even with the new set of parameters, so only minimal recalibration is then required.

Null-space Mote Carlo analysis was performed for predictions made with both the well field water quality model and the subregional model. The sensitivity of the model outputs to the model parameters is encapsulated in the Jacobian matrix which is comprised of the first order partial derivatives of all model outputs with respect to the model parameters. Using the methodology described above a suite of 500 parameter realisations were generated for both models.

Recalibration was undertaken using PEST to adjust each of these nearly calibrated parameter fields. This resulted in 500 sets of fully calibrated parameter fields for both the well field water quality model and subregional model. Predictive simulations were then run,in a batch mode, with the 500 parameter sets for both models. Uncertainties in the flow and transport predictions quantified using this Monte Carlo simulation framework are now described in the following sub-sections.

4.3 Groundwater head increase in Precipice BSF

The groundwater head increase close to the injection well field up to a distance of 16 km was simulated using the well field water quality model. The subregional model also simulated the groundwater head increase at 16 km, but additionally was able to simulate head responses farther away from the well field, up to a distance of to 160 km. These simulations are now both described below.

4.3.1 NEAR WELL FIELD GROUNDWATER HEAD INCREASE

The Null-space Monte Carlo analysis on the well field water quality model resulted in 500 realisations of the predicted groundwater head hydrograph for all observation locations. Three observation locations were selected to provide calibration targets for the subregional model, as illustrated in Figure 28. The average of the 500 hydrographs for each of the three monitoring bores was used as the calibration targets for the subregional model. This resulted in the subregional model mimicking the average predictions of the well field water quality model over the overlapping model domain. Null-space Monte Carlo analysis of the subregional model followed this inversion based upscaling.

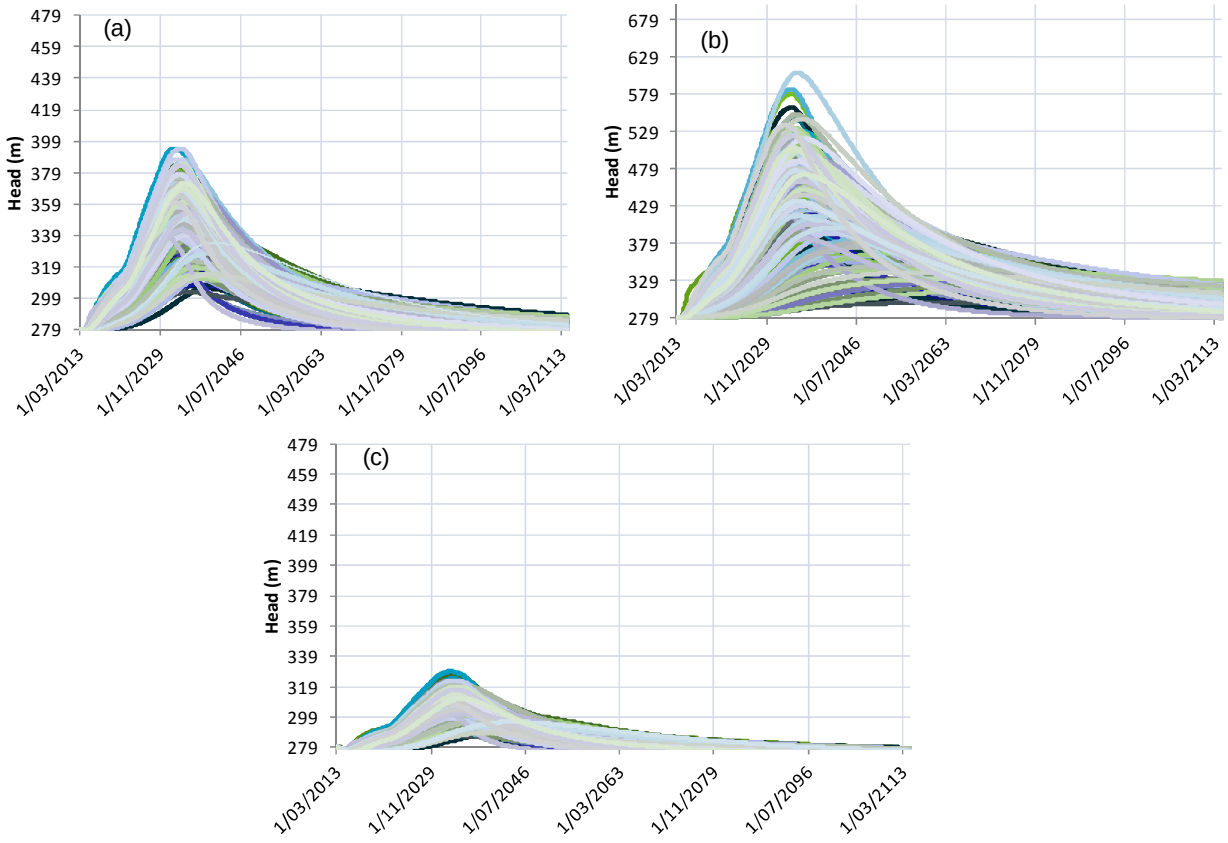

Figure 28: Bore hydrographs for three bores viz, (a) R-INJ2-P (b) R-INJ4-P and (c) pseudo bore simulated using the well field water quality model

It is readily observable from the plots that the uncertainty is large for the simulated heads, particularly for the peak values. This is because the simulated heads are very sensitive to both the hydraulic conductivity distribution around the well field as well as to the GHB conductance at the model boundaries. Considering that the hydraulic conductivity distribution is calibrated with the limited information available from the injection trial conducted for one well, this large uncertainty was expected. When simulating the dilution process, the velocity field is proportional to the head gradients and not the absolute value of heads, and

hence the uncertainty in the dilution simulated using these uncertain flow fields is proportionally less than for the head values.

4.3.2 SUBREGIONAL GROUNDWATER HEAD INCREASE

The groundwater head hydrographs at the same three bore locations shown in Figure 28, were also simulated using subregional model, as shown in Figure 29. Essentially the hydraulic parameters of the subregional model which are located close to the injection well field were upscaled in such a way that the simulations of the groundwater head increase by the subregional model mimics the simulated average obtained using the well field water quality model. However, it should be noted that the primary purpose of the subregional model is to predict the groundwater head changes far away from the injection well field.

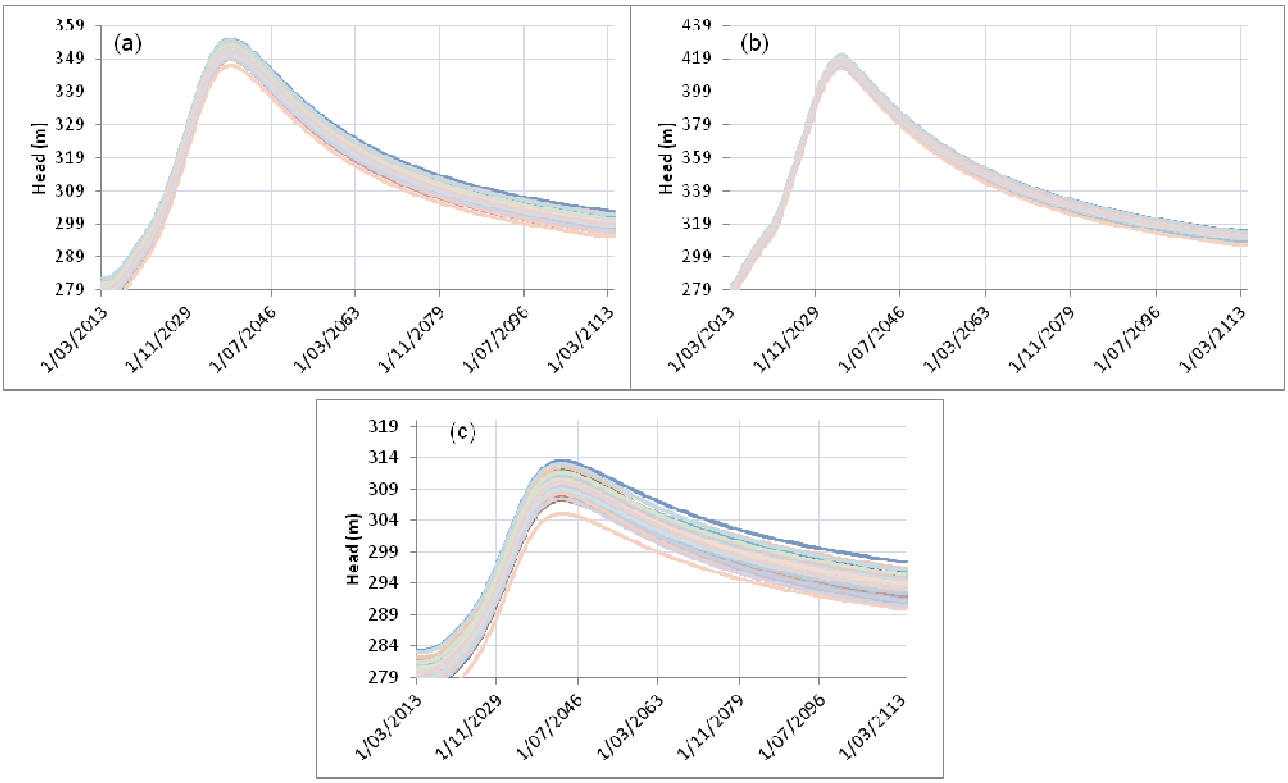

Figure 29: Bore hydrographs for three bores viz, (a) R-INJ2-P (b) R-INJ4-P and (c) pseudo bore simulated using the subregional model

The head increase hydrographs were obtained for all locations within the subregional model domain, and the hydrograph of groundwater head increase for the risk receptor domestic bore RN123030 is illustrated in Figure 30. Although head hydrographs corresponding to only Precipice bores are shown here, the hydrographs of groundwater head change in other aquifer layers are also available from the subregional model simulations if required. However, significant groundwater head changes were not indicated in any domestic bore in the Hutton or other aquifer layers.

The maximum groundwater head increase simulated at the four bores, R-INJ2-P, R-INJ4-P, the “pseudo bore” and RN123030 are given in table 2. The maximum simulated head increase over a 100 year period simulated for the closest risk receptor bore was 4.3 m. Groundwater head changes in bores at farther distances would be much lesser than this value. Given that groundwater head changes of this order of magnitude occur even with the natural unsteady nature of flow in the confined aquifers in Surat Basin, the injection induced temporary increase in the groundwater head in Precipice sandstone does not necessarily indicate a hydrogeologically negative impact. Simulated groundwater head increase contours for different snapshots in time are presented in Figure 31, Figure 32 and Figure 33.

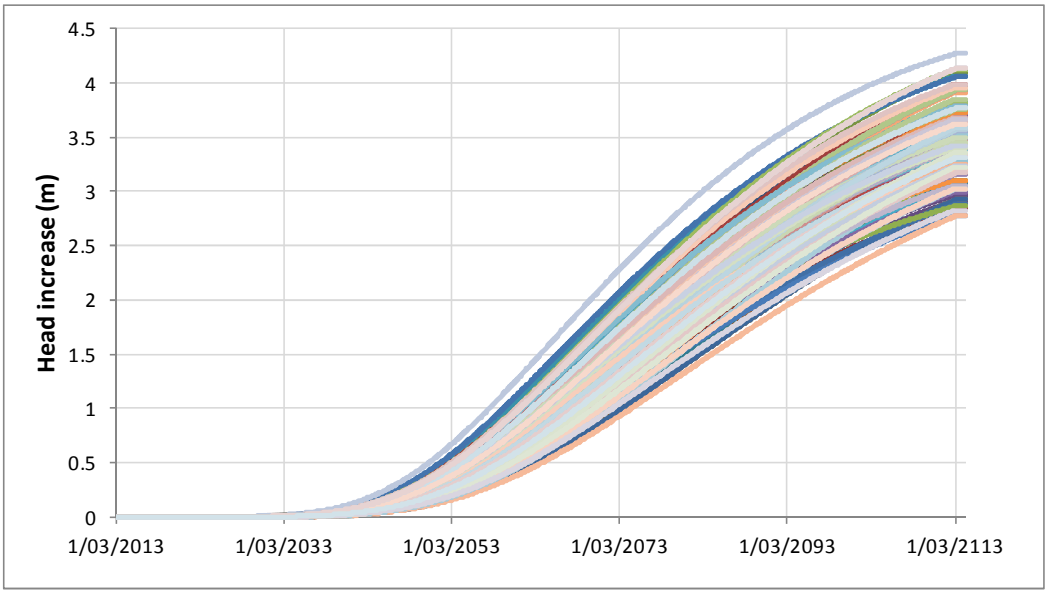

Figure 30: Bore hydrograph for the risk receptor domestic bore RN123030

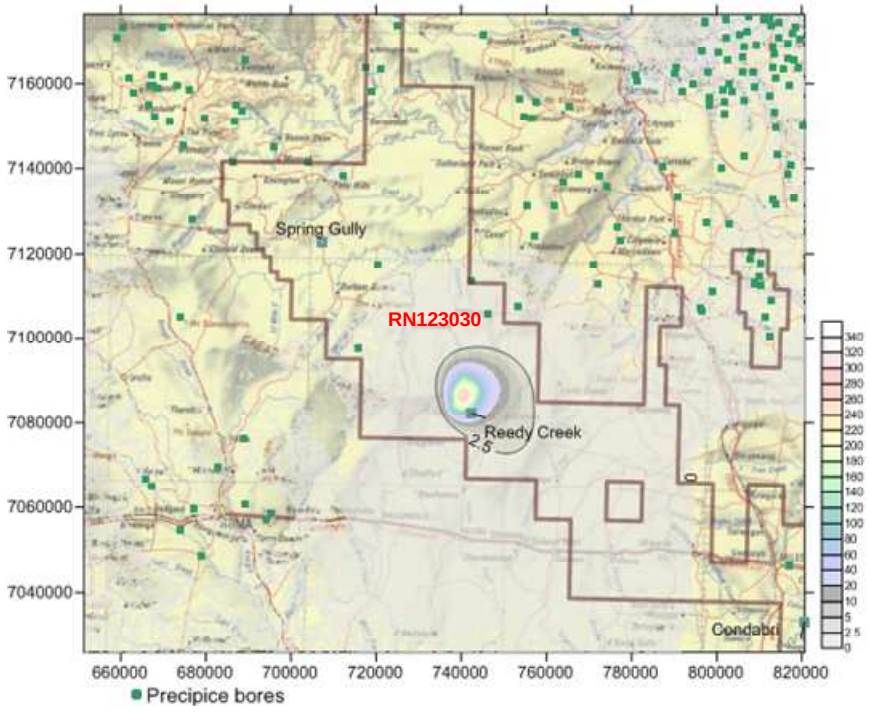

Figure 31: Simulated average head increase (m) in the Precipice BSF when the injection ceases after 22 years.

Table 4: Maximum head increase simulated by the subregional model for the observation bores and indicative risk receptor

Bore	Maximum head increase (m)
R-INJ2-P	72.7
R-INJ4-P	140.1
Pseudo bore	30.5
RN123030	4.3

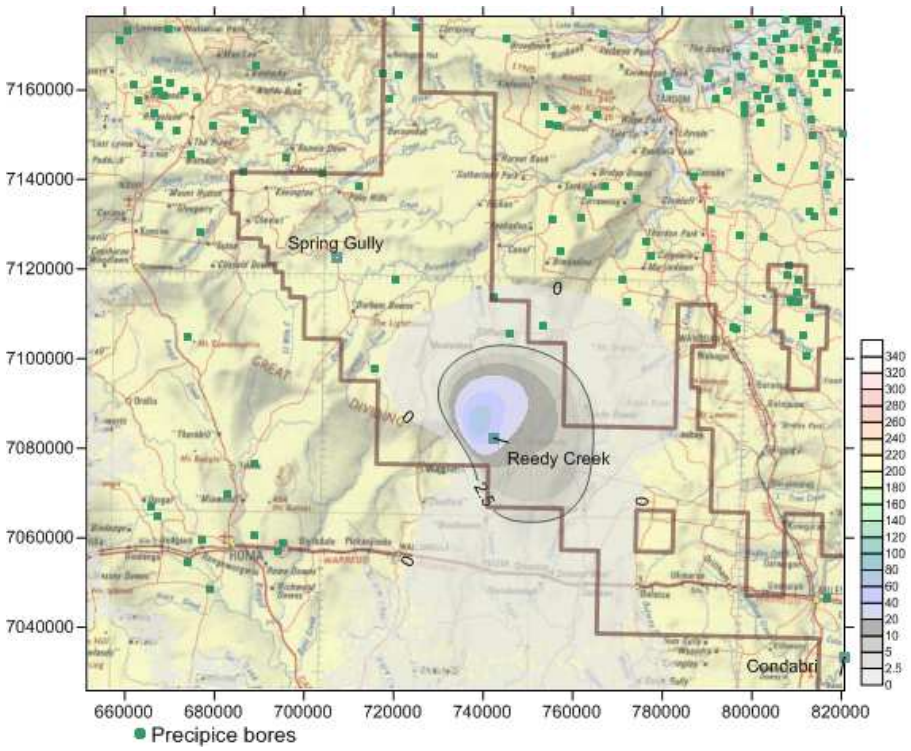

Figure 32: Average head increase (m) in Precipice BSF after 50 years from the start of injection (Injection stops at 22 yrs)

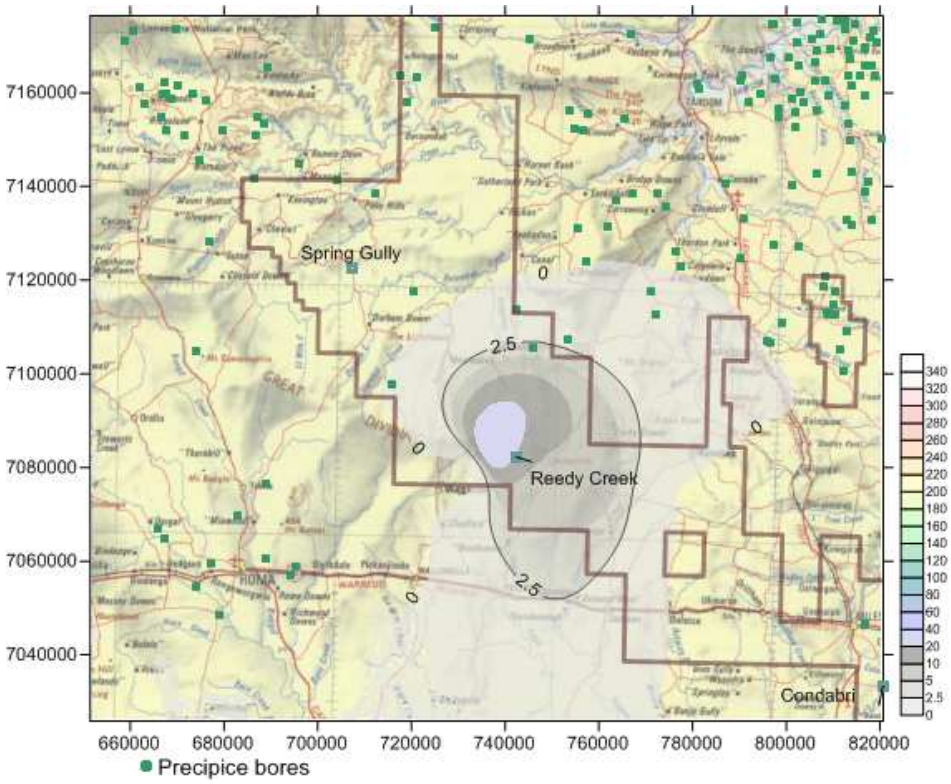

Figure 33: Simulated head increase (m) in Precipice BSF at the end of 100 years

4.4 Groundwater head changes in overlying aquifers

Groundwater head changes in the aquitards and fresh water aquifers above Precipice sandstone were also simulated using the subregional model. The average head increase in the model layers representing the upper Precipice, Evergreen formation and Hutton sandstone were also computed from the Null-space

Monte Carlo analysis already described. In the model layer 8 representing upper Precipice, local head increases were simulated close to the injection wells. The maximum simulated head increase in the upper Precipice layer was approximately 20 m towards the centre of the well field. The simulated head increase in the upper Precipice at the end of the injection scheme and after 50 years is shown in Figure 34 and Figure 35. The simulated head increase in the Evergreen formation at the end of injection and after 50 years are shown in Figure 36and Figure 37. Only a slight change in the head distribution in the Evergreen formation is shown to result from the injection and no change in the groundwater head distribution was simulated in the Hutton sandstone (which overlies the Precipice sandstone and Evergreen formation). It therefore follows that changes in the groundwater head distribution in any shallower overlying freshwater aquifers, such as the Gubberamunda, are very unlikely.

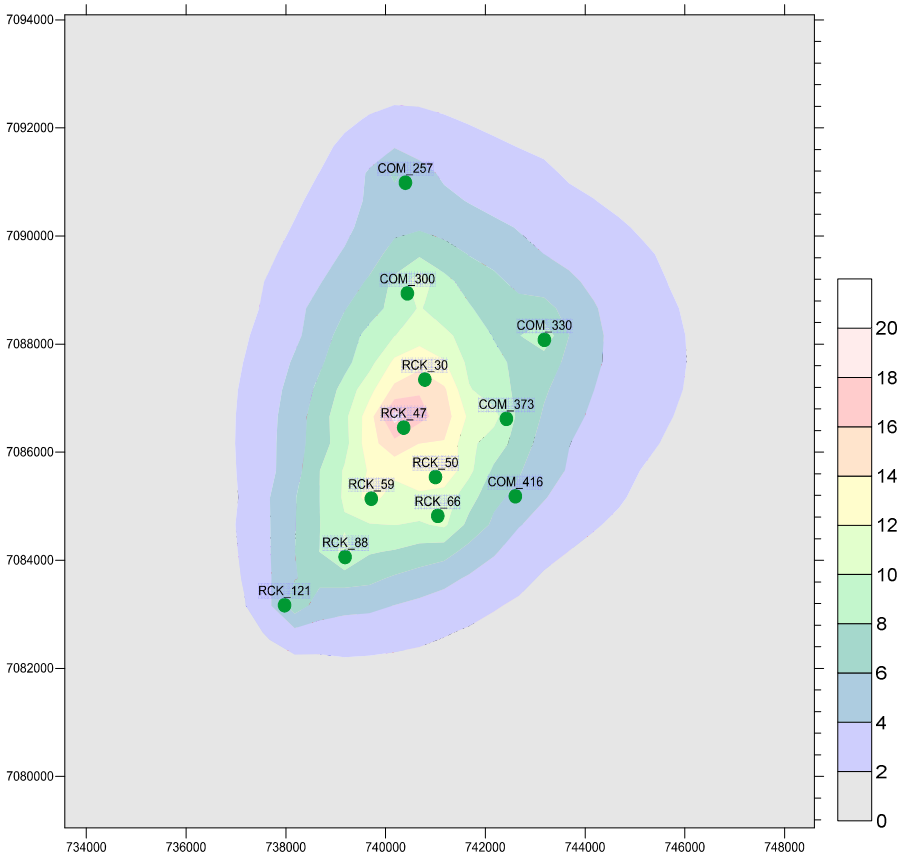

Figure 34: Groundwater head increase (m) in the upper Precipice layer when the injection ceases after 22 years.

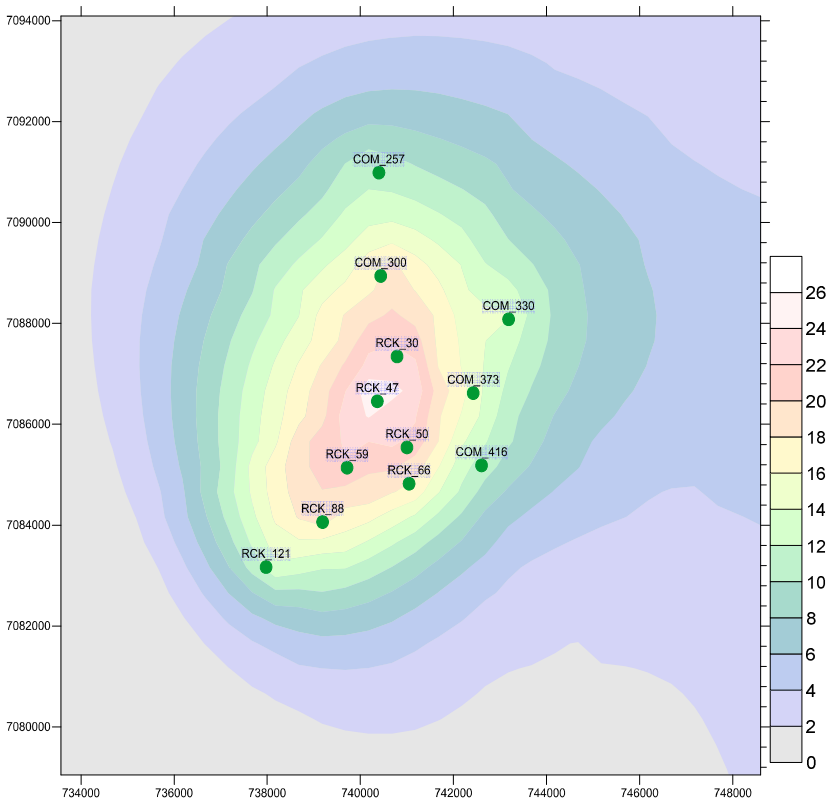

Figure 35: Groundwater head increase (m) in the upper Precipice layer after 50 years

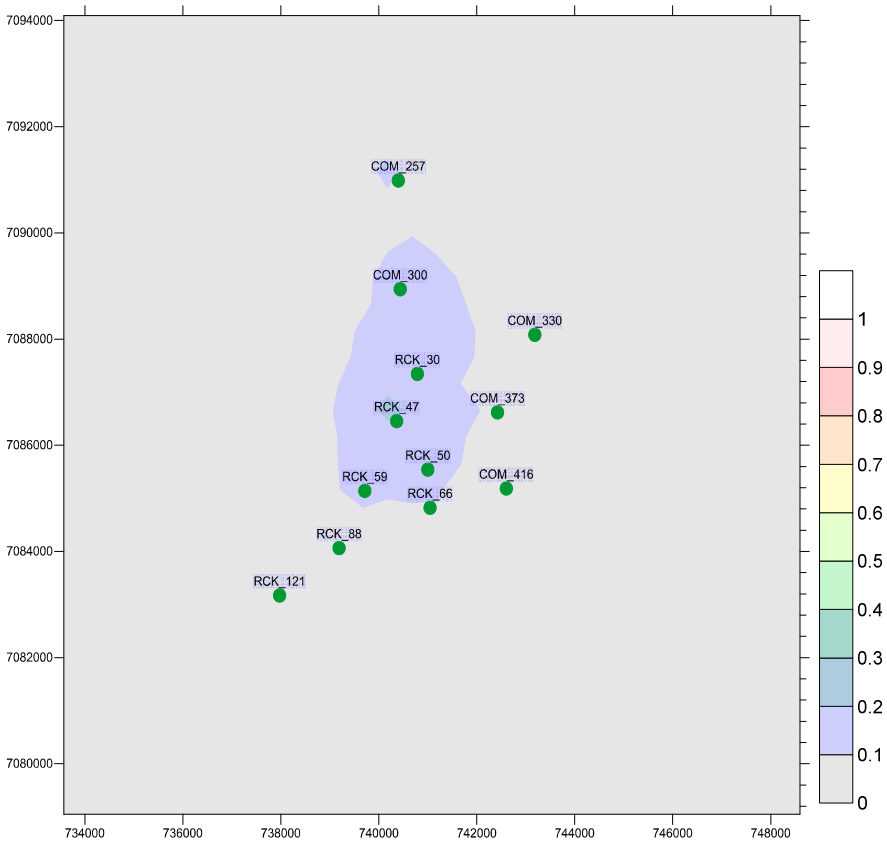

Figure 36: Groundwater head increase (m) in Evergreen formation at the end of 22 years of injection

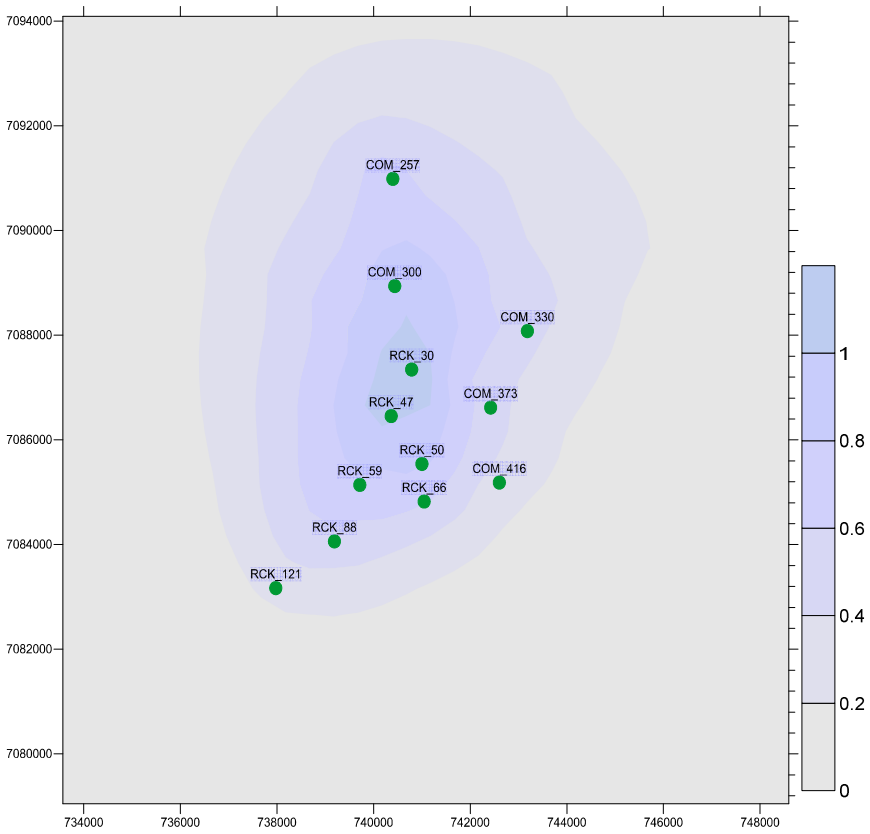

Figure 37: Groundwater head increase (m) in Evergreen formation after 50 years.

4.5 Dilution of reinjected water in the Precipice aquifer

Dilution of the reinjected CSG water was simulated using the well field water quality model. The flow field was simulated using MODFLOW and the transport within this flow field was simulated using MT3D. The transport modelling scenario analysed the fate of the injected water with an hypothesised concentration of 1kg per m^3. It was assumed that this was injected into all the 12 wells continuously over the injection period of 22 years. It is emphasised that this simulation is an hypothetical scenario adopted only to establish dilution rates for a conservative tracer. Testing of the treated CSG water indicates there is no risk of contaminants, even at very low concentration levels, being present in the injection water. However, a potential cause of contamination is the mobilization of geogenic contaminants resulting from high pressure injection. A detailed investigation of injection induced transport of geogenic contaminants in the vicinity of the injection wells is being carried out in the GISERA surface and groundwater hydrology project 1 titled 'Geochemical response to injection' (http://www.gisera.org.au/research/waterprojects/water-project-1-response-injection.pdf). The objective of the transport simulation in the current study was to simply investigate the expected dilution over the region represented by the well field water quality model.

The dilution of the injectate to $1/10^{th}$, $1/100^{th}$ and $1/1000^{th}$ of its initial concentrations were investigated. Initially, the calibrated model was used to simulate dilution that would occur over the life of the injection scheme (22 years). Figure 38 shows the contours of predicted peak dilution within this period. In this context, peak dilution refers to the maximum concentration that would occur over the 22-year period. Contours of the times at which peak dilution occurs for this scenario are shown in Figure 39.

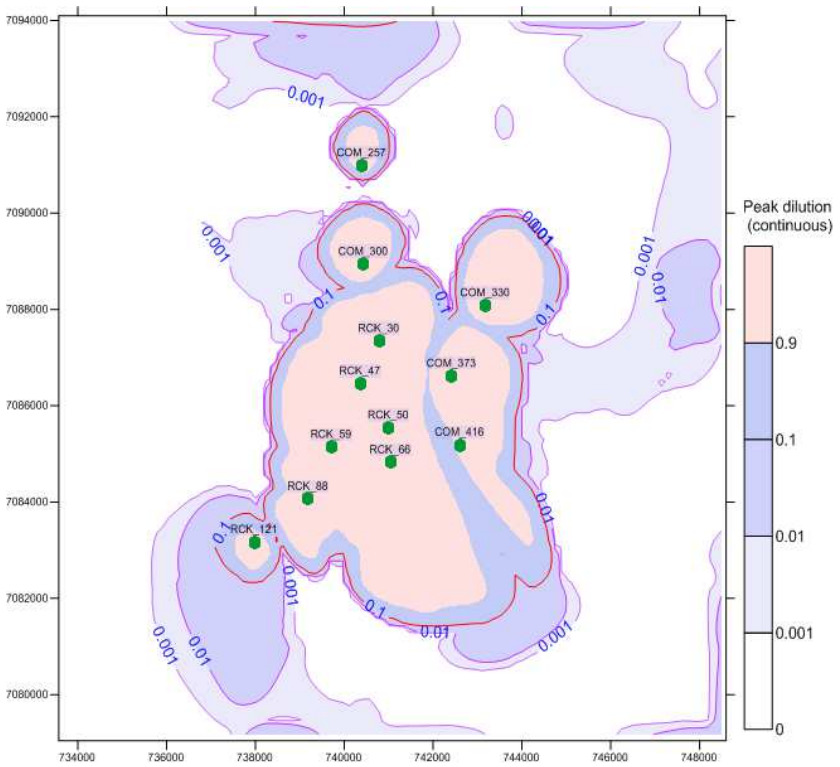

Figure 38: Contours of dilution to 1/10th, 1/100th and 1/1000th concentration (Note that this contour plot does not represent a snapshot in time, but the peak dilution over the 22 year period)

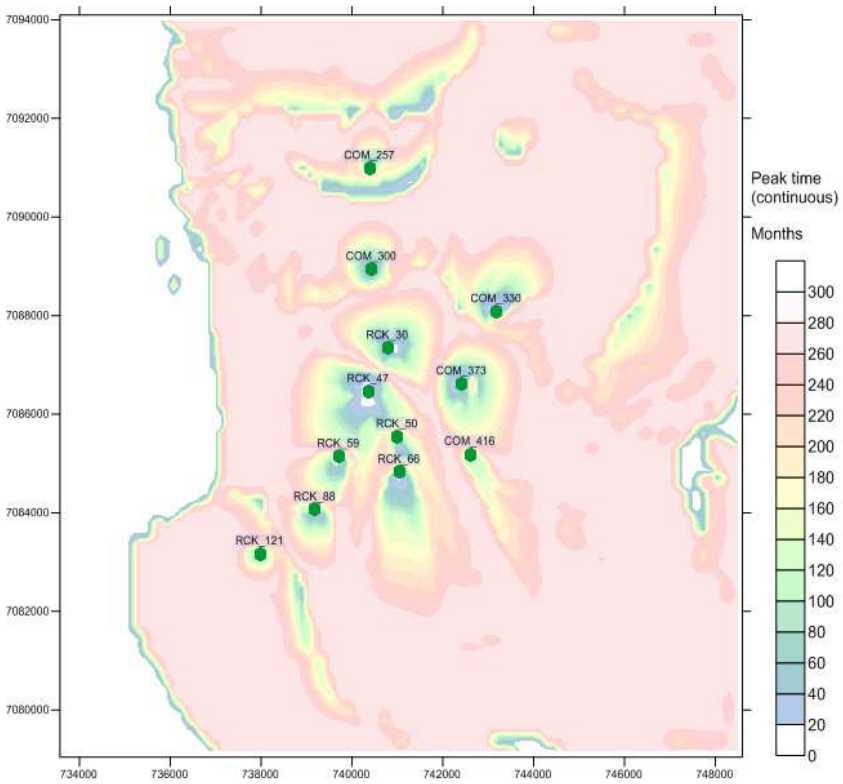

Figure 39: Contours of the travel times at which the peak dilution occurs

Subsequently, stochastic simulation of the dilution process was undertaken using Null-space Monte Carlo analysis. The contours of the mean peak dilution obtained from the Null-space Monte Carlo are shown in Figure 40 and the corresponding uncertainty is shown in Figure 41. Uncertainty was quantified as the standard deviation of the predicted dilution over 500 simulations.

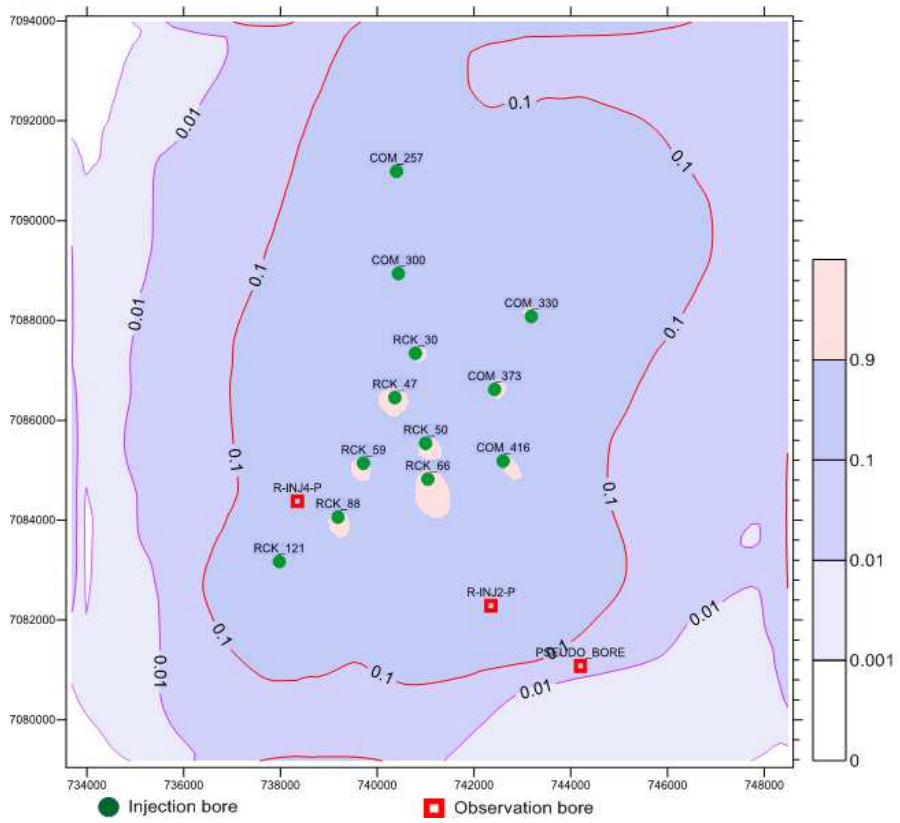

Figure 40: Mean peak dilution obtained from the Null-space Monte Carlo simulation

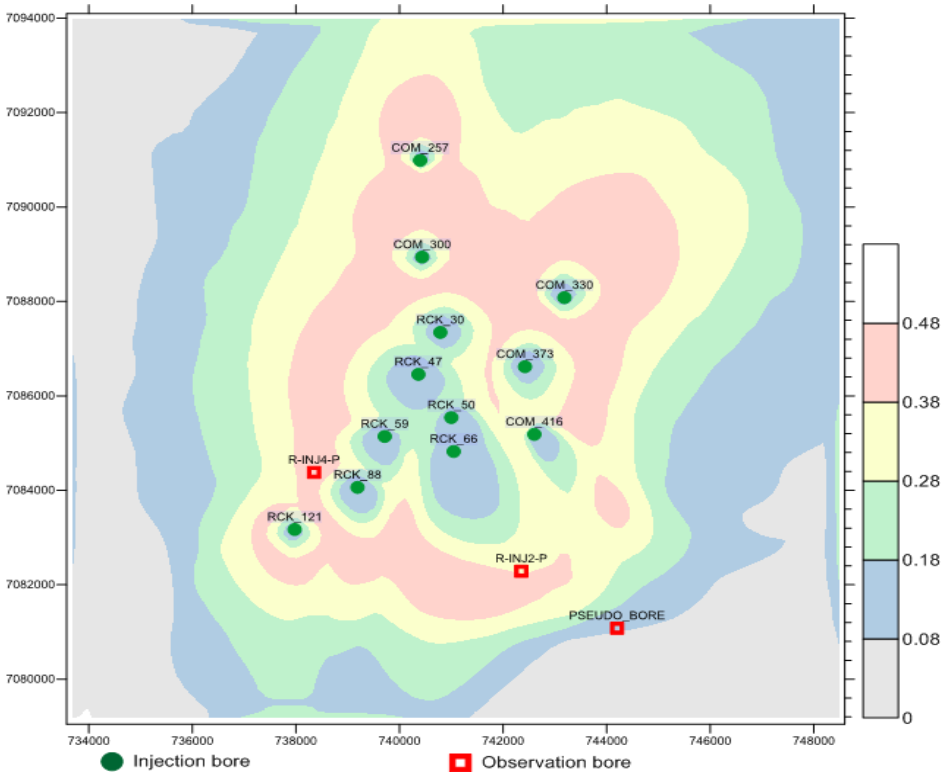

Figure 41: Uncertainty (prediction standard deviation) in the peak dilution

The mean time at which peak dilution occurs was also computed from the outputs of Null-space Monte Carlo analysis. The mean time and the corresponding uncertainty are shown in Figure 42 and Figure 43 respectively.

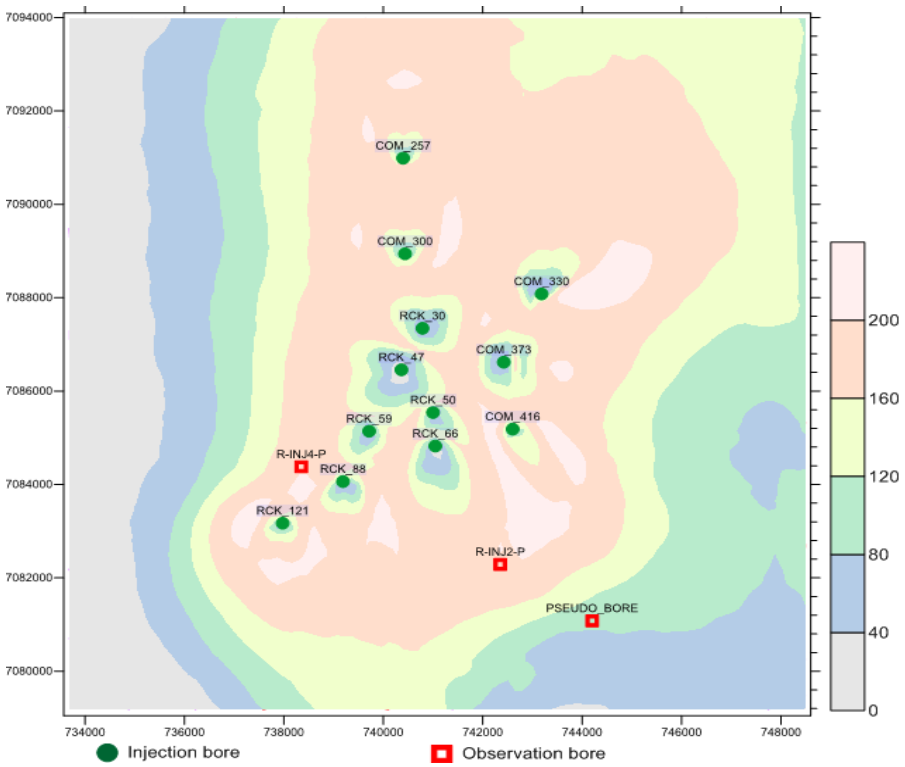

Figure 42: Contours of the mean time (months) at which peak dilution occur.

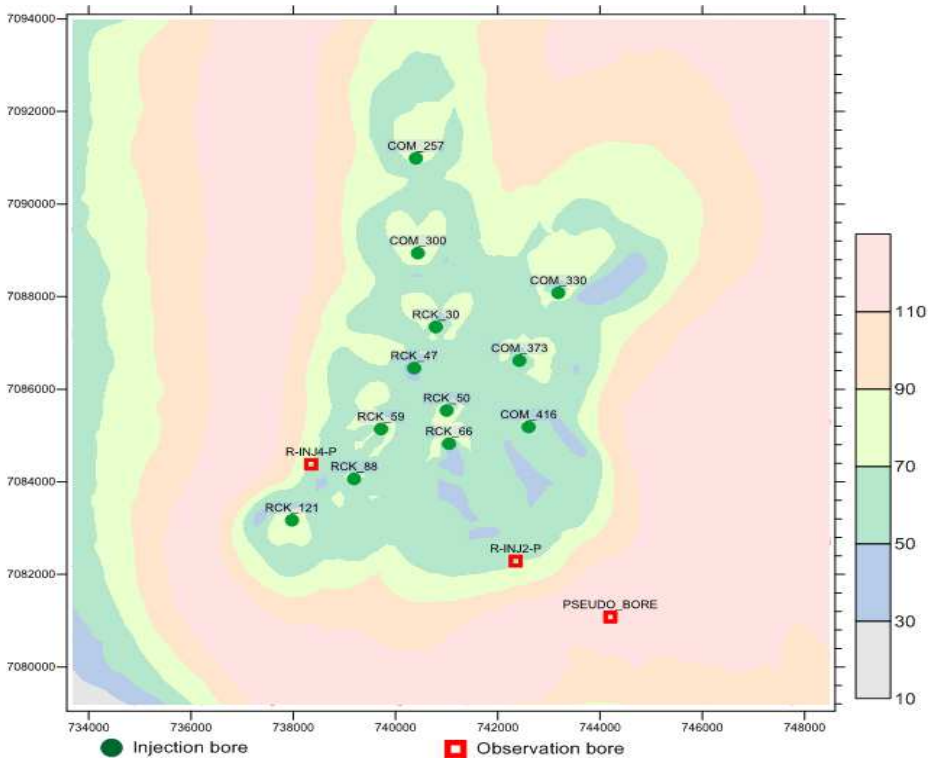

Figure 43: Contours of the uncertainty (prediction standard deviation) in the time (months) at which peak dilution occurs.

Mean peak dilution contours indicated that a dilution to 1/10th of the initial concentration occurs mostly within the block of area represented by the well field water quality model for the hypothesised worst case scenario. Also, contours of dilutions to 1/100th and 1/1000th of the initial concentration are very close to the 1/10th dilution contour. The ”pseudo bore” represents a location which is 5 km from the nearest injection well in one of the key directions of flow (Figure 33) of the reinjected water. The dilution simulated for this location is 0.02 with a prediction standard deviation of 0.08. This value indicates dilution to 1/50th of the

initial concentration. The average time at which the peak dilution occurs at this location was computed as 86 months with a prediction standard deviation of 120 months, indicating that the peak dilution occurs within the 264-month period of injection. This implies that an increase in concentration beyond this may not be expected at this location given that the injection ceases after 22 years duration, thus the groundwater gradient driving the plume movement is reduced over time. No domestic or stock bores are located closer to the injection bores than this pseudo bore.

In spite of relatively large uncertainties in the predicted dilutions and travel times, nevertheless these simulations indicate that dilution to very low concentrations would occur within the block represented by the well field water quality model. Thus contamination risks to Precipice domestic bores located much farther from the well field are considered negligible. However, given that the proposed injection wells are dispersed over a large area, continual monitoring of the groundwater quality in the well field is essential for early detection of any undesirable changes.

4.6 Linear uncertainty analysis

While Null-space Monte Carlo analysis is a robust approach for quantifying the uncertainty in the groundwater model predictions, considerable computational burden is involved in the calibration of all plausible realisations in the Monte Carlo simulation frame work, particularly for the transport simulations using the well field water quality model. Calibration of the well field water quality model had more than a month, when using a 64-bit operating system server (Intel(R)Xeon(R) 4 processers 2.26 GHz) after parallelising the PEST runs onto the 4 processors using BEOPEST (Doherty, 2010b). This computational burden was commensurately increased when calibrating the 500 realisations for the subsequent Null-space Monte Carlo simulations.

An alternative pragmatic approach for the quantification of the uncertainty of targeted predictions is based on linear predictive uncertainty analysis. This approach is based on the assumption that the Jacobian matrix is able to mimic the model parameter-output relationship near those parameter values for which the Jacobian was computed. If appropriate, use of this approximation, allows the user to circumvent computationally demanding model runs, so that an approximate evaluation of the prediction uncertainty can be obtained. Estimation of the uncertainty using this approach was performed to compare the performance of the linear uncertainty analysis method with the more comprehensive Null-space Monte Carlo approach. This comparison of approaches was utilized for quantifying the prediction uncertainty of the dilution at the pseudo bore.

The linear uncertainty analysis required the following inputs- (a) The calibrated parameter field of the well field water quality model (b) the inherent parameter variability encapsulated in the covariance matrix (c) sensitivity of the dilution at the pseudo bore to the calibrated parameters and (d) the Jacobian matrix computed for the calibrated parameter field.

The standard deviation of dilution prediction at the pseudo bore obtained from the linear analysis was 0.074. The corresponding value obtained from the Null-space Monte Carlo analysis was 0.082 as shown in Figure 41. The satisfactory comparison warranted the use of linear uncertainty analysis principle in the data worth optimisation described in section 6.

4.7 Impact of faults

Potential changes in the dilution impacts caused by the presence of faults in the injection well field were explored by simulating the transport processes while considering the presence of hypothesised faults (Figure 44) in the well field water quality model. The presence of faults and the associated changes in the hydraulic property field were simulated using a program called FAULTSIM (Moore et al., 2014). By using this program, effect of faults is simulated by modifying the hydraulic properties (horizontal and vertical K values) of the model cells in which the fault lies. This program was used to simulate the effects that faults produce on the groundwater flow. FAULTSIM has the advantage that effects of faults can be incorporated into an already existing model. A detailed description of the FAULTSIM program is given in APPENDIX A.

In the FAULTSIM program the fault is defined using the following parameters - (a) fault throw (b) fault core thickness and (c) damage zone thickness.

A fault may act as a barrier to the horizontal movement of water or it may provide a means through which horizontal or vertical flow can take place. FAULTSIM undertakes weighted arithmetic averaging of horizontal permeability and weighted harmonic averaging of vertical permeability over a vertical distance of half the user-designated throw length over layers above and below that cell.

Weighting is calculated in accordance with the fraction of the fault plane that is intersected by each layer over this total distance. The fault core is then assumed to be comprised of these same materials, effectively layered in the direction of the fault plane; as Bense and Person (2006) describe, this allows ready calculation of the anisotropic permeability of fault plane material. Harmonic averaging of vertical hydraulic conductivities of the protolith material intersected by the fault are employed in the former calculation, and arithmetic averaging of intersected protolith horizontal hydraulic conductivities are employed in the latter calculation. The horizontal and vertical permeabilities of the fault-affected cell are then modified in order to accommodate the presence of the core zone, taking into account the fraction of the cell that this zone occupies, as dictated by its thickness.

Within any cell that is demarked by the user as containing a fault, further modifications are made to the vertical permeability assigned to that cell in order to accommodate the presence of the damage zone. Suppose that the overall damage zone width is provided as w_d and that the fault core width is provided as w_c. Suppose also that the width of the cell is w_e. Then a new vertical conductivity is calculated for the cell based on the following premises:

- Vertical permeability within the a width of cell given by w_c (i.e. the core zone), is enhanced in the manner described above;
- The vertical permeability within a width of cell given by w_d-w_c (i.e. the fault damage zone with the core excluded) is the same as its horizontal permeability, so that anisotropy is been effectively reduced to 1.0 in the damage zone.
- Vertical permeability within a width of cell given by w_e-(w_d+w_c) (i.e. non fault-affected parts of the cell) is unchanged.

The faults were assumed to pervade both the model layers in the well field water quality model. Fault throw length of 200 m, fault core thickness of 5 m and fault damage zone of 20 m were assumed and the uncertainty in these values were addressed during the uncertainty analysis.

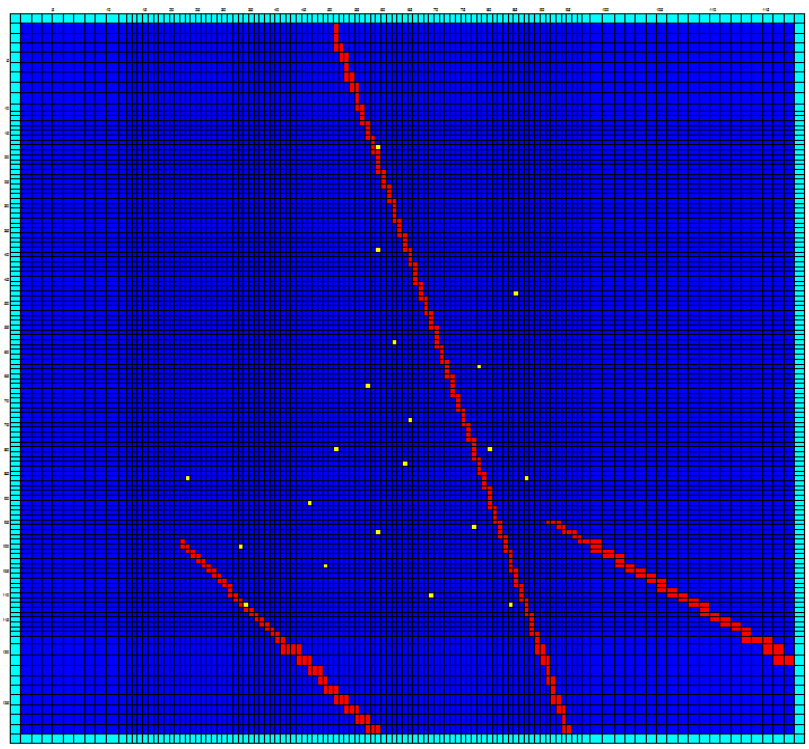

Figure 44: Hypothesized faults in the well field water quality model grid. The injection well locations are indicated by the yellow dots.

The FAULTSIM program was used together with the stochastic simulation framework provided by Null-space Monte Carlo approach for the prediction of dilution and travel times. The ratios of modified to unmodified horizontal and vertical conductivities were considered as variable parameters in the Null-space Monte Carlo analysis by introducing a power factor to these ratios. These parameters accounted for the uncertain impact that the fault causes to the groundwater flow system in terms of reducing the horizontal flow and/or increasing he vertical flow. These parameters were varied stochastically in the range 0.66 to 1.5 equivalent to a standard deviation of 0.089 in the log-transformed scale. In addition to the variability permitted for these fault parameters the variability of other model parameters within their uncertainty bounds as described in section 4.2, was also considered in this Null-space Monte Carlo simulation for the fault scenario.

For the fault scenario, means of the simulated peak dilution was computed for all model cells in the well field water quality model from the Null-space Monte Carlo simulations. The contours of $1/10^{th}$ mean peak dilution is shown in Figure 45 and the corresponding uncertainty contours are shown in Figure 46.

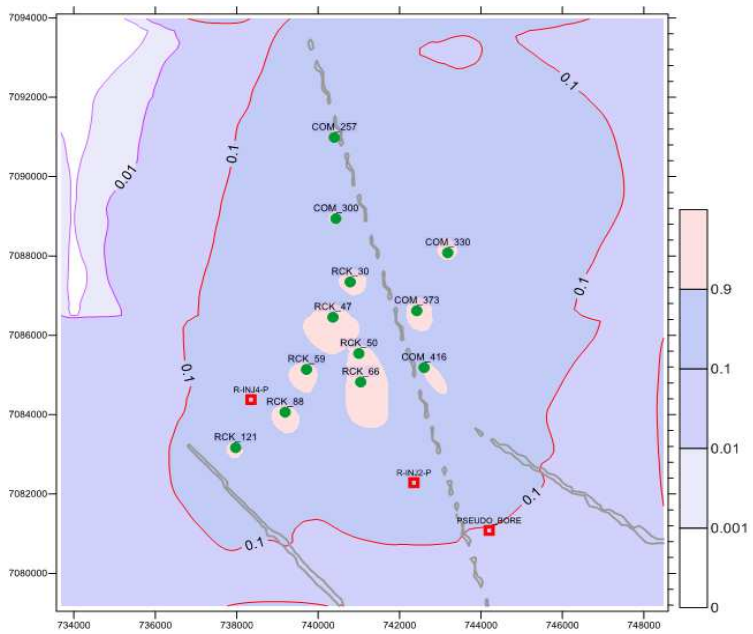

Figure 45: Mean peak dilution contours for the scenario considering faults in the well field water quality model

Comparing with Figure 32, it is readily observed that the 1/10th dilution contours have moved slightly farther from the well field.

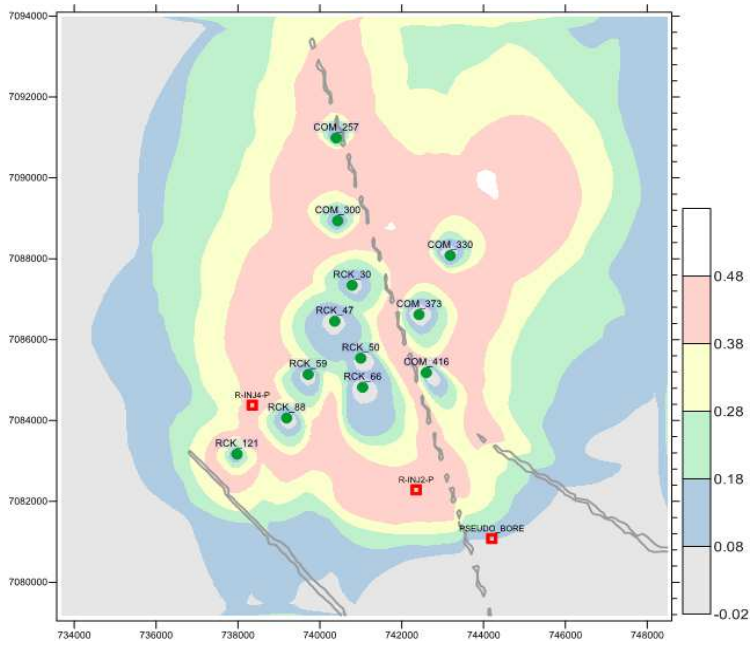

Figure 46: Uncertainty in the dilution prediction for the scenario considering the presence of faults

Comparing Figure 46 to Figure 41, it is notable that there is an increase uncertainty along the fault for the peak dilution predictions. Contours of time taken until peak dilution and corresponding uncertainty for the fault scenario are shown in Figure 47 and Figure 48. Simulation of the fault scenario indicated slight changes in the time to peak dilution and its uncertainty induced by the presence of faults in the well field.

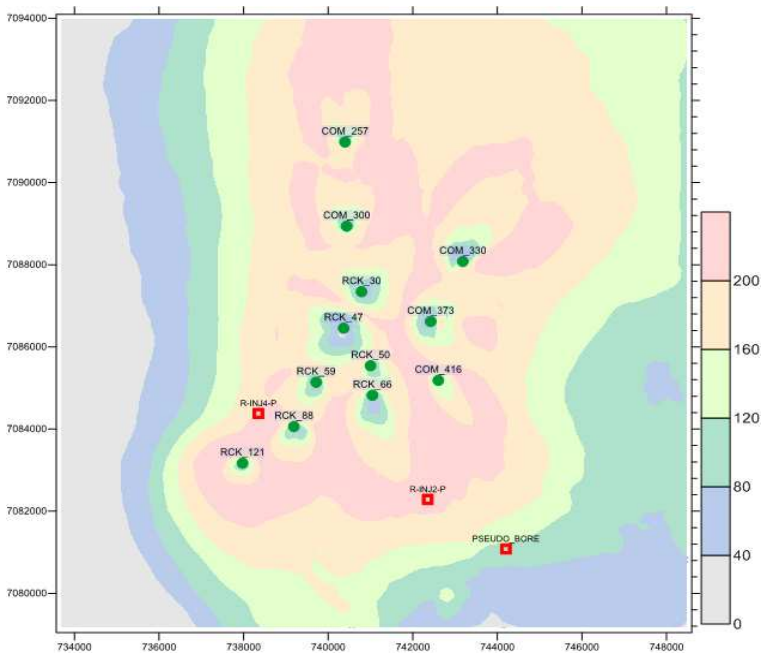

Figure 47: Contours of mean time (months) at which peak dilution occurs for the scenario with the fault

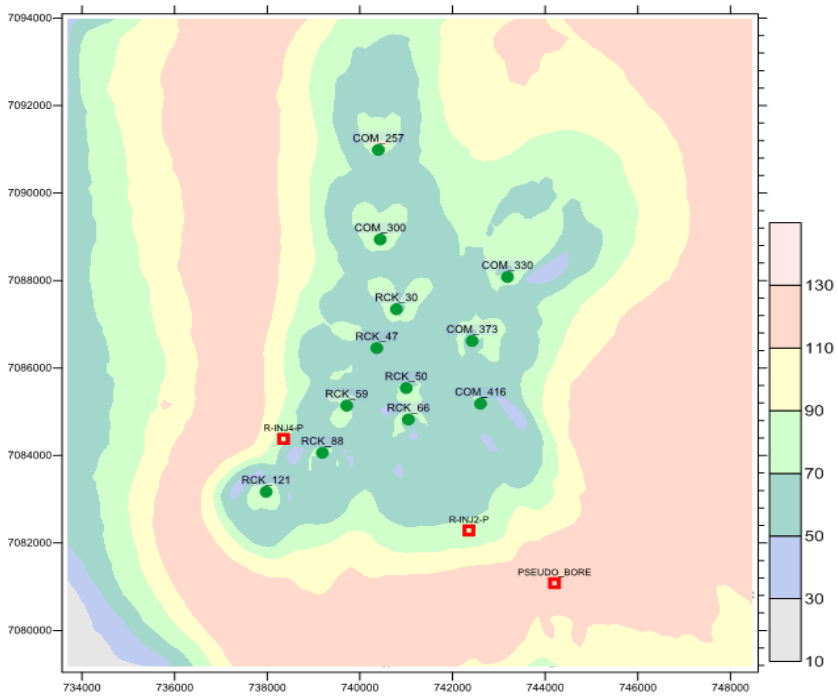

Figure 48: Contours of uncertainty in the time at which peak dilution occurs for the scenario with the fault

4.8 Conclusions

Comprehensive Null-space Monte Carlo analyses were carried out using the subregional and well field water quality model to quantify the uncertainty in the groundwater head changes, dilution and travel times. The subregional model was used to predict the head increase in the risk receptor domestic bore closest from the injection well field. Well field water quality model was used to predict the distances and times at which an injectate would dilute to 1/10th, 1/100th and 1/1000th of its initial concentration of 1 kg/m^3. The uncertainties in these predictions were quantified using Null-space Monte Carlo analysis. These analyses helped quantify the entire range of uncertainty associated with the head, dilution and travel time predictions. It was found that the uncertainty associated with these predictions were large, rightly

reflecting that limited amount of groundwater monitoring data was used in the development of these models and points to the fact that more measured data is required to reduce the uncertainty in the predictions.

Simulation of the groundwater head increase using the subregional model indicated that the maximum head increase in the closest risk receptor bore (RN123030) of 4.3 m. The standard deviation of the predicted average head increase at this location was 1.2 m. Average peak dilution and travel times simulated using the well field water quality model indicated a dilution to $1/10^{th}$ of the initial concentration within a distance of 5 km from the closest injection bore in all directions. The uncertainty in the dilution and concentration were also computed from the Null-space Monte Carlo analysis. An independent linear uncertainty analysis approach was employed to quantify the uncertainty at a chosen location. The linear analysis indicated similar values of uncertainty of the predicted dilution at this location in comparison to that obtained from Null-space Monte Carlo analysis. This warranted the use of linear analysis technique for the hypothesis testing described in section 6.

5 Hypothesis testing

5.1 Overview

The Null-space Monte Carlo analysis described in section 4, facilitated the generation of multiple realisations of the parameter fields honouring the calibration constraints. Model simulations using these parameter fields enabled quantification of the uncertainty in the prediction of groundwater impacts of the injection scheme. The probability distribution of the impact variable (e.g. head increase, dilution at a location) was obtained from the Monte Carlo simulations. However, there could be many more parameter realisations which could calibrate the model, but were not tested in the Null-space Monte Carlo analysis. Thus the possibility of occurrence of an undesirable impact cannot be nullified even if it did not feature in the predictive simulations using the Null-space Monte Carlo approach. To address this possibility, hypothesis testing was performed to test if the occurrence of an undesirable impact could be rejected with high confidence.

Recall that there are no domestic bores or other risk receptors identified in the Precipice sandstone aquifer within the domain represented by the well field water quality model. In spite of this, it remains important to quantify the potential changes to the water quality as the Precipice sandstone is an important freshwater aquifer in the Great Artesian Basin. Hypothesis testing was initially included in the scope of this project when the target aquifers being considered for injection included the Gubbaramanda sandstone or Hutton sandstone. A larger number of stock and domestic bores located closer to the Reedy Creek injection well field tap these aquifers and hence it would have been more important to do hypothesis testing to quantify the likelihood of the injection impacts at these risk receptors with high confidence. The choice of the Precipice sandstone as the target aquifer for injection, in itself, minimised the risk of any negative impacts as the Precipice aquifer is deep (-1300 m) at this Reedy Creek location and not many bores tap this aquifer in the vicinity of the injection well field.

In the absence of any proximal domestic bores, a location 5 km from the injection bore RCK_66 was chosen as a representative bore location (pseudo bore) to focus the hypothesis testing. Simulated head gradients in the direction of this chosen pseudo bore were the steepest. For this reason, it represented one of the most vulnerable directions for any risk of contamination in comparison to other radial directions. Hypothesis testing was conducted for the scenario considering faults in the well field water quality model domain.

5.2 Methodology

In the method adopted in this study, hypothesis testing was done by evaluating the model setting in which the hypothesized impact could be simulated. This was achieved by incorporating the chosen undesirable environmental impact to be investigated as a member of the expanded calibration data set. A prediction specific calibration was performed in the following to find the parameter set that simultaneously satisfies the following two conditions;

a) The identified parameter set allows the model to honour the hypothesised prediction without incurring excessive misfit to the original calibration data sets indicated by the covariance matrix of the measurement noise.
b) The identified parameter set is reasonable in terms of physically realistic values and spatial dependence represented by the covariance matrix of innate parameter variability. This covariance matrix also encapsulates the expert knowledge on the spatial distribution of the hydraulic properties.

If the identified parameter set satisfies both these conditions then the proposed hypothesis cannot be rejected indicating some probability of its occurrence. However, at times, the calibration exercise cannot match the hypothesised impact without affecting the fits to the observations or it may require

parameter set identified in the process to take unrealistic values or spatial dependence. Such instances indicate that hypothesised impact cannot be simulated while the model honours the calibration data. This gives high confidence to reject the hypothesis.

The hypothesis tested in this study was that the proposed injection scheme could result in the peak dilution of only 50 % at the location indicated by the pseudo bore. This hypothesis was tested for the scenarios considering faults in the well field. Peak dilution of 0.5 at the pseudo bore was added as an observation to the calibration data set and the model was re-calibrated using PEST. The objective of this recalibration was to match the simulated peak dilution at pseudo bore to the hypothesised peak dilution while still retaining the calibration with respect to other calibration data sets. Then, the two conditions described above were tested. To test if the identified parameters are 'unreasonable' a PEST utility called ASSESSPAR (Moore et al. 2014) was used. ASSESSPAR computed two variates, a chi-square variate and a normal variate. The prediction specific normal variate was computed based on the sensitivities of the prediction of interest to model parameters.

5.3 Results

The Null-space Monte Carlo analysis using the well field water quality model predicted the mean peak dilution at the pseudo bore as 0.02 with a prediction standard deviation of 0.08. Considering a Gaussian distribution for the peak dilution, the value of dilution with a 95% confidence level (mean + 2 × standard deviation) will be 0.18. This indicates with a 95% confidence that an injectate would dilute to at least $1/6^{th}$ of its initial concentration at the considered location. Hypothesis testing was performed to test if the possibility of occurrence of dilution of 0.5 at this location could be rejected with very high confidence given the available information from the groundwater monitoring data. Thus the selected impact for hypothesis testing is of extreme nature.

With the new pseudo bore observation defined by the hypothesis, the well field water quality model was recalibrated to simulate the hypothesised dilution at this location. Tikhonov regularisation constraints were used to constrain the departure of the hydraulic property values from their calibrated values. To the extent possible these constraints also try to ensure that the resulting parameter fields obey the pertinent variograms that define the spatial variability of these fields.

The parameter fields which enabled simulation of the hypothesised prediction were then tested using ASSESSPAR to obtain the prediction specific normal variate which defines a likelihood of the specific combination of the parameters. The assessment resulted in a normal variate values for the fault scenario of -1.8 indicating that the hypothesised dilution of 0.5 would fall within a 95% confidence interval. While this result indicates that the hypothesised impact is unlikely to occur, it also indicates it is indeed possible if faults were present in the vicinity of the injection bore. This result emphasises the need for sentinel monitoring of the impacts from injection.

5.4 Summary and Conclusion

Modelling using the hypothesis testing framework was employed to investigate whether incidence of specified undesirable impacts could be rejected with high confidence levels. The approach involved hypothesising the undesirable impact as an outcome of the proposed injection scheme and then using the model to simulate this outcome while still honouring the calibration data used in model development. In this process if the model parameters assume unreasonable values defying the spatial properties of these parameters elucidated by measurements and expert knowledge it indicates that the impact is highly unlikely. A PEST utility ASSESSPAR was used to evaluate the parameter fields identified using the approach. The hypothesis testing was performed for the fault scenario using the well field water quality model. The possibility of a peak dilution of only 50% at a location 5 km from the injection bore RCK_66 was investigated using this approach. The results indicated that high values of peak dilution in this range were unlikely at a distance of 5 km from the closest injection bore.

6 Data-worth analysis

6.1 Overview

The groundwater models developed and used for the simulation of predictions of CSG produced water injection impacts used different types of groundwater monitoring data comprising the regional groundwater head observations, head observations from the pump tests and injection trial and tracer concentrations from the tracer tests. The worth of each monitoring data type and its measurement density in space and time was assessed in terms of the extent to which the uncertainty in the prediction of a chosen impact is reduced upon data acquisition. The model-based data worth analysis can be used to prioritise and optimise future data collection with the objective of minimising the uncertainty of a predicted impact.

Data worth analysis was carried out to assess the relative worth of different types of groundwater monitoring data including groundwater head and concentration measurements in informing the model predictions. Data worth analysis was applied to three different contexts in this study *viz*;

a) Analysis of the worth of the different data types used in inversion based upscaling for the prediction of the dilution and travel times at the Reedy Creek injection site.
b) Data-worth analysis to optimise injection tracer test monitoring for Spring Gully injection site.
c) Data-worth analysis for the long term monitoring for the Reedy Creek injection site.

6.2 Methods

In this study the worth of different data types was computed in terms of their relative contribution to reducing the uncertainty of a key model prediction. Variance of the key model prediction was chosen as the measure of uncertainty. Variance was computed by applying linear uncertainty analysis principles using the PEST utility software PREDUNC. In this approach the prediction variance is computed using the following formula;

$$\sigma_s^2 = \mathbf{y}^t\mathbf{C}(\mathbf{p})\mathbf{y} - \mathbf{y}^t\mathbf{C}(\mathbf{p})\mathbf{X}^t[\mathbf{X}\mathbf{C}(\mathbf{p})\mathbf{X}^t + \mathbf{C}(\boldsymbol{\varepsilon})]^{-1}\mathbf{X}\mathbf{C}(\mathbf{p})\mathbf{y} \qquad \textbf{(1)}$$

where ***y*** is a vector representing the sensitivity of the prediction to the parameters, ***p*** is the parameter vector, ***X*** represents the Jacobian matrix which gives a linear approximation of the model, ***ε*** is the measurement noise vector, and ***C*** refers to the covariance matrix of a vector. Sensitivities of different observations to the model are captured in the Jacobian matrix (first derivatives of the observation data to model parameters). Thus, equation (1) relates the prediction uncertainty to the sensitivity of the model to different observations. The data worth can be assessed either as (I) increase in the prediction uncertainty upon removal of the observations or as (II) decrease in the prediction uncertainty upon the addition of the observations into the observation data set. In the first approach all the observations are included in the monitoring data set and they are removed one-by-one and prediction uncertainty is calculated using equation (1) each time to compute the prediction uncertainty increase resulting from the removal of the observation. In the second approach observations are sequentially added to an initially empty data set with the execution of equation (1) to compute the prediction uncertainty decrease resulting from addition of each observation. The absolute value of the 'worth' or prediction uncertainty change computed using these two approached would be different; however generally the relative worth is consistent, unless there already exists a more than sufficient monitoring network. Both these approaches were employed in the data worth analysis for the three different applications in this project as mentioned in 6.1.

A similar analysis can also be performed to compute the relative contributions of different parameters and parameter groups to the prediction uncertainty. A very similar approach is employed for this as described above except that model parameters comprising the vector $\mathbf{p}$ in equation (1) are sequentially added or

removed from the data sets instead of observations and observation groups when computing the prediction variance.

6.3 Data-worth analysis for inversion based upscaling

Different data sets were used to calibrate the well field water quality model. These calibration data sets for inversion based upscaling comprised of,

a) Tracer breakthrough data obtained from 2D radial transport model;
b) Injection trial head observations;
c) Steady-state head observations from OGIA model; and
d) Regional inflow and outflow across the well field water quality model boundaries obtained from the OGIA model.

Data worth analysis was performed in this application to evaluate the relative contribution of the different data sets in reducing the predictive uncertainty of the peak dilution at the location indicated by the pseudo bore in figure 45. Similarly the relative contributions of the uncertainty in different model parameter groups to the prediction uncertainty were also computed. Figure 49 depicts pre-calibration and post-calibration relative contributions of uncertainty in different parameter groups to the prediction uncertainty.

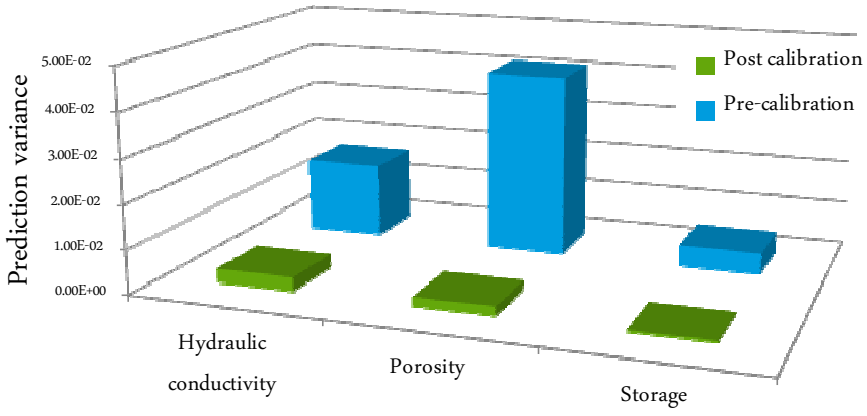

Figure 49: Relative contribution of different parameter groups to the prediction uncertainty of the well field water quality model

In Figure 49 it can be seen that uncertainty in the porosity contributes most to the pre-calibration uncertainty in the dilution prediction. While hydraulic conductivity is an important factor contributing to the uncertainty in the flow field, close to the injection bores the flow is governed by the high pressure injection and hence porosity becomes the single most important factor governing the prediction of dilution driven by advection-dispersion transport.

Figure 50 depicts the relative worth of different observation groups in predicting the dilution. Information obtained from the tracer break through curve contributes most to reducing the prediction uncertainty compared to the information obtained from the groundwater head and fluxes. This result is in agreement with the parameter contributions to uncertainty shown in Figure 49. Concentration measurements best inform the porosity estimates and thus help most in achieving biggest reduction in prediction uncertainty.

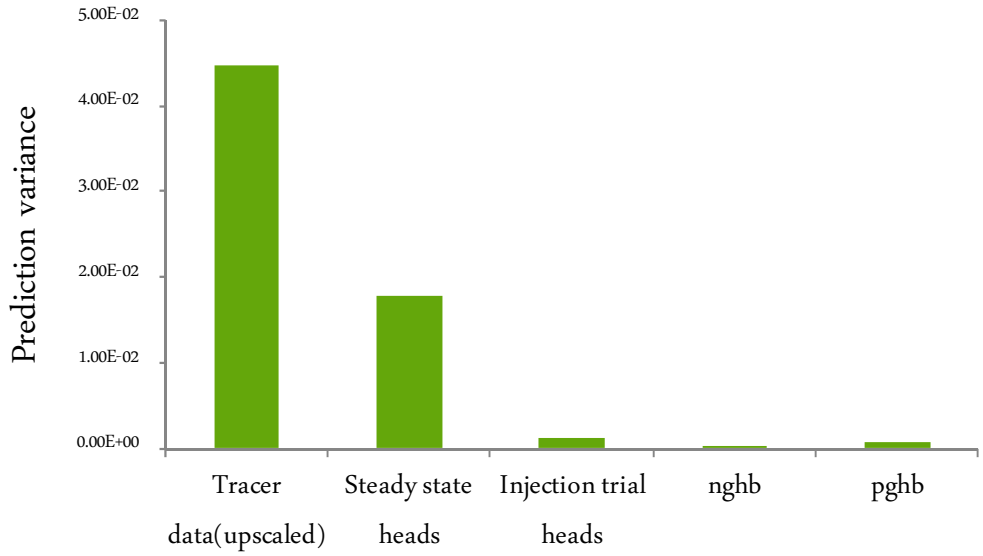

Figure 50: Data-worth of different data types in informing the dilution predictions

6.4 Spring Gully injection trial data-worth

For the Spring Gully site, we again adopted linear predictive uncertainty analysis (Moore and Doherty 2005) to quantify the usefulness of different tracer types (e.g. bromide, temperature, methane and chloride) and head measurements in the context of a field scale aquifer injection trial of coal seam gas (CSG) co-produced water. Data worth was evaluated in terms of tracer test design (e.g. injection rate, duration of the test, and the applied measurement frequency) and monitoring disposition to increase the reliability of injection impact assessments. This was followed by an uncertainty targeted Pareto analysis, which allowed the interdependencies of cost and predictive reliability for alternative monitoring campaigns to be compared directly.

Comparing data worth at three selected times (Figure 51) illustrates the transient nature of ‘‘best monitoring location’’, which is related to the changing signal to noise ratio between the plume and surrounding groundwater that occurs as the plume migrates from the tracer injection point. Therefore observations close to the injection point (<50 m) are most informative at the start of the trial, but lose information content soon thereafter as groundwater rapidly attains the concentrations of the injectate. With time the region of greatest data worth moves outwards into the aquifer. However, because groundwater velocities decrease rapidly away from the injection point due to the radial expansion in aquifer volume, the outward movement of the plume slows successively.

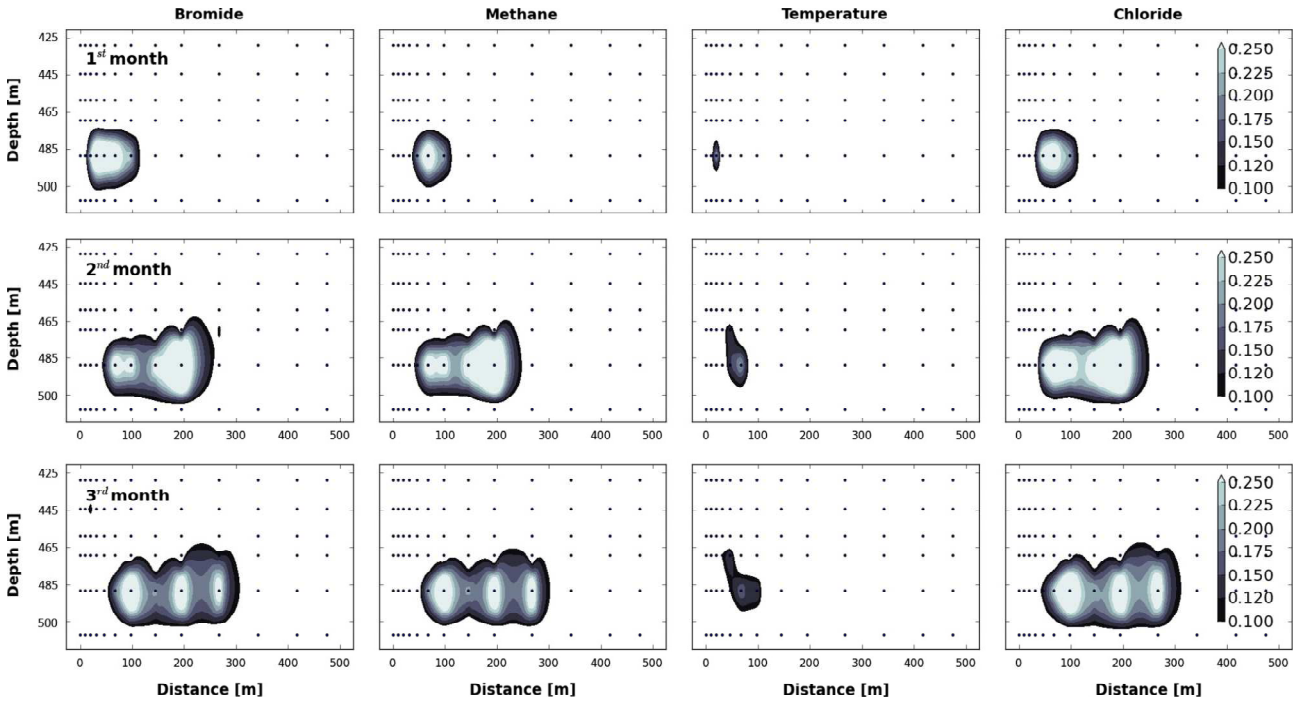

Figure 51: The spatial distribution of data-worth within the 2nd week and 8th week of injection for all tracer observations with respect to the solute dilution prediction at 106 m from the injection well.

The impact of measurement frequency is shown in Figure 52. It depicts the contours of the standard deviation of travel time error for all tracers and combinations of measurement frequency, versus the distance at which a prediction of travel time is sought. As expected, with a coarsening sampling frequency, the uncertainty increases. If all monitoring observations are available, e.g., at 78 observation locations, the calculated standard deviation of predictions of travel time is less than 1 day within a radial distance of about 100 m, assuming all tracers are sampled at least every three days. When sampling frequency is reduced to once per week, such accuracy can only be achieved up to a radial distance of about 40 m, reduced further to about 20 m if a monthly sampling regime was adopted.

The analysis of the influence of the total number of available bores on predictive accuracies (Figure 52b, scenarios 1–4) indicated that data from a single optimally located observation bore, sampled daily for all tracers within the region of greatest data worth, achieves a reduction of uncertainty of almost two orders of magnitude. This can be compared with two optimally located observation wells, sampled daily for all tracers, which achieves a further halving of predictive uncertainty compared to the case of a single bore. Thereafter, additional observation wells provide diminishing returns in terms of the rate of decrease in predictive error. The addition of a third, fourth and fifth bore within the area of greatest data worth, i.e., between 50 m and 250 m radial distance, leads to only minor reductions in uncertainty. This analysis indicates that two appropriately located observation bores provide the greatest reduction in uncertainty; with any further addition of monitoring bores incurring disproportionally low reductions in uncertainty in this relatively homogeneous radial flow case.

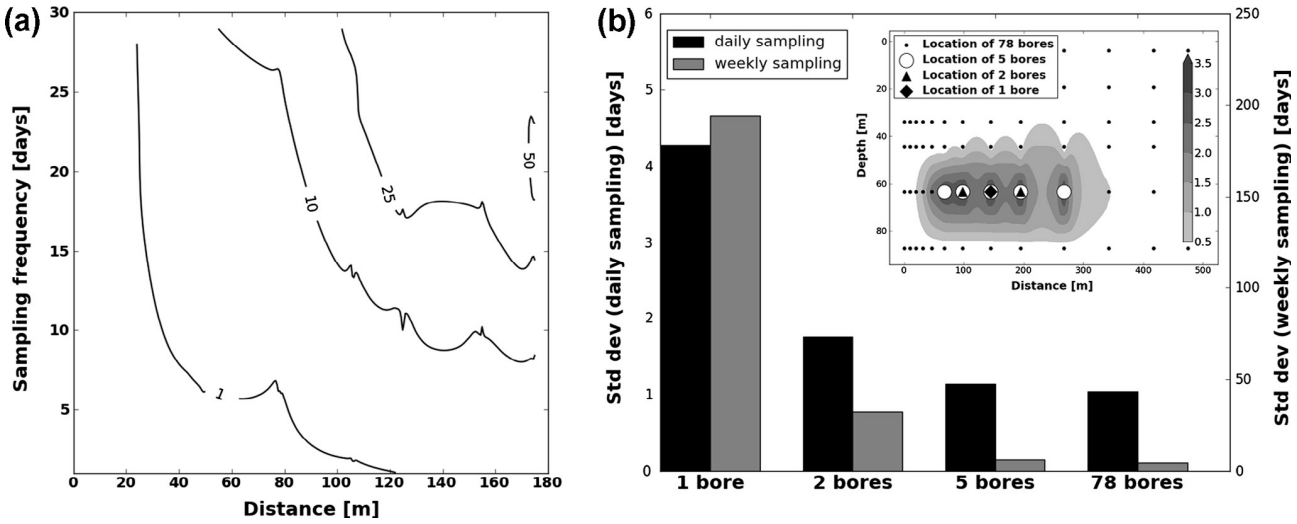

Figure 52: Predictive uncertainty standard deviation of peak solute breakthrough [days] as a function of (a) frequency of sampling events and radial distance from the injection well (based on 78 observation bores and (b) number of available observation bores for a prediction at 106 m. Location of observation bores and integrated data-worth over the duration of the injection trial (i.e. 100 days) is also shown. Sampling frequencies (1) = daily, (2) = every second day…(30) = monthly sampling

For the evaluated injection test, the data worth analysis assessed bromide as superior to head data and all other tracers during early sampling times. However, with time, chloride became a more suitable tracer to constrain simulations of physical transport processes, followed by methane. Temperature data was assessed as the least informative of the solute tracers. However, taking costs of data acquisition into account, it could be shown that temperature data when used in conjunction with other tracers was a valuable and cost-effective marker species due to temperature's low cost to worth ratio. In contrast, the high costs of acquisition of methane data compared to its muted worth, highlighted methane's unfavourable return on investment. Areas of optimal monitoring bore position as well as optimal numbers of bores for the investigated injection site were also established.

This work is fully summarised in Wallis et al (2014) and the reader can consult that publication for further details of this study.

6.5 Injection well field long-term monitoring data-worth

The data-worth analysis carried out in this section addressed the challenge of optimising future data collection to quantify the impacts of the proposed injection scenario at the Reedy Creek injection site. The example described here illustrates the application of data-worth analysis to assess the relative worth of concentration measurements at five existing monitoring bores in the prediction of peak dilution at a target location indicated as 'point' in Figure 53. The injection locations and monitoring locations are also indicated in Figure 53.

The data-worth analysis presented here is specific to the injection scenario described in section 3. This scenario considered a continuous stream of injectate emerging from all the 12 injection wells in the well field. Considering that this is a hypothesised scenario for simulating the worst case contaminant transport, the scope of the data-worth analysis performed for this scenario is intended for demonstrating the applicability of the methodology rather than for informing the actual sampling at these locations.

The relative worth of concentration measurements at these 5 locations is indicated by the relative size of the bubbles surrounding each monitoring location in Figure 53. Contours of the simulated peak dilution are also shown in the background. It may be noted that although Comb291 and Comb352 are the two closest monitoring bores of the prediction location, the data-worth of the these two bores was computed to be less than that of the monitoring bore Comb395. Considering these bore locations in relation to the dilution contours it could be observed that these two bores miss capturing the peak of the plume emerging from

any of the injection wells. But monitoring bore Comb395 is located sufficiently near the injection well COM_373 to capture the peak dilution. Thus monitoring data collected from this bore will have more information content about the peak dilution characteristics and is useful in informing the peak dilution at the target location "point".

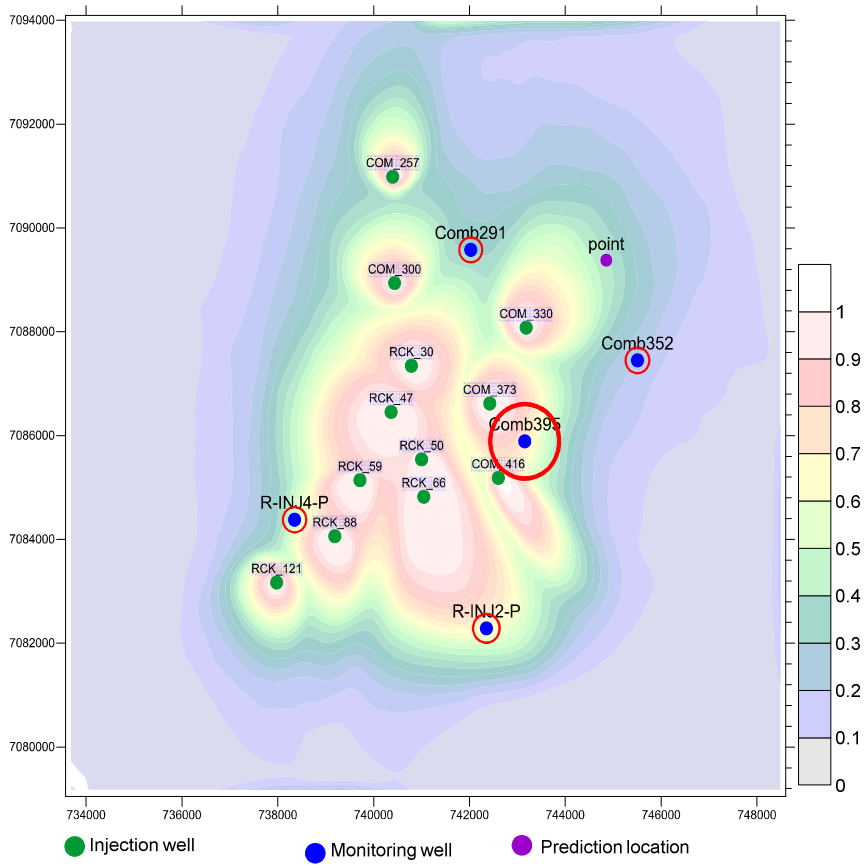

Figure 53: Injection scenario-specific data-worth for the monitoring bores at Reedy Creek. The size of the red circles indicates the relative worth of concentration measurements at these locations.

Data-worth analysis also provides a description of the worth of the data collection in the temporal domain. Figure 54 illustrates the relative data-worth of concentration measurements at the monitoring locations Comb291 and Comb352 over a period of 264 months.

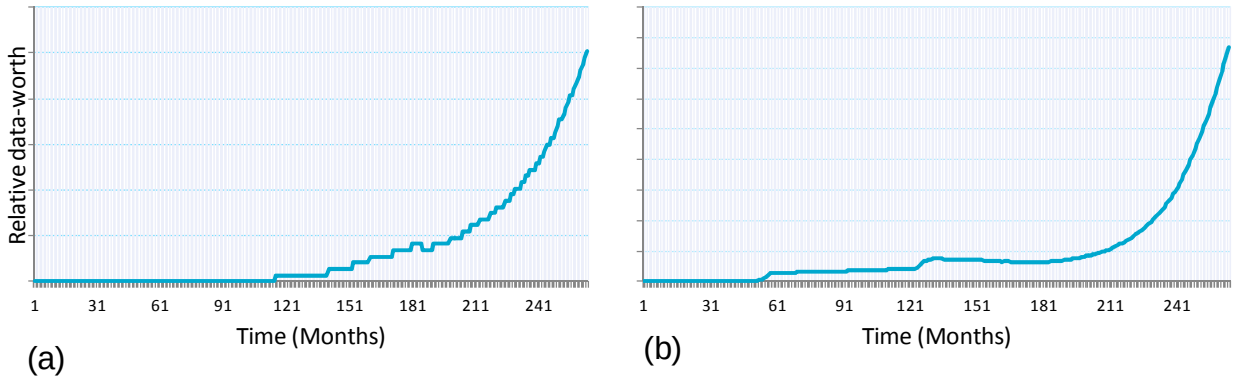

Figure 54: Relative data-worth of concentration measurements at the monitoring locations (a) Comb291 and (b) Comb352

The relative data-worth of concentration measurements seemed to increase towards the end of the simulation period. Peak concentrations occur at these monitoring locations towards the end of the simulation period. Since the prediction of interest at the target location 'point' for the data-worth analysis

was the peak dilution, information on peak dilution at the monitored locations would be more useful in making this prediction.

6.6 Summary

The spatial and temporal trends in the groundwater quantity and quality changes resulting from the proposed injection scenario were simulated using the well field water quality model. The stochastic simulation of these spatial and temporal trends enabled the quantification of relative contribution of various data types and the worth of their spatial and temporal measurements in reducing the model prediction uncertainty. Data-worth analysis was performed for three different purposes. In the first application relative contributions of the tracer test data, pump tests and injection trial head measurements and regional groundwater head measurements towards reducing the uncertainty of model predictions of dilution were estimated. This analysis was done for the Reedy Creek injection site. The results indicated that the tracer test data was most useful in informing the prediction of contamination transport resulting from the proposed injection scenario.

The second application of data-worth analysis was performed for the optimal design of injection trial tests for the Spring Gully site. This analysis explored the data-worth in terms of the tracer type (bromide, temperature and chloride), tracer test design (injection rate, duration of test and measurement frequency) and monitoring disposition to increase the reliability of injection impact assessments. Bromide tracer measurements were found to be superior to the head data and all other tracers during early sampling. However, data-worth of chloride followed by Methane became more suitable with time. Optimal number and locations of the bores were also established from the data-worth analysis.

The third analysis considered the long-term monitoring of the well field over the 22-year period of operational injection. In this exercise the worth of concentration measurements in the existing monitoring bores with the aim of minimising the prediction uncertainty in peak dilution at a target location. In general, it was found that more frequent sampling towards the last 12 years of injection has more worth than the measurements in the first 10 years.

7 Modelling the groundwater ages

7.1 Overview

The regional (OGIA) and subregional models used in this study were calibrated to the groundwater head observations in different aquifer layers in the Surat Basin. Thus, estimation of the hydraulic parameters in different model layers is informed only by the head measurements. The uncertainty in the hydraulic parameters and the recharge rates are correlated and different combinations of recharge and hydraulic parameters can provide equal fit to the groundwater head observations. Ideally multiple lines of evidence are required to minimise the uncertainty in the characterisation of the complex groundwater system. For instance, information from the isotopic characterisation of the groundwater in different formations can be used to constrain the hydraulic parameters in different model layers. To this end a preliminary analysis was conducted in this study to simulate advective transport of particles from recharge areas to chosen locations in different formations in the Surat Basin. Such simulations are useful to estimate the age of groundwater in different formations. The model-based age estimates could be compared to the age information obtained from isotopic studies to have better understanding of the groundwater system.

Simulation of advection transport was undertaken in this study to estimate the age of groundwater in different formations in the Surat Basin. Groundwater age in this context is defined as the time elapsed between when the water entered the saturated zone and when the water was sampled at a specific location downstream in the groundwater flow system (IAEA, 2013). The advection transport simulation was undertaken in a Null-space Monte Carlo analysis framework to generate the probability distribution of groundwater ages at different sampling locations in different formations in the Basin. The age distributions were simulated for 12 sampling locations for which isotopic characterisation of the groundwater system is being undertaken in the GISERA surface and groundwater project 4 titled 'monitoring of geochemical and isotopic characteristics of CSG formation waters, adjacent aquifers and springs' (http://www.gisera.org.au/research/waterprojects/water-project-4-baseline-monitoring.pdf). This project is referred henceforth in this section as project 4. The age distribution obtained from this exercise is expected to complement the isotope analysis that is being conducted in the project 4.

7.2 Methodology

Particle tracking analysis was used to simulate the groundwater ages. Locations at which groundwater samples were taken for isotope analysis were chosen for the particle track analysis. Particle tracks originating from these sampling locations (in the respective aquifer) were simulated back in time which enabled computation of the time taken by the particles to travel from the recharge areas to the sampling locations. Particle tracking was undertaken using the advection transport observation package (ADV2) for MODFLOW (Anderman and Hill, 2001). The subregional model was chosen for the particle tracking analysis. In using the ADV2 package it was assumed that advection driven by the recharge is the only transport process. Owing to the very slow velocity of flow in the Surat Basin it is known that molecular diffusion also contributes to the transport processes in the Basin. But owing to the computational burden involved, advection-diffusion modelling of the transport processes in the Surat Basin using the subregional model was beyond the scope of this preliminary analysis.

A steady state groundwater head field corresponding to pre-CSG period was simulated using the subregional model. Thus the groundwater stresses from neither CSG extraction nor the injection were considered in the simulation for obtaining the particle tracks. The velocity of flow in each model cell is then obtained using the formula $v = {KI}/{n}$ where v is the flow velocity, K is the hydraulic conductivity in the cell, I is the hydraulic gradient and n is the porosity of the cell. Then, based on these velocities, particle displacement is simulated by tracking successive Cartesian components through the groundwater model grid over time until the particle traces back to the recharge location. Particle tracks were simulated in a stochastic modelling framework using the 350 sets of hydraulic parameters generated by the Null-space

Monte Carlo analysis described in section 4. The hydraulic conductivity-porosity relationship shown in Figure 9: Hydraulic conductivity-porosity relationship for the Precipice sandstone aquifer. was used to generate the porosity distribution corresponding to different K realisations. This resulted in 350 particle tracks and ages for each sampling location. The cumulative time elapsed was recorded for each particle as it travels from the sampling location to the recharge area. Histograms of groundwater ages for all sampling locations were obtained from this data.

The sampling locations for which particle tracks were simulated are shown in Figure 55. The formations for which particle tracks were simulated at these locations are also indicated (in brackets) along with the location sampling ID.

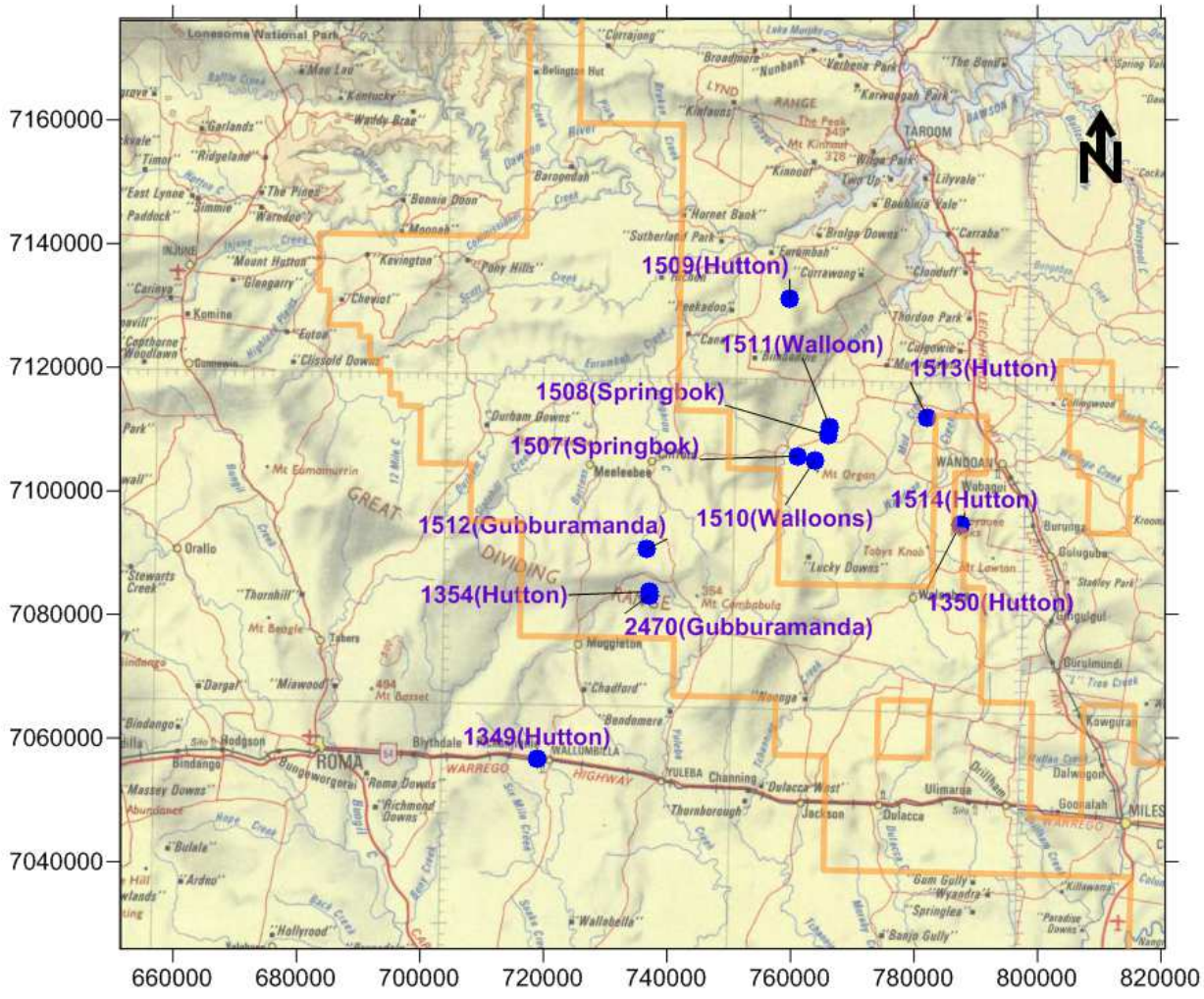

Figure 55: Sampling locations and formations for which particle tracks were simulated.

7.3 Results

Null-space Monte Carlo simulation of particle tracks resulted in 350 values of groundwater age for each sampling location. Histograms were plotted for the age distribution at each location. Age corresponding to the highest frequency interval for each location is shown in Figure 56.

The simulations indicated a general trend of increasing ages from North to South. The northern Hutton sampling location 1509 had a highest frequency age of 50,000 years. As we move to the deeper parts of the Hutton, simulated age increased with highest frequency age of 500,000 years for the sampling location 1349. Plan (X-Y) and cross-sectional (Y-Z, X-Z) views of the particle tracks within the subregional model grid for the bore locations 1349(Hutton) and 1350(Hutton) are shown in Figure 57 and Figure 58 respectively.

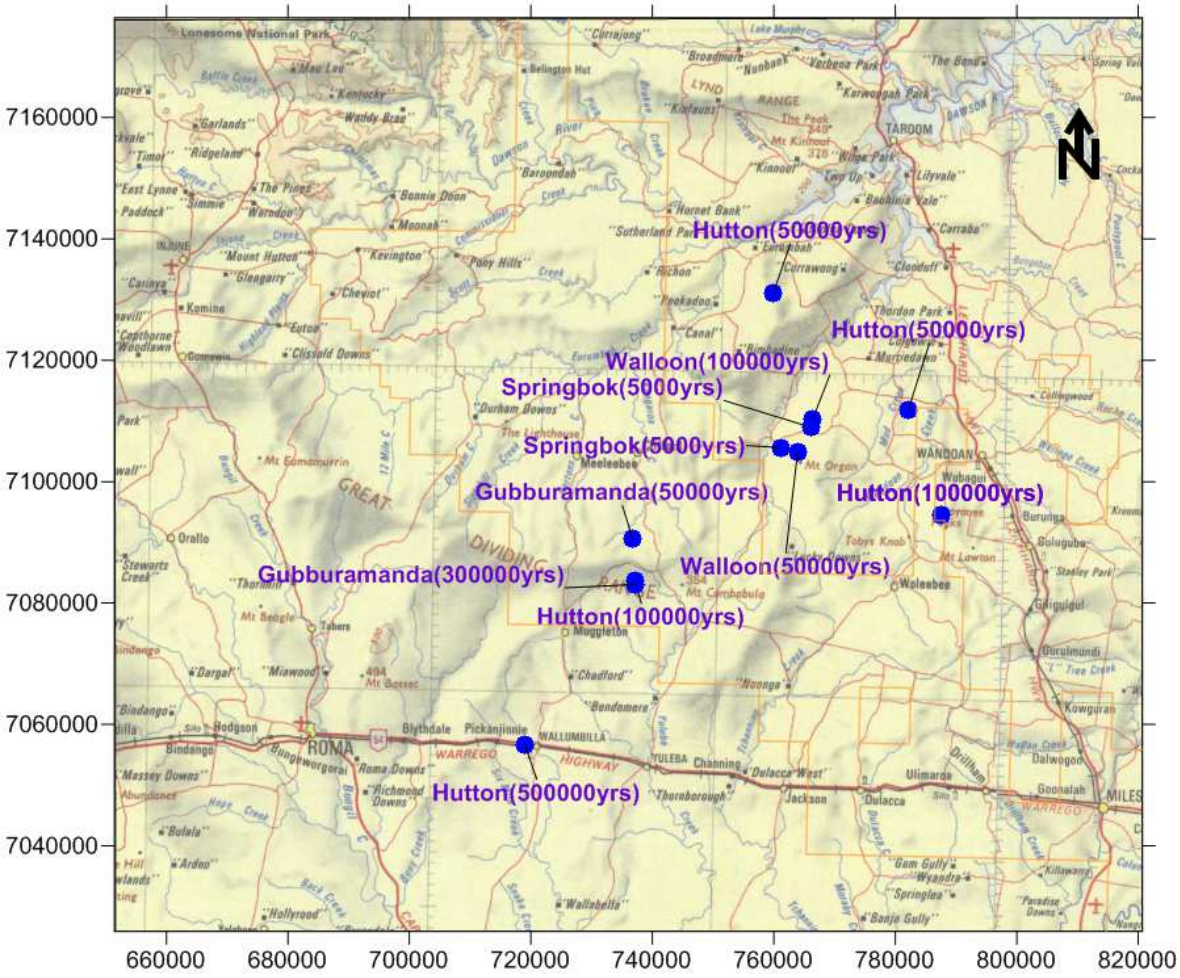

Figure 56: Highest frequency ages obtained from the particle track analysis

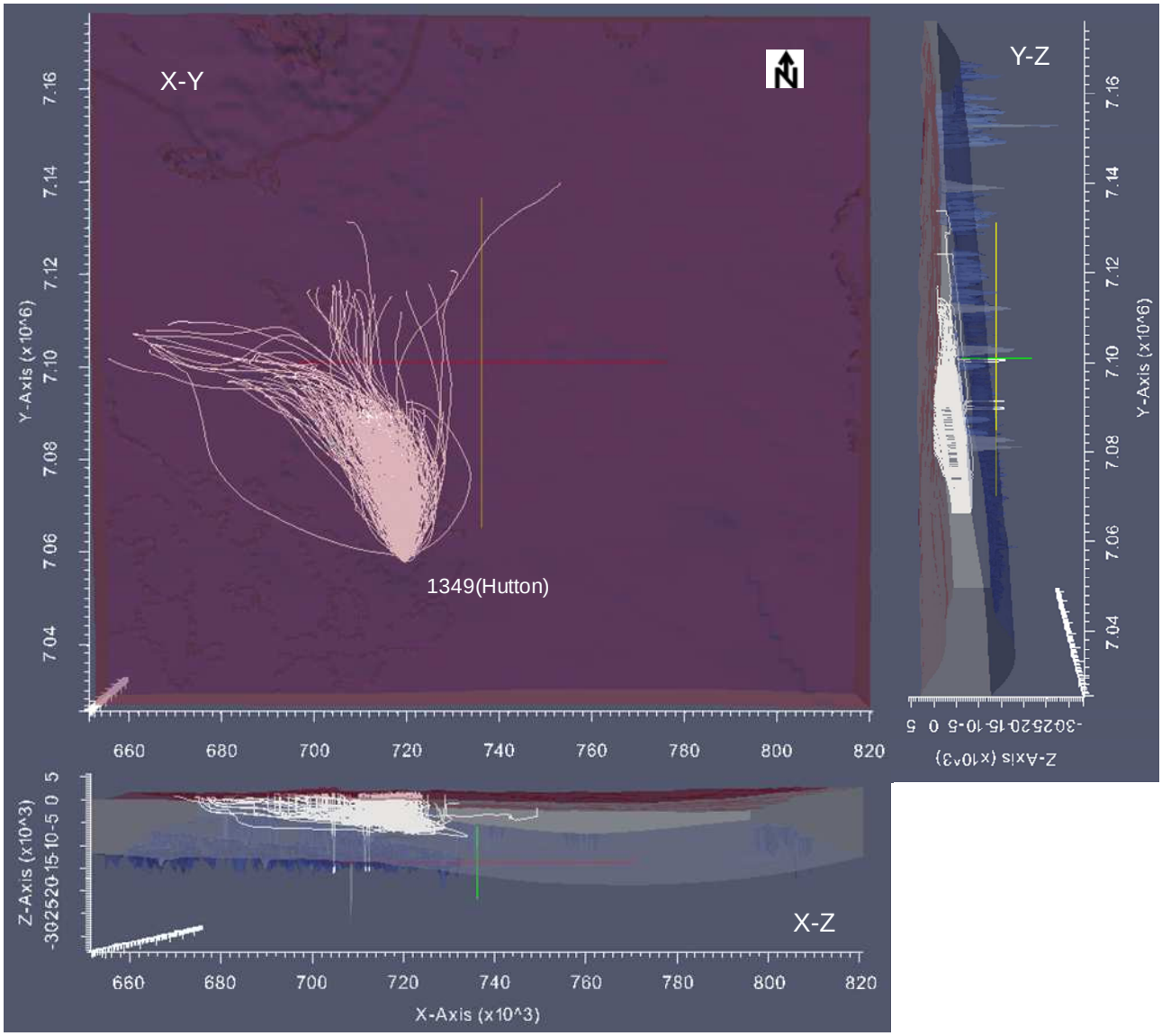

Figure 57: Particle tracks simulated for the bore location 1349(Hutton)

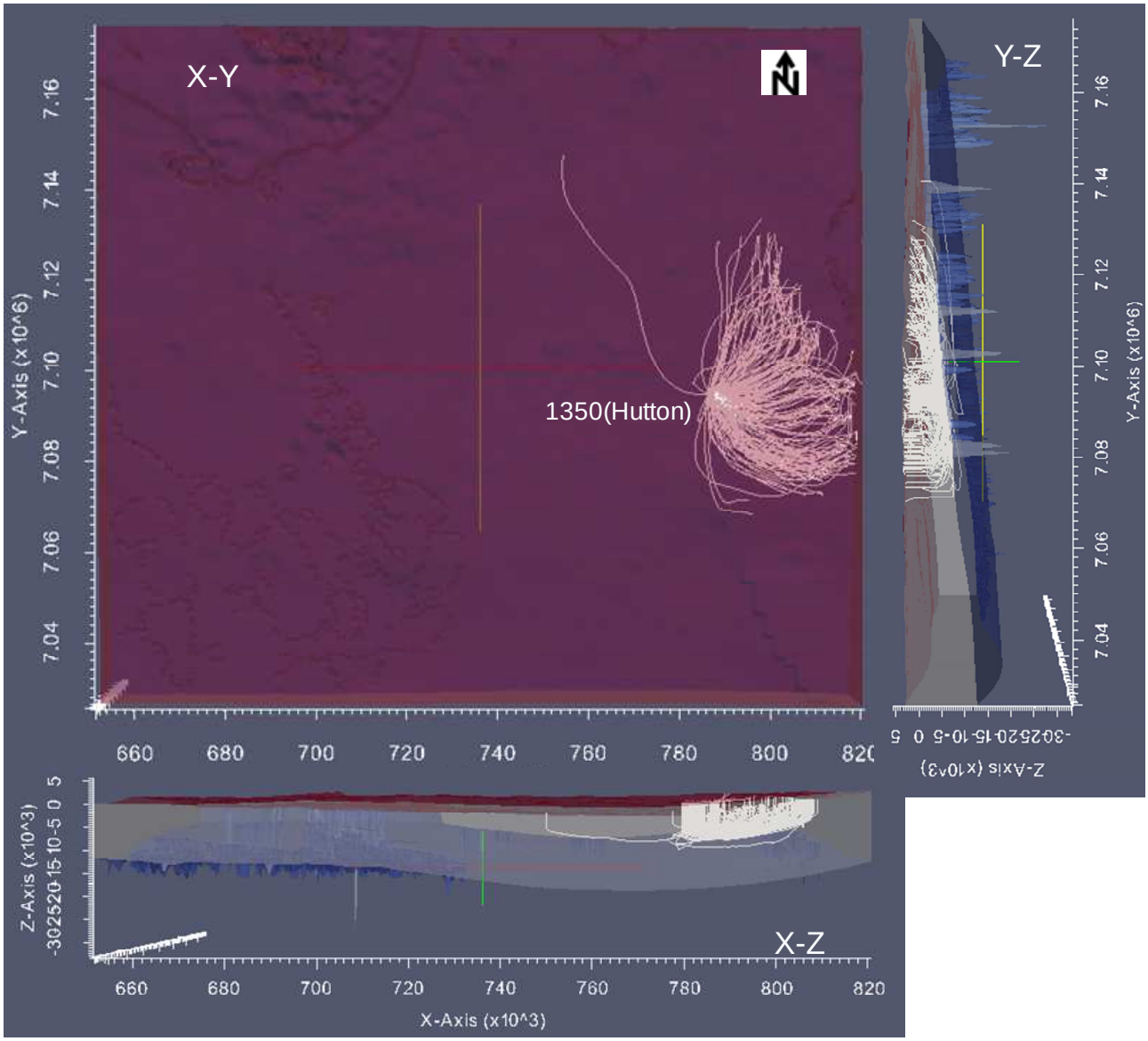

Figure 58: Simulated particle tracks for the bore location 1350(Hutton)

In general, the particles followed the direction of flow and the tracks differ from each other due to the uncertainty in the flow resulting from the model parameter uncertainty. From the vertical profiles (X-Z and Y-Z plots) it can be seen that some tracks vertically move across different model layers and emerge out at the top layer whereas some tracks move a large distance horizontally in different model layers before emerging out into the recharge area. Thus the travel times vary over a wide range for these tracks resulting in a distribution of groundwater age estimates for each location. The age distributions for the 12 locations are shown in Figure 59 and Figure 60. Simulated groundwater age for different locations in Hutton sandstone varied from 20,000 to over 700,000 years.

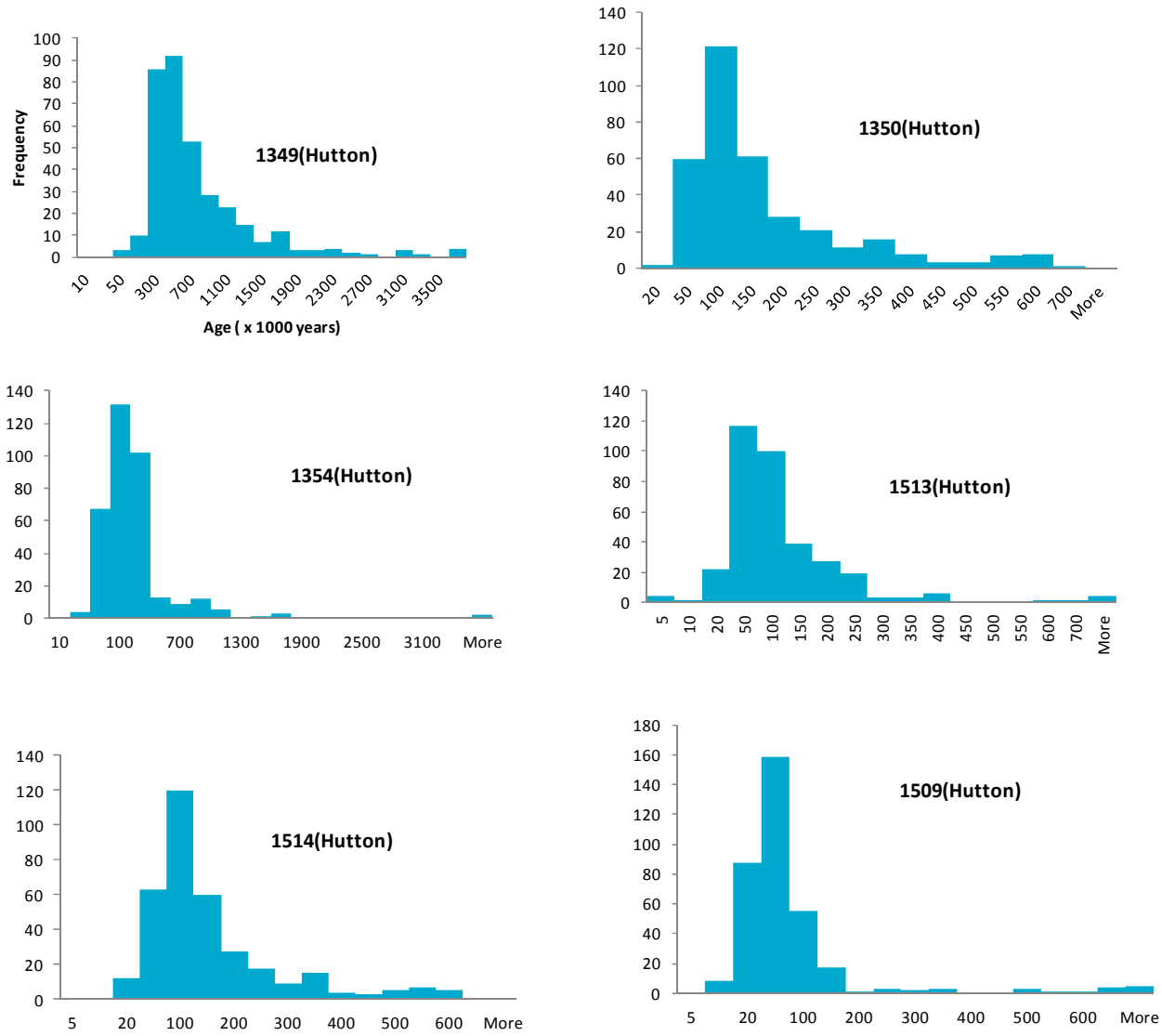

Figure 59: Distribution of groundwater ages for the Hutton sampling locations.

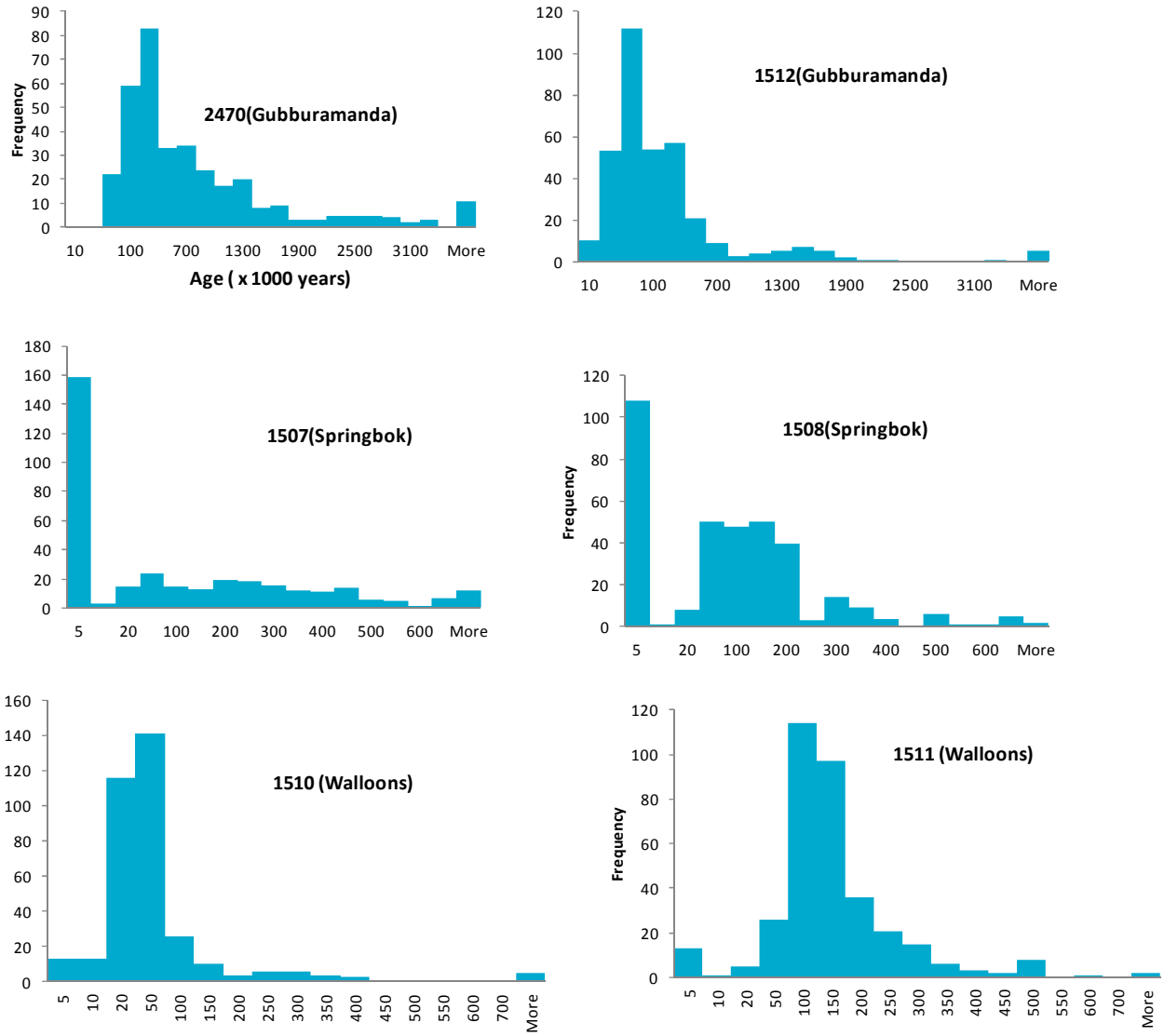

Figure 60: Groundwater age distribution for Gubberamunda, Springbok and Walloon coal measures sampling locations

It was observed that the simulated age distribution for the sampling location 2470, which is screened in the Gubberamunda aquifer was inconsistent with the ages for other locations. One possible reason is that this sampling location is located close to the Great Dividing Range where many formations pinch out. Thus the large values in the tail end of the age distribution may be a modelling artefact where pinching out of the model layers resulted in ambiguous and long particle tracks.

Since the velocity of flow in these formations is very slow, molecular diffusion would also play a significant role in the transport processes. Hence more realistic modelling of the groundwater age should account for the diffusive processes. Chlorine 36 dating study (Torgersen et al., 1991) conducted for the Surat Basin indicated ages in the range 100,000 to 1 million years with an increasing trend towards the deeper parts of the Basin. Ages with similar order of magnitude and directional trend were obtained from the current preliminary study as well.

7.4 Summary

The subregional model (section 3) was used for particle track analysis to estimate the groundwater age for different formations in the Surat Basin. ADV2 package of MODFLOW was used for simulating the particle

tracks with the assumption that advection is the dominant and only mechanism behind the transport process. Particles were tracked in a reverse order to determine the groundwater age at specified target locations. Each target location corresponded to a bore that was sampled for isotopic analysis. In this way the age distribution obtained from this modelling exercise could complement the results from the isotopic analysis.

Simulation of particle tracks was undertaken in a stochastic modelling framework using Null-space Monte Carlo analysis (Section 4). The hydraulic parameters and model boundary conditions were stochastically varied to simulate 350 particle tracks for each sampling location. The groundwater age distribution for each location was computed from the resulting particle tracks. The groundwater ages determined by using this approach varied between 50,000 to 500,000 years for most sampling locations. Particle tracks were simulated for 6 locations in the Hutton sandstone and the estimated groundwater ages indicated an increasing trend towards the deeper parts of the basin.

8 Design of optimal injection well field – Proof of concept

8.1 Overview

Design of a well field for the injection of CSG produced water is constrained by a number of criteria including available budget, capacity of the Reverse Osmosis treatment plants, characteristics and depth of the aquifer into which injection is planned at different locations within the injection well field, environmental and regulatory constraints etc. Budgetary constraints apply to the number of wells, locations of drilling and associated infrastructure. Similarly the capacity of the RO plants, characteristics of the target aquifer and environmental constraints govern the rate and total volume of injection. An ideal design of the injection well field should address all these constraints to optimally locate the injection wells and determine the injection rates to satisfy the objectives like maximisation of the total injection at minimal cost within the constraints set by the limited information on the target aquifer properties and environmental regulations.

This section illustrates the development of a methodology based on simulation and optimisation for the optimal design of an injection well field. Optimal design refers to the identification of the optimal locations and injection rates to maximise the design objective. The methodology was tested for a synthetic aquifer system and was **NOT** based on the models developed for Reedy Creek injection site in this project. But the algorithms and computed codes implementing this methodology could be readily used with the Reedy Creek models.

8.2 Methodology

A multi-objective stochastic optimisation approach was developed to optimise the injection well locations and injection rates. In this approach the groundwater flow simulation model is coupled to a multi-objective optimisation algorithm in order to optimise the injection well field design. While the simulation model predicts the aquifer response to each candidate design the optimisation algorithm searches for the best design amongst a large number of candidate designs. The optimal well locations and injection rates are to be determined subject to the constraint that the resulting groundwater head increase in a set of risk receptor bores should not exceed a prescribed target. Two objectives of management were considered for this illustrative well field design problem viz.,

1) Maximisation of the total injection into the well field for a given maximum number of wells
2) Minimisation of the total uncertainty in the predicted groundwater head changes at the control bores subject to the limited amount of information available about the aquifer system.

A set of control bores were considered where the groundwater head increase above a specified level was not permissible. In practice, these represent regulatory constraints to the development activity. A multi-objective optimisation problem was formulated to solve the injection well design problem. The solution of this optimisation problem requires the evaluation of the groundwater system responses to different alternative well field designs obtained from the groundwater flow simulation model. The simulation model was coupled to a multi-objective optimisation algorithm NSGA II (Deb et al., 2002) in a simulation-optimisation framework to do this.

To capture the prediction uncertainty, different realizations of the uncertain model parameters were simultaneously considered within the simulation-optimisation model. Thus, groundwater flow field resulting from each candidate solution is simulated across all the different realizations of the hydraulic parameter field. The variance of the simulated head increase was computed from these simulations and was used as a measure of the prediction uncertainty. Minimisation of the sum of the prediction variances computed for all the control bores constituted the second objective function.

The solution of the multi-objective optimisation problem is a Pareto-optimal front which gives the trade-off between two conflicting objectives. Each point in the front corresponds to one optimal well field design. The reliability of the solution was defined as the probability that the constraints defined for the groundwater head at the control bores are not violated. Reliability of each optimal solution in the front was computed by performing a post-optimisation Monte Carlo simulation using 200 hydraulic conductivity fields.

8.3 Synthetic case study

The simulated injection well field is located in an idealized rectangular confined aquifer with dimensions of 8000m × 5000 m and a uniform thickness of 100m. Dirichlet (i.e. specified head) boundary conditions of -8 and -12 m are applied to the northern and southern boundaries of the model respectively. This equates to a hydraulic gradient of 4 m / 8000 m = 5×10^{-4}, which is consistent with typical hydrogeological conditions. Neumann (i.e. specified flux) boundary conditions of 0 $m.d^{-1}$ are applied to the eastern and western boundaries. A uniform 100m × 100m cell discretization was adopted for the entire model grid. The synthetic model domain is depicted in Figure 61. The boundary of the well field within which the injection wells can be located and the locations of the control bores are also indicated. A hypothetical regulatory constraint was imposed that the groundwater head at these control bores should be less than -5m. The synthetic aquifer system was simulated numerically using MODFLOW [Harbaugh et al., 2005].

Uncertainty in hydraulic conductivity was considered as the only factor contributing to prediction uncertainty. This uncertainty is represented in the optimisation problem using stochastic characterisations of $\log_{10}$ hydraulic conductivity ($Y = \log_{10} K$). The $\log_{10}$ hydraulic conductivity field can be characterised using three parameters: the mean, covariance and correlation length of Y. This requires the assumption of stationarity of the first two moments of Y and that the covariance of Y is a function of the separation distance between interpolated locations. An unconditioned field generation was performed using sequential Gaussian simulation [GSLIB; Deutsch and Journel,1988] to generate the "true" K field (Figure 61). From this true K distribution, point measurements were extracted at uniform intervals of 1200 m. Log_{10} hydraulic conductivity distributions conditioned on these extracted values were then generated also using sequential Gaussian simulation to obtain multiple K fields for the optimisation and post-optimisation Monte Carlo analysis.

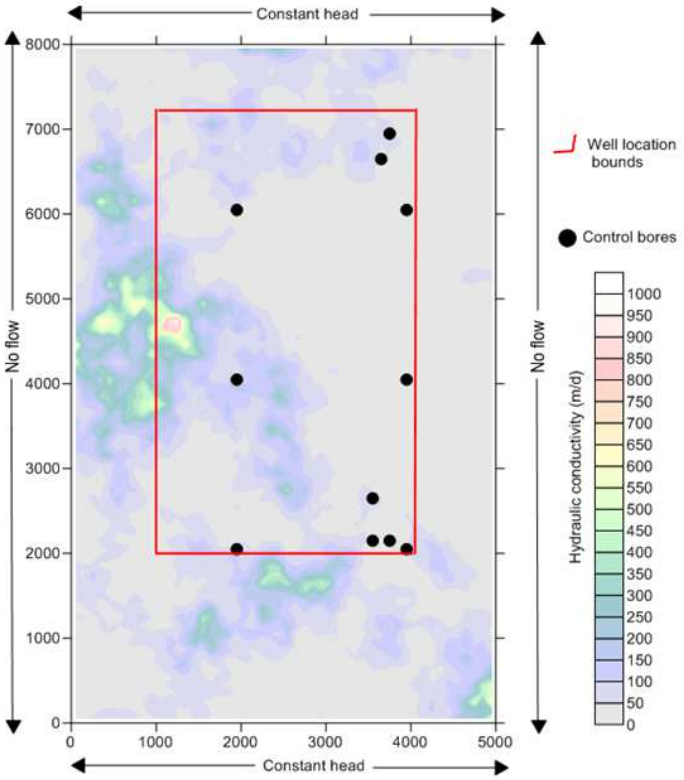

Figure 61: Synthetic model area indicated the 'true' hydraulic conductivity field and location of the well field and control bores.

8.4 Results

Pareto-optimal front obtained by solving this simulation optimisation problem is shown in Figure 62. The two axes represent the two objectives of the well field design problem. Each point in the front corresponds to a solution of the well field design problem. Thus each point corresponds to a set of optimal well locations and their injection rates. The histograms of the simulated groundwater head increase at one control bore for selected (numbered) solutions are also shown in Figure 62. These histograms were obtained from the post-optimisation Monte Carlo analysis. The distribution of the heads in the histogram indicates that majority of the simulated heads are below -5 m, thus satisfying the regulatory constraint on the injection scheme. Also, as we move from point 1 to point 6 the well field design is further constrained to ensure higher reliability in meeting these regulatory constraints. However, it is noteworthy that this increased reliability results in a lower total injection rate. In this way the Pareto-optimal front gives an entire range of well field design options for the decision maker to choose from, depending on different operational, design and regulatory constraints.

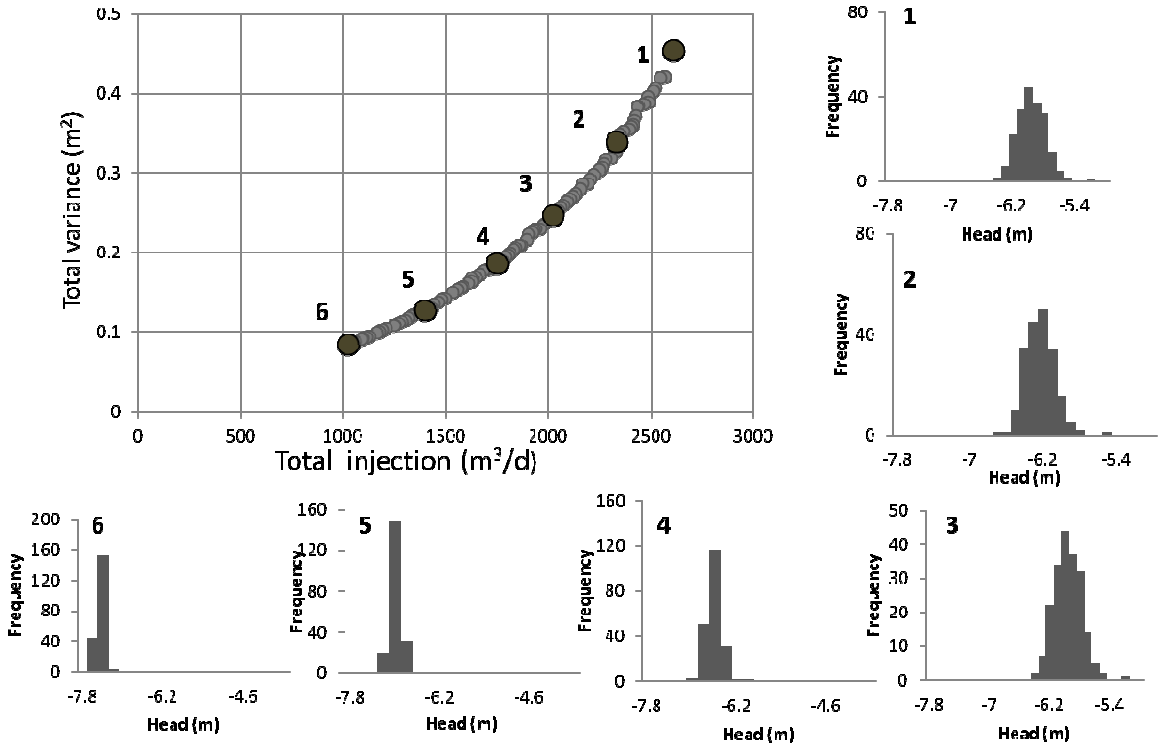

Figure 62: Pareto-optimal front representing the trade-off between the two objectives for different well field designs. Each point in the front correspond to a well field design (i.e. optimal well locations and injection rates)

Optimal well locations

The simulation optimisation algorithm proposed in this study identifies both the optimal location for the injection wells and the optimal injection rates meeting the objectives and constraints for the well field design problem. The optimality of such solutions depend on the information available to characterise the aquifer system in the models. Figure 63 illustrates the optimal well locations identified by the simulation-optimisation model when information regarding the hydraulic conductivity is available only at a number of locations scattered around the well field. The Kriging estimates of the uncertainty in the hydraulic conductivity are shown by the background colour flood in Figure 63. It is noteworthy that the optimal well locations identified by the simulation-optimisation model coincide with areas of least uncertainty. Also, on comparison with Figure 61 it could be observed that these well locations also coincide with high hydraulic conductivity values thus permitting intake of more injection water with less change in the groundwater head at the nearby control bores.

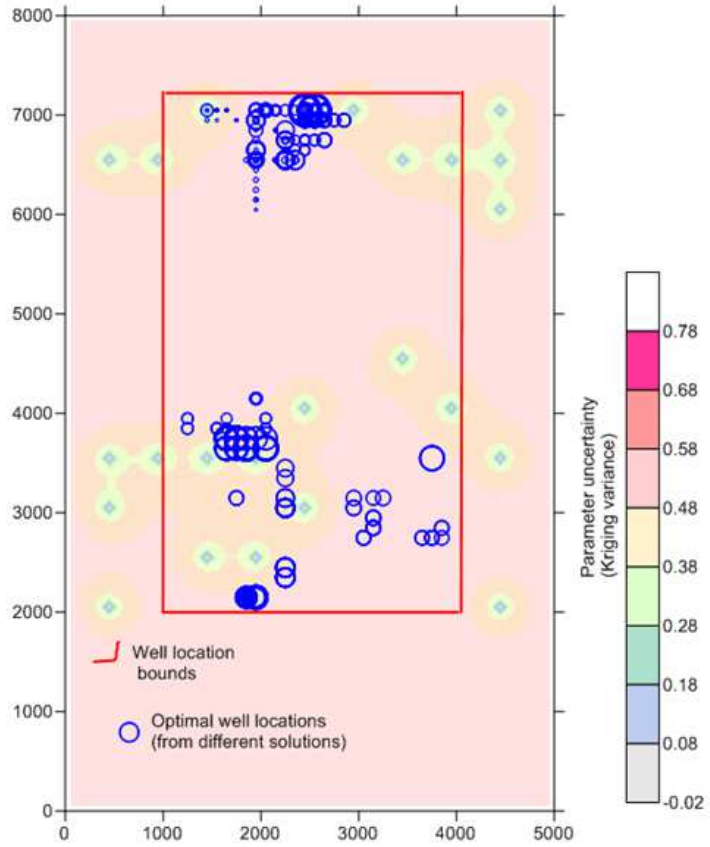

Figure 63: Optimal well locations identified by different solutions (scheme 3) in a Pareto front (blue circles; size is proportional to injection rate). Also shown is the Kriging variance of the hydraulic conductivity field (pastel colour scheme) and the candidate area for injection bore locations (red outline).

8.5 Summary

This section describes the methodology and a proof-of-concept case study to illustrate the applicability of simulation-optimisation approach for the design of optimal injection well fields. Once the groundwater flow model is built based on the available information of the aquifer characteristics, the model is used in a stochastic simulation-optimisation framework to determine the optimal locations for the injection wells and their injection rates. The uncertainty of the hydraulic parameter field is accounted by multiple realisations of the field generated using sequential Gaussian simulation. The reliability of the optimal well field design solutions in meeting the regulatory constraints was tested using post-optimisation Monte Carlo simulations.

The results indicated that high reliability designs which comply with the operational and regulatory constraints can be obtained using the proposed approach.

9 Conclusions

9.1 Overview

This study developed and applied a suite of methods based on numerical groundwater modelling and uncertainty analysis to quantify the regional impacts of a large scale coal seam gas produced water injection scheme in Surat Basin. The study specifically focused on a proposed scheme at the Reedy Creek site in Surat Basin where APLNG is developing a facility to reinject approximately 30 ML/d in to the Precipice sandstone. Groundwater quantity and quality impacts of the injection scheme were predicted using a stochastic modelling framework to address the uncertainties in the groundwater system and its representation in the models. The study has;

- Developed and applied a multi-scale integrated groundwater modelling approach for the prediction of water quantity and quality changes resulting from an injection scheme that APLNG has proposed for the disposal of CSG produced water in Surat Basin.
- Developed an inversion based upscaling approach for efficiently upscaling the information from limited injection trials, pump tests and tracer tests conducted in the field to constrain regional scale groundwater models.
- Applied state-of-the-art uncertainty analysis techniques to quantify the uncertainty in the estimated water quality and quantity changes.
- Explored the potential impacts of the presence of faults in the injection well field on the water quality changes.
- Explored a hypothesis testing framework to test whether the occurrence of an undesirable level of water quality at a specified location can be rejected with high confidence.
- Investigated the relative worth of different data types and their spatial and temporal disposition to optimise injection trial design for the Spring Gully site as well as for the long-term monitoring water quality monitoring.
- Developed a simulation-optimisation modelling methodology for the stochastic optimisation of injection well field design and tested it for a proof-of-concept model.

9.2 Conclusions

- The simulations of the proposed injection scenario using the OGIA model and the subregional model indicated that groundwater head increase would occur on a regional scale. The simulations indicated that the groundwater head increase resulting from the injection could extend over 50 km from the well field over hundreds of years. The domestic and stock bores in the region are located far from the Reedy Creek injection well field, the nearest bore (Combabula - RN 123030) being 15 km from the well field. The maximum simulated head increase in this bore was 4.3 m. The fluctuations of the water level in this range usually occur even due to the natural unsteady state of the flow in the Surat Basin and may not necessarily indicate a hydrogeological risk.
- Water quality simulations indicated dilutions to very low concentrations ($1/100^{th}$ of initial concentration) would occur over a distance of 5 km from the injection wells. Thus water quality changes resulting from the large scale injection, if any, are not likely to propagate to risk receptors like the domestic bores.
- Inversion based upscaling methodology proved useful in upscaling the information from the injection trial tracer tests and fine scale models for the upscaled prediction of regional scale impacts of operational scale injection scheme. The methodology provided a computationally efficient approach for simulating the impacts at different scales using multi-scale models and was useful to perform the uncertainty analysis in a computationally efficient manner.

- Null-space Monte Carlo analysis illustrated large uncertainty in the groundwater flow and transport predictions close to the injection field reflecting the limited amount of spatial and temporal data available from the injection trial in comparison to the vast spatial and temporal extent influenced by the operational scale injection. The stochastic prediction of the water quantity and quality changes helped in a more realistic characterisation of these perceived risks.
- Stochastic simulation of the groundwater quality changes considering the presence of faults in the injection well field indicated that presence of faults contribute to increased uncertainty in the prediction of dilution and travel times close to the location of faults.
- Relative worth of different types of data in informing the dilution predictions was computed using the uncertainty based modelling framework. Data-worth analysis highlighted the importance of water quality measurements over head measurements in informing the dilution predictions. In terms of designing the injection trial tracer tests for Spring Gully site, the data-worth analysis indicated the worth of bromide tracers over other tracer types.
- The results from the proof-of-concept study indicated that the simulation-optimisation modelling is a useful tool to assist the design of injection well field in terms of optimising the operational and design goals while simultaneously meeting the regulatory requirements.

9.3 Shortcomings and scope for future work

- The inversion based upscaling approach proposed in this work is a robust and efficient methodology to upscale point and local estimates of groundwater flow system properties into regional scale modelling framework. In this study, the pump tests, injection trials and tracer tests conducted in only one injection well were available for implementing this methodology. The method will be most efficient when such fine scale data is available at multiple locations.
- Few domestic and stock bores are present in the vicinity of Reedy Creek site which taps the Precipice sandstone aquifer. As a result of this, there were not many real risk receptors in the study area trivialising the outcome of novel approaches like hypothesis testing used in this study. Notwithstanding the lack of real risk receptors, hypothesis testing is a useful tool to test whether environmentally undesirable outcomes could be rejected with high confidence given the amount of data that is currently available.
- The impact of the presence of faults in the injection well field was tested using a novel and efficient approach. While the fault properties were varied probabilistically to quantify the uncertainty in the impacts, uncertainty in the fault locations were not explored in this study. It is very well possible to incorporate a stochastic descriptor defining variable fault locations into the Null-space Monte Carlo analysis and may be incorporated in any of the future analysis using these models.
- Groundwater age modelling undertaken in this study considered only advective transport of particles. For a comprehensive analysis of the groundwater age distribution it is required to consider the dispersive and diffusive processes of transport. Development of a 2 dimensional flow and transport model considering all these processes would be useful for a more comprehensive estimation of the groundwater ages in different formations.

REFERENCES

Anderman, E R and Hill, M C (2001), MODFLOW-2000, The US Geological survey modular groundwater model – documentation of the advective-transport observation(ADV2) package, version2, US Geological Survey.

Barrett, D. J., Couch, C. A., Metcalfe, D. J., Lytton, L., Adhikary, D. P., & Schmidt, R. K. (2013). Methodology for bioregional assessments of the impacts of coal seam gas and coal mining development on water resources. *A report prepared for the Independent Expert Scientific Committee on Coal Seam Gas and Large Coal Mining Development through the Department of the Environment*.

Bense, V.F., and Person, M.A., 2006. Faults as conduit-barrier systems to flow in siliciclastic sedimentary aquifers. *Water Resources Research*. 42, W05421, doi:10.1029/2005WR004480

Bense, V.F., Gleeson, T., Loveless, S.E., Bour, O. and Scibek, J., 2013. Fault zone hydrogeology. *Earth Science Reviews*. 127, p171-192.

Deb, K., Pratap, A., Agarwal, S., & Meyarivan, T. A. M. T. (2002). A fast and elitist multiobjective genetic algorithm: NSGA-II. *Evolutionary Computation, IEEE Transactions on*, *6*(2), 182-197.

Deutsch, C. V., and A. G. Journel (1998), GSLIB Geostatistical Software Library and User's Guide, 2nd edition, Oxford University Press, Oxford, UK.

Dockrill, B. and Shipton, Z/K/, 2010. Structural controls on leakage from a natural CO2 geologic storage site: central Utah. U.S.A. *Journal of Structural Geology*. 32 (11), 1768-1782.

Doherty J (2010a) *PEST model-independent parameter estimation user manual*, Watermark Numerical Computing, Brisbane, Australia, 336p.

Doherty J (2010b) *Addendum to the PEST manual*, Watermark Numerical Computing, Brisbane, Australia, 272p.

Doherty J, (2010c). Methodologies and Software for PEST-Based Model Predictive Uncertainty Analysis.Watermark Numerical Computing report. *www.pesthomepage.org/Training.php.*

Doherty J, Fienen MN, and Hunt RJ, (2010). Approaches to highly parameterised inversion: Pilot-point theory, guidelines, and research directions: *U.S. Geological Survey Scientific Investigations Report* 2010-5168, 36p.

Egholm, D.L., Clausen, O.R., Sandiford, M., Kristensen, M.B. and Korstgard, J.A., 2008. *The mechanics of clay smearing along faults*. *Geology*. 36, 787-790.

Faulkner, D.R., Jackson, C.A.L., Lunn, R.J., Schlische, R.W., Shipton, Z.K., Wibberley, C.A.J. and Withjack, M.O., 2010. A review of recent developments concerning the structure, mechanics and fluid flow properties of fault zones. *Journal of Structural Geology*. 32, 1557-1575.

Fredman, N., Tveranger, J., Cardozo, N. Braathen, A., Soleng, H., Roe, P., Skorstad, A., and Syversveen, A.R., 2008. Fault facies modeling: technique, and approach for 3D conditioning and modeling of faulted grids. *AAPG Bulletin*. v92 (9), 1-22.

Fulljames, J.R., Zijerveld, L.J.J., Franssen, R.C.M.W., Ingram, G.M. and Richard, P.D., 1996. Fault seal processes. *In* Norwegian Petroleum Society eds., Hydrocarbon seals – importance for exploration and production (conference abstracts): Oslo, Norwegian Petroleum Society, p5.

GHD (2011) Report for QWC17– 10 Stage 2 Surat cumulative management area groundwater model report, December 2011. Queensland Water Commission, Brisbane, Australia

Harbaugh, A. W. (2005), MODFLOW-2005, the US Geological Survey modular ground-water model: The ground-water flow process, United States Geological Survey Techniques and Methods 6-A19, US Department of the Interior, Reston, VA, USA.

Hsieh, P.A., and Freckleton, J.R., 1993, Documentation of a computer program to simulate horizontal-flow barriers using the U.S. Geological Survey modular three- dimensional finite-difference ground-water flow model: U.S. Geological Survey Open-File Report 92-477, 32 p.

IAEA, 2013. Isotope methods for dating old groundwater, International Atomic Energy Agency, Vienna, 2013.

Lindsay, N.G., Murphy, F.C., Walsh, J.J. and Watterson, J., 1993. Outcrop studies of shale smear on fault surfaces. International Association of Sedimentologists Special Publication 15, 113-123.

Manzocchi, T., Walsh, J.J., Nell, P., and Yielding, G., 1999. Fault transmissibility multipliers for flow simulation models. *Petroleum Geoscience*. 5, 53-63.

Manzocchi, T., Childs, C. and Walsh, J.J., 2010. Faults and fault properties in hydrocarbon flow models. *Geofluids*. 10, 94-113.

Moore, C., Doherty, J.E., 2005. Role of the calibration process in reducing model predictive error. Water Resour. Res. 41 (5). http://dx.doi.org/10.1029/2009WR008627.

Moore C, Cui T, Doherty J, Turnadge C, Pagendam D, and Peeters L (2014) Uncertainty analysis, data worth analysis and hypothesis testing: Assessments to support Environmental impact Assessments related to cumulative impacts of Coal Seam Gas extraction in the Surat Basin, Queensland. CSIRO, Australia.

QWC (2012) Underground Water Impact Report for the Surat Cumulative Management Area, Queensland Water Commission.

Sperrevik, S., Gillespie, P.A., Fisher, Q.J., Halvorsen, T., and Knipe, R.J., 2002. Empirical estimation of fault rock properties. *Hydrocarbon Seal Quantification*. Edited by A.G. Koestler and R. Hunsdale. Norwegian Petroleum Society Special Publication 11, pp109-125.

Tonkin M. and Doherty J., 2009a. Calibration-constrained Monte Carlo analysis of highly parameterized models using subspace techniques. *Water Resources Research* 45, WOOB10, doi:10.1029/2007WR006678.

Torgersen, T., Habermehl, M. A., Phillips, F. M., Elmore, D., Kubik, P., Jones, G. B., ... & Gove, H. E. (1991). Chlorine 36 dating of very old groundwater: 3. Further studies in the Great Artesian Basin, Australia. *Water Resources Research*, *27*(12), 3201-3213.

Wallis, I., Moore, C., Post, V., Wolf, L., Martens, E., Prommer, H., 2014. Using predictive uncertainty analysis to optimise tracer test design and data acquisition. Journal of Hydrology 515 (2014) 191–204.

Yielding, G., Freeman, B. and Needham, T., 1997. Quantitative fault seal prediction. *AAPG Bulletin*. 81 (6), 897-917.

Appendix A FAULTSIM

INTRODUCTION

Program FRACSIM adds faults to an existing groundwater flow model. It does this by modifying the horizontal and vertical permeabilities (this word is used interchangeably with "hydraulic conductivities" in the discussion that follows) of cells in which faults lie. Modifications to permeability take account of the two effects which a fault may have on groundwater flow, as described in petroleum and groundwater literature. These are:

- A fault may present a barrier to horizontal water movement; and
- It may provide the means through which flow to upper and lower layers can take place through otherwise impermeable material.

THE EFFECTS OF FAULTS ON GROUNDWATER FLOW

Fault architecture is normally characterized by two components, these being the "fault core", and the surrounding "damage zone". The former is the zone through which displacement occurs. The latter is comprised of the "halo" surrounding this zone in which rock properties are affected by the presence of the fault and in which permeability is consequentially enhanced. The actual values of permeabilities in these (normally very heterogenous) zones depend on a number of factors. These include the following.

- the type of rock displaced by the fault (i.e. the so-called "protolith");
- the throw of the fault;
- the nature of the stress regime that give rise to faulting;
- the extent to which fragments of protolith are entrained by the fault through gouging as displacement takes place;
- the nature of these entrained lithologies;
- the depth of burial of rocks at the time of faulting;
- the depth of burial since the time of faulting, increased depth of burial promoting compaction and cementation.

See papers such as Sperrevik et al (2002), Fredman et al (2008), Faulkner et al (2010), Bense et al (2013), and references cited therein, for a full discussion of these issues.

The effect that faults, particularly in sedimentary sequences, have on fluid movement has been widely discussed on the petroleum literature. In that context, much attention has been paid to their ability to act as seals on fluid movement in general, and hydrocarbon movement in particular. Part of their ability to form effective hydrocarbon traps rests on the fact that fault surfaces are often smeared with shale that has been "gouged" from displaced stratigraphic layers. The low permeability of material which then coats the fault plane and (particularly in the hydrocarbon context) the barrier that such material presents to hydrocarbon entry because of the high capillary pressure differential that must be overcome before such entry takes place, is responsible for the effectiveness of faults as hydrocarbon traps; see for example, Manzocchi et al (2010) for a full discussion.

A number of methodologies have been developed for estimating the amount of fine-grained material that may coat a fault plane. These include the use of indices such as clay shear potential (CSP) (Fulljames et al 1996), shale smear factor (SSF) (Lindsay et al, 1993) and shale gouge ratio (SGR) (Yielding et al 1997), all of which are relatively easily calculated from information available in petrophysical logs; in this context the host rock clay content (often referred to as V_m) is particularly important. Calculations made of differential

failure plane orientations in juxtaposed weak and strong lithologies support the notion of entrainment of weaker, low permeability, material along fault planes; see for example, Egholm et al, 2008. The presence of thus entrained fine-grained material on fault surfaces presents an impediment to horizontal fluid flow in sequences of high silt and clay content above that which is incurred through movement of the fault itself, with consequential offsetting of permeable strata and their juxtapositioning against less permeable layers.

Methodologies such as that described by Manzochhi et al (1996) can be used for modifying reservoir and other models to account for the presence of impermeable material on fault surfaces. These methods rely on introduction of so-called “transmissibility multipliers” to cell connections which cross fault planes. Calculation of these multiplies often follows estimation of fault permeability, this in turn being calculable from indices such as SGR described above.

It has been pointed out by some authors (for example Sperrevik et al, 2002) that lithologies such as coal and carbonates can also contribute to fault plane shearing, with consequential reduction in cross-fault horizontal permeability, as these too can be entrained into the fault plane as movement takes place along the fault. Bense and Person (2006) further suggest that commonly-used indices such as SGR do not necessarily provide a complete means through which across-fault permeability can be calculated, as they neglect the presence within the fault core of considerable amounts of material which may be more permeable than shale/clay, and which can also be gouged from neighouring strata. The fact that such material may be present in abundance, particularly in sequences that are not fully lithified, is evinced by the fact, documented by other authors, that fault widths tend to be wider where shale abuts sand or where sand abuts sand than elsewhere, this indicating a considerable amount of sand entrainment during the faulting process.

Even in areas where little shale exists within the stratigraphic sequence, or which are not sedimentary at all, fault planes are still likely to constitute impediments to horizontal subsurface as a consequence of the cataclasis that is induced by rock movement. This is especially the case where the host rock is deeply buried and accommodation of movement by mechanisms such as grain alignment and dilation that are available in shallow environments is not possible.

While the sealing role of faults has received much attention in the literature, that same literature provides little guidance on the likely nature of the fault damage zone in sedimentary environments, nor on what hydraulic properties should be assigned to it, particularly those that pertain to vertical flow. This suggests that faulting in sedimentary sequences, especially shale and siltstone-rich sedimentary sequences, does not enhance vertical fluid movement to a great degree. Alternatively, it may reflect the fact that where it does, such locations would not be the focus of petroleum industry attention, because a trap would not exist.

Within the Surat Basin, it is believed that at least some springs within the Surat Basin owe their existence to faulting; hence they must play some role in promoting vertical movement of water in at least some locations. It has been suggested that where a fault does promulgate vertical movement of water, such movement is likely to be confined to discrete channels either along the fault place or through the damage zone associated with the fault, rather than being uniform along the fault structure (Faulkner et al, 2010; Dockrill and Shipton, 2010).

REPRESENTATION OF FAULTS IN MODELS

The “corner point grid” concept employed by ECLIPSE and supported by other reservoir models, allows representation of stratigraphic offsets along faults, and variation of this offset along fault strike and dip. This concept of unstructured grid design allows a model cell on one side of a fault to connect to one or multiple cells on the other side of a fault as required by displacement along the fault and the consequential introduction of new juxtapositional relationships. At the same time, obstacles to horizontal flow across cell boundaries can be addressed through the use of directional tranmissibilitiy multipliers as described by Manzocchi et al (1999). It is worthy of note, however, that calculation of these multipliers is a complex matter where multiple cells linkages take place a fault.

In the single phase modelling context, cross-fault connectivity of offset stratigraphies can be accommodated using MODFLOW-USG’s unstructured grid functionality. While use of the corner point grid

concept is not directly supported for MODFLOW-USG, its input protocols are flexible enough for this to be readily accommodated with a little programming – either within the MODFLOW-USG code itself, or within a supporting program. Meanwhile, concomitant cross-fault permeability reduction could be readily accommodated through use of the MODFLOW Horizontal Flow Barrier package (Hsieh and Freckleton, 1993), which is also supported by MODFLOW-USG.

REPRESENTATION OF FAULTS IN REGIONAL AND SEMI-REGIONAL GROUNDWATER MODELS

The FAULTSIM program described herein attempts to introduce groundwater-flow-salient features of faults to a model that lacks the detail of a typical reservoir model. Nevertheless, the algorithm on which the program is based attempts to encompass some of the techniques that have been developed in the petroleum industry for representation of faults in a model, and the effects that faults have on subsurface fluid flow. However as the algorithm does not have the same data requirements as these methodologies, it is easier to implement.

It is assumed that a model has been constructed. It is further assumed that this model does not simulate displacement of strata at the fault plane. While this can be seen as a disadvantage in some respects, it can also be construed as an advantage, particularly if fault displacement is not likely to be large in relation to model layering (as is often the case in regional and sub-regional models). Use of this algorithm also allows faults to be emplaced anywhere within an existing model domain. In particular, it readily allows stochastic emplacement of faults in different realizations of a regional or semi-regional impact assessment model.

The user supplies an integer array in which non-zero elements indicate cells in which faults exist. Fault planes are thus assumed to occur within a cell rather than at the boundaries between two neighbouring cells. While this makes representation of impediments to horizontal flow incurred by a fault slightly more difficult, representation of enhanced vertical flow becomes rather easy. This can be construed as a beneficial aspect of the algorithm, as the propensity for vertical flow enhancement is probably more important in the regional impact assessment modelling context than the propensity of faults to impede horizontal flow.

As presently programmed, a fault is assumed to pervade all layers of a model grid. While this is appropriate for smaller sub-regional models focussed on only a small number of stratigraphic layers, it is not appropriate broader scale models encompassing larger areas and greater depth ranges. The FRACSIM program can be easily modified to accommodate this situation.

Fault zone architecture is assumed to be comprised of two elements, a core zone and a damage zone. The user is asked for the width of each of these. The damage zone is assumed to include the core, so that its width must be supplied as greater than that of the fault core. If its width is supplied as equal to that of the fault core, then the thickness of the damage zone halo around the core is effectively zero.

Within a regional or semi-regional modelling context, data for calculation of indices such as shale gouge ration (SGR), clay smear potential (CSP) etc., at each fault-effected cell will probably not be available. Furthermore, use of these indices in stratigraphic layers where shale is not abundant may yield unrealistic estimates of fault-induced groundwater flow impediments as it fails to take account of entrainment of lithologies other than clay into the fault plane. Instead the FAULTSIM algorithm employs a method that is somewhat similar to that proposed by Bense and Person (2006). The entrained constituents of a fault plane are assumed to originate in all layers intersected by the fault and that could be transported by the fault to a particular layer through movement along the fault, this being dictated by its throw. In a similar manner to Bense and Person (2006), fault permeability anisotropy (with flow up and down the fault plane being easier than across it) is accommodated through conceptual layering of entrained lithologies along the fault plane. The permeabilities of materials which constitute this layering are those of entrained prototype rocks. This allows ready computation of hydraulic properties of the fault core through appropriate arithmetic and harmonic averaging of protolith horizontal and vertical permeabilities that are within “reach” of a certain location along the fault plane as determined by the throw of the fault.

In the damage zone which surrounds the fault plane, stratigraphic anisotropy is assumed to have been eradicated through local reorientation of rocks and the introduction of drag folding. Hence, within this damage zone, the vertical anisotropy becomes effectively 1.0. It follows that, in the vicinity of a fault, shale layers are locally unable to present the impediment to vertical water movement that they normally by virtue of decreased vertical permeability; however they will still be able to present an impediment to vertical water movement because of their low intrinsic horizontal permeability.

The user is asked for the throw of the fault. As presently programmed only a single value for fault throw can be supplied; in future versions of the program, layer-specific throws will be provided if this is warranted. For any cell in the model that is deemed to be fault-affected (as indicated by the integer array discussed above), the FAULTSIM program then undertakes weighted arithmetic averaging of horizontal permeability and weighted harmonic averaging of vertical permeability over a vertical distance of half the user-designated throw length over layers above and below that cell. Weighing is calculated in accordance with the fraction of the fault plane that is intersected by each layer over this total distance. The fault core is then assumed to be comprised these same materials, effectively layered in the direction of the fault plane; as Bense and Person (2006) describe, this allows ready calculation of the anisotropic permeability of fault plane material. Harmonic averaging of vertical hydraulic conductivities of the protolith material intersected by the fault are employed in the former calculation, and arithmetic averaging of intersected protolith horizontal hydraulic conductivities are employed in the latter calculation. The horizontal and vertical permeabilities of the fault-affected cell are then modified in order to accommodate the presence of the core zone, taking into account the fraction of the cell that this zone occupies, as dictated by its thickness.

Within any cell that is demarked by the user as containing a fault, further modifications are made to the vertical permeability assigned to that cell in order to accommodate the presence of the damage zone. Suppose that the overall damage zone width is provided as w_d and that the fault core width is provided as w_c. Suppose also that the width of the cell is w_e. Then a new vertical conductivity is calculated for the cell based on the following premises:

- Vertical permeability within the a width of cell given by w_c (i.e. the core zone), is enhanced in the manner described above;
- The vertical permeability within a width of cell given by w_d-w_c (i.e. the fault damage zone with the core excluded) is the same as its horizontal permeability, so that anisotropy is been effectively reduced to 1.0 in the damage zone.
- Vertical permeability within a width of cell given by w_e-(w_d+w_c) (i.e. non fault-affected parts of the cell) is unchanged.

ADDITIONAL FLEXIBILITY

Further flexibility is provided in calculation of revised horizontal and vertical permeabilities for fault-effected cells. Suppose that the existing horizontal permeability for a fault-effected is cell is Kh_o (“o” stands for “old”). Suppose that its revised horizontal permeability (calculated as above) is Kh_n (where “n” stands for “new”). Denote the ratio of these two as *rh*. That is:

$$rh = Kh_o/Kh_n$$

FAULTSIM ensures that this ratio is always greater than 1.0. However a power can be applied to this ratio if desired, so that the impediments to horizontal flow provided by faulting are amplified beyond those calculated above. Kh_n is then calculated as:

$$Kh_n = Kh_o * rh^{ph}$$

where *ph* is the user-supplied horizontal conductivity reduction power. This can be supplied as 1.0 if outcomes of the above algorithm are to be left unmodified.

Similarly, let *rv* denote the ratio of modified to existing (i.e. new to old) vertical permeability (i.e. *Kv*) of a fault-affected cell calculated using the above algorithm. Hence:

$rv = Kv_n/Kv_o$

FAULTSIM ensures that this is always greater than 1.0. The actual vertical conductivity of the fault affected cell is calculated by FRACSIM as:

$$Kv_n = Kv_o * rv^{pv}$$

where *pv* is the user-supplied vertical permeability enhancement power. This can be supplied as 1.0 if outcomes of the above algorithm are to be left unmodified.

ADVANTAGES AND DISADVANTAGES

The above methodology has the advantage of being easily programmed. Furthermore, its data requirements are met mainly by the existing model. These are layer elevations, cell permeabilities, and locations of fault-affected cells. The output of the program is a new set of horizontal and vertical permeabilities arrays which are then used by the model. Additional user inputs include only the locations of fault affected cells (these being supplied through an integer array), fault throw, and fault core and overall damage zone widths. Optionally the effect of the fault on horizontal and vertical conductivities can be amplified by user-supplied enhancement powers.

Enhanced versions of FAULTSIM can easily accommodate introduction of cell-specific fault throws and widths if this is required. It is also an easy matter to allow fault-cell identification to be layer-specific rather than pertaining to all layers.

However the main drawback of FAULTSIM as presently programmed is that no horizontal anisotropy is introduced to fault-affected cells. Thus the permeability reduction in the across-fault horizontal direction is the same as that in the fault-parallel horizontal direction. This is not expected to present too much of a problem where a fault is long, as flow parallel to a fault within fault-effected cells is probably not great. Furthermore, if a fault is a significant flow barrier and orientated perpendicular to a regional flow field, then flow adjustment will tend to take place in cells that are in front of and behind the fault but separated from the fault by greater distances than half the width of one model cell.

Lack of provision of horizontal anisotropy is also not likely to be disadvantageous where faults that are introduced to a model domain are not parallel to grid cells and columns, and or exists in local swarms.

Nevertheless, in future versions of FAULTSIM, it may be possible to introduce horizontal anisotropy to fault-effected cells. The appropriate anisotropy direction for each fault affected cell could be gleaned from the values of the integer array(s) that indicate fault-affected cells.

RUNNING FAULTSIM

Typical FAULTSIM prompts and responses are as follows.

```
Enter name of grid specification file: model.spc
- file model.spc read ok.

How many layers in model? 13

Enter name of fault integer array (assumed same for all layers): fault.inf
- file fault.inf read ok.

Enter filename base of bottom elevation arrays: bot
- file bot0.ref read ok.
- file bot1.ref read ok
  etc

Enter filename base of Kx arrays: kx
- file kx1.ref read ok.
- file kx2.ref read ok.
  etc
```

```
 Enter filename base of Kz arrays: kz
 - file kz1.ref read ok.
 - file kz2.ref read ok.
   etc

Enter throw of fault: 200
Enter thickness of fault core: 5
Enter thickness of fault damage zone (includes core): 20

Enter fault vertical K enhancement power: 2.0
Enter fault horizontal K reduction power: 3.0

Enter filename base for new Kx array files: newkx
Enter filename base for new Kz array files: newkz

- file newkx1.ref written ok.
- file newkx2.ref written ok.
  etc

- file newkz1.ref written ok.
- file newkz2.ref written ok.
  etc
```

The following should be noted.

- The contents of a grid specification file are described in documentation of the PEST Groundwater Data Utilities.
- An extension of "*.ref*" is expected for real array files.
- The layer-numbers associated with real array files should be built into their filenames; the layer number should immediately precede the dot prior to the filename extension.
- The layer numbers associated with bottom elevation arrays begin at zero; the bottom of layer zero is the top of layer 1.
- All elements of the integer array denoting the presence of a fault must be zero except for elements pertaining to those cells in which the fault exists. As presently programmed, the values of these elements can be any number other than zero. Because only one integer array is supplied to the present version of FAULTSIM the fault is assumed to pervade all model layers.

Appendix B - Assesspar utility description

GENERAL

The ASSESSPAR utility can be used to assist in model-based hypothesis-testing.

Suppose that a model has been calibrated. Suppose that it is then re-calibration with an extra "observation" included in the calibration process, this being the value of a prediction of interest. (This is effectively done when using PEST in Pareto mode.) If parameter values that emerge from this second calibration process are "unreasonable", then the prediction can be construed as unlikely.

The integrity of model-based hypothesis-testing conducted in this way rests upon the model's ability to allow predictive values to be computed if, indeed, these values are compatible with an expert-knowledge-based assessment of hydraulic properties. In the groundwater modelling context, this will normally require that calibration be undertaken using highly-parameterized inversion, so that predictive possibilities are not artificially prevented by a parameterization scheme that is incapable of representing geologically realistic heterogeneity. Both the first and second calibration exercises discussed above will therefore probably employ Tikhonov regularisation in which preferred values are assigned to parameters through regularisation prior information. A PEST control file will probably therefore exist in which "expected parameter values" from a pre-calibration (or pre-re-calibration) point of view are represented as initial values within this file. Assessment of parameter sets which emerge from the calibration process (these are assumed to reside in a parameter value file) is then based on differences between calibrated parameter values and these prior expected parameter values. ASSESSPAR allows this comparison to be made on a statistical basis.

ASSESSPAR computes two variates, one a chi-square variate and one a normal variate. (Here it is assumed that prior parameter probabilities are multiGaussian in nature.) Optionally, a prediction-specific normal variate can be computed based on sensitivities of a prediction of interest to model parameters. If this is to be done, the model calibration dataset will need to include this prediction so that the sensitivity of this prediction to model parameters is available from the JCO file.

If desired, other statistics can be calculated by the user on the basis of information recorded in the ASSESSPAR output file. This file tabulates the values of "eigen-parameters"; the standard deviation of each of these is 1.0, and each is statistically independent of other eigen-parameters. If a Gaussian prior parameter distribution is assumed, parameter (and hence predictive) confidence intervals are readily calculated from the values of these eigen-parameters.

THEORY

Let **k** denote a parameter set. Actually, let it denote the differences between an actual parameter set and a "base" parameter set whose values are prior expected parameter values. Thus the expected value of the **k** parameter vector is the vector **0**.

Let the covariance matrix of **k** be denoted as C(**k**). Because C(**k**) must be a symmetric, positive-definite matrix, it can be written (through singular value decomposition) as:

$$C(\mathbf{k}) = \mathbf{E}\mathbf{F}\mathbf{E}^t \qquad (1)$$

where **F** is a diagonal matrix with positive and non-zero diagonal elements.

Let the "eigen-parameter set" **m** be defined through the transformation:

$$\mathbf{m} = \mathbf{F}^{-1/2}\mathbf{E}^t\mathbf{k} \quad (2)$$

It is easily verified that the covariance matrix of **m** (i.e. C(**m**)) is the identity matrix **I**. Hence, by definition, the scalar variable $\mathbf{m}^t\mathbf{m}$ has a chi-square distribution with *n* degrees of freedom, where *n* is the number of elements of **k** and hence of **m**. Basic matrix manipulation demonstrates that:

$$\mathbf{m}^t\mathbf{m} = \mathbf{k}^t\mathbf{E}\mathbf{F}^{-1/2}\mathbf{F}^{-1/2}\mathbf{E}^t\mathbf{k} = \mathbf{k}^t\mathbf{E}\mathbf{F}^{-1}\mathbf{E}^t\mathbf{k} = \mathbf{k}^t\mathbf{C}^{-1}(\mathbf{k})\mathbf{k} \quad (3)$$

Hence $\mathbf{k}^t\mathbf{C}^{-1}(\mathbf{k})\mathbf{k}$ also has a chi-square distribution. Tables of probabilities associated with chi-square values are readily available; calculators are also available on the internet. Note that as the number of degrees of freedom increases, the chi-square distribution approaches a normal distribution with mean *n* and variance 2*n*. This relationship can be used to assess parameter credibility in highly parameterized cases as standard tables do not usually extend beyond *n* values of about 100.

Let *t* be a scalar that is calculated from **m** (defined as above) through use of a vector ***j*** as:

$$t = \mathbf{j}^t\mathbf{m} \quad (4)$$

Through basic propagation of variance relationships, the variance of *t* is given by:

$$\sigma^2_t = \mathbf{j}^t\mathbf{C}(\mathbf{m})\mathbf{j} = \mathbf{j}^t\mathbf{j} \quad (5)$$

If follows that if **j** is a unit vector then the variance (and hence standard deviation) of **j** is 1.0. If C(**m**) pertains to a normal distribution, then this provides us with a normal variate through which parameter credibility can be assessed. Useful options for **j** may include vectors for which all elements except that pertaining to a parameter of interest are zero; this allows the credibility of individual parameter to be assessed.

For predictive assessment a more useful vector unit may be:

$$\mathbf{j} = \mathbf{v} = \mathbf{w}/(\mathbf{w}^t\mathbf{w})^{1/2} \quad (6)$$

where **w** encompasses sensitivities of a prediction of interest to elements of the eigen-parameter set **m**.

Suppose that the sensitivity of a prediction *s* to the real parameter set **k** is given by the vector **y**. Then:

$$s = \mathbf{y}^t\mathbf{k} \quad (7)$$

If **w** is calculated as:

$$\mathbf{w} = \mathbf{F}^{1/2}\mathbf{E}^t\mathbf{y} \quad (8)$$

then:

$$\mathbf{w}^t\mathbf{m} = \mathbf{y}^t\mathbf{E}\mathbf{F}^{1/2}\mathbf{F}^{-1/2}\mathbf{E}^t\mathbf{k} = \mathbf{y}^t\mathbf{k} \quad = s \quad (9)$$

the second last equality holding through orthonormality of **E**. Because **v** is a unit vector, it follows that the scalar:

$$s' = \mathbf{v}^t\mathbf{m} = \mathbf{w}^t\mathbf{m}/(\mathbf{w}^t\mathbf{w})^{1/2} = \mathbf{y}^t\mathbf{k}/(\mathbf{w}^t\mathbf{w})^{1/2} \quad (10)$$

has a standard deviation of 1. From (4.27.8) it follows that:

$$\mathbf{w}^t\mathbf{w} = \mathbf{y}^t\mathbf{E}\mathbf{F}^{1/2}\mathbf{F}^{1/2}\mathbf{E}^t\mathbf{y} = \mathbf{y}^t\mathbf{C}(\mathbf{k})\mathbf{y} \quad (11)$$

Hence:

$$s' = \mathbf{y}^t\mathbf{k}/[\mathbf{y}^t\mathbf{C}(\mathbf{k})\mathbf{y}]^{1/2} \quad (12)$$

has a standard deviation of 1. If C(**k**) pertains to a multi-Gaussian distribution, then *s*′ is a standard normal variate. Its value is then easily employed for assessing parameter confidence, where parameter values are "calibrated" to ensure the occurrence of a prediction *s*. In doing so, predictive confidence is also assessed. Calibration to ensure the occurrence of a prediction can be achieved through a single calibration exercise in which the prediction is included in the calibration dataset, or through use of PEST in Pareto mode.

USING ASSESSPAR

ASSESSPAR is run using the command:

```
assesspar parfile pestfile uncfile outfile [senfile]
```

where

parfile is a parameter value file,

pestfile is a PEST control file containing prior expected parameter values,

uncfile is a parameter uncertainty file,

outfile is the eigen-parameter output file, and

senfile is an optional predictive sensitivity file.

As stated above, it is assumed that expected parameter values are housed as initial values in the user-nominated PEST control file. The transformation status of parameters is also read from this file. As is normal practice, parameter sensitivities and uncertainties pertaining to parameters must pertain to the logs of parameters where parameters are denoted as log-transformed in the PEST control file.

If a predictive sensitivity file is not supplied, then the normal variate s' of equation (12) is not calculated. Only the chi-square variable $\mathbf{k}^t\mathbf{C}^{-1}(\mathbf{k})\mathbf{k}$ is calculated in this case. Inversion of the C(**k**) matrix is undertaken using SVD. This may take a while where the matrix is large; a 64bit version of ASSESSPAR may then be required.

Whether or not a predictive sensitivity vector is supplied, the output file written by ASSESSPAR lists all eigen-parameters. If numerical singular value decomposion of C(**k**) is undertaken (which occurs if C(**k**) has any off-diagonal elements), these are listed in order of decreasing singular value. Otherwise they are listed in the same order as parameters in the PEST control file as there is then a one-to-one relationship between actual parameters and eigen-parameters. Eigen-parameters are the elements of the vector **m** of equation (2). Where C(**k**) pertains to a Gaussian distribution, then each of these are standard normal variates whose credibility is thereby easily assessed.

The values of the chi-square variable and (when the predictive sensitivity file is supplied) the prediction-specific normal variate are each written to the screen and recorded in the ASSESSPAR output file. Note that the degrees of freedom associated with the chi-square distribution is the number of adjustable parameters contained in the PEST control file. This is also listed to the screen and to the ASSESSPAR output file.

Note also that a predictive sensitivity file is easily obtained from a PEST Jacobian matrix file using the JROW2VEC utility.

Appendix C Injection rates (ML/d) across 12 wells over 264 months

Month	COM_257	COM_300	RCK_30	COM_330	COM_373	COM_416	RCK_47	RCK_50	RCK_59	RCK_66	RCK_121	RCK_88
1	0.01	0.01	0.01	0.01	0.01	0.00	0.02	0.01	0.01	0.01	0.00	0.01
2	0.01	0.02	0.03	0.03	0.02	0.01	0.05	0.02	0.02	0.02	0.01	0.02
3	0.03	0.04	0.07	0.06	0.05	0.01	0.11	0.03	0.03	0.04	0.02	0.03
4	0.03	0.04	0.07	0.07	0.06	0.02	0.12	0.04	0.04	0.05	0.03	0.04
5	0.27	0.36	0.58	0.54	0.46	0.12	0.98	0.30	0.29	0.37	0.21	0.29
6	0.26	0.35	0.57	0.53	0.45	0.12	0.96	0.29	0.29	0.36	0.21	0.29
7	0.27	0.36	0.58	0.54	0.46	0.12	0.98	0.30	0.29	0.37	0.21	0.29
8	0.30	0.40	0.66	0.61	0.52	0.14	1.11	0.34	0.33	0.42	0.24	0.33
9	0.29	0.39	0.64	0.59	0.51	0.14	1.07	0.32	0.32	0.40	0.23	0.32
10	0.49	0.65	1.07	0.99	0.85	0.23	1.79	0.54	0.54	0.67	0.39	0.54
11	0.90	1.21	1.98	1.84	1.57	0.42	3.33	1.01	0.99	1.25	0.72	0.99
12	0.99	1.33	2.18	2.03	1.73	0.47	3.66	1.11	1.09	1.38	0.80	1.09
13	1.09	1.46	2.38	2.22	1.89	0.51	4.01	1.21	1.20	1.51	0.87	1.20
14	1.19	1.60	2.62	2.44	2.08	0.56	4.40	1.33	1.31	1.65	0.96	1.31
15	1.25	1.68	2.74	2.55	2.18	0.59	4.61	1.39	1.38	1.73	1.00	1.38
16	1.28	1.72	2.81	2.61	2.23	0.60	4.72	1.43	1.41	1.77	1.03	1.41
17	1.30	1.74	2.85	2.65	2.26	0.61	4.79	1.45	1.43	1.80	1.04	1.43
18	1.47	1.98	3.23	3.01	2.57	0.69	5.43	1.64	1.62	2.04	1.18	1.62
19	1.41	1.89	3.09	2.88	2.45	0.66	5.20	1.57	1.55	1.95	1.13	1.55
20	1.34	1.79	2.93	2.73	2.32	0.63	4.92	1.49	1.47	1.85	1.07	1.47
21	1.27	1.71	2.79	2.60	2.22	0.60	4.69	1.42	1.40	1.76	1.02	1.40
22	1.20	1.61	2.64	2.46	2.09	0.57	4.44	1.34	1.32	1.67	0.96	1.32
23	1.14	1.53	2.50	2.33	1.99	0.54	4.21	1.27	1.26	1.58	0.91	1.26
24	1.08	1.45	2.37	2.21	1.88	0.51	3.99	1.21	1.19	1.50	0.87	1.19
25	1.08	1.45	2.36	2.20	1.88	0.51	3.98	1.20	1.19	1.49	0.86	1.19
26	1.01	1.36	2.22	2.07	1.77	0.48	3.74	1.13	1.12	1.41	0.81	1.12
27	0.94	1.26	2.06	1.92	1.64	0.44	3.47	1.05	1.04	1.31	0.75	1.04
28	0.87	1.17	1.92	1.78	1.52	0.41	3.22	0.98	0.96	1.21	0.70	0.96
29	0.82	1.10	1.80	1.68	1.43	0.39	3.03	0.92	0.90	1.14	0.66	0.90
30	0.77	1.04	1.69	1.58	1.35	0.36	2.85	0.86	0.85	1.07	0.62	0.85
31	0.78	1.04	1.71	1.59	1.36	0.37	2.87	0.87	0.86	1.08	0.62	0.86
32	0.76	1.02	1.66	1.55	1.32	0.36	2.80	0.85	0.84	1.05	0.61	0.84
33	0.71	0.95	1.56	1.45	1.24	0.33	2.62	0.79	0.78	0.98	0.57	0.78
34	0.70	0.93	1.53	1.42	1.21	0.33	2.57	0.78	0.77	0.96	0.56	0.77
35	0.71	0.95	1.56	1.45	1.24	0.33	2.63	0.79	0.78	0.99	0.57	0.78
36	0.77	1.03	1.68	1.56	1.33	0.36	2.82	0.85	0.84	1.06	0.61	0.84
37	0.83	1.11	1.82	1.69	1.45	0.39	3.06	0.93	0.91	1.15	0.66	0.91
38	0.80	1.07	1.75	1.63	1.39	0.38	2.95	0.89	0.88	1.11	0.64	0.88

39	0.83	1.11	1.82	1.69	1.44	0.39	3.06	0.93	0.91	1.15	0.66	0.91
40	0.86	1.15	1.88	1.75	1.49	0.40	3.16	0.96	0.94	1.19	0.69	0.94
41	0.86	1.16	1.89	1.76	1.50	0.41	3.19	0.96	0.95	1.20	0.69	0.95
42	0.90	1.21	1.98	1.85	1.57	0.43	3.33	1.01	1.00	1.25	0.72	1.00
43	0.87	1.17	1.91	1.78	1.52	0.41	3.22	0.97	0.96	1.21	0.70	0.96
44	0.84	1.13	1.84	1.72	1.46	0.40	3.10	0.94	0.93	1.16	0.67	0.93
45	0.84	1.12	1.83	1.70	1.45	0.39	3.08	0.93	0.92	1.16	0.67	0.92
46	0.82	1.10	1.80	1.68	1.43	0.39	3.03	0.92	0.90	1.14	0.66	0.90
47	0.82	1.09	1.79	1.66	1.42	0.38	3.01	0.91	0.90	1.13	0.65	0.90
48	0.83	1.12	1.83	1.70	1.45	0.39	3.07	0.93	0.92	1.16	0.67	0.92
49	0.84	1.13	1.84	1.72	1.46	0.40	3.10	0.94	0.93	1.17	0.67	0.93
50	0.85	1.14	1.86	1.74	1.48	0.40	3.14	0.95	0.94	1.18	0.68	0.94
51	0.82	1.10	1.80	1.68	1.43	0.39	3.03	0.92	0.90	1.14	0.66	0.90
52	0.78	1.05	1.71	1.59	1.36	0.37	2.87	0.87	0.86	1.08	0.62	0.86
53	0.75	1.00	1.64	1.53	1.30	0.35	2.76	0.83	0.82	1.04	0.60	0.82
54	0.76	1.02	1.67	1.55	1.32	0.36	2.81	0.85	0.84	1.05	0.61	0.84
55	0.78	1.05	1.71	1.60	1.36	0.37	2.88	0.87	0.86	1.08	0.63	0.86
56	0.77	1.03	1.69	1.58	1.34	0.36	2.85	0.86	0.85	1.07	0.62	0.85
57	0.75	1.00	1.64	1.53	1.30	0.35	2.76	0.83	0.82	1.04	0.60	0.82
58	0.74	0.99	1.61	1.50	1.28	0.35	2.72	0.82	0.81	1.02	0.59	0.81
59	0.73	0.98	1.60	1.49	1.27	0.34	2.70	0.82	0.81	1.01	0.59	0.81
60	0.72	0.97	1.59	1.48	1.26	0.34	2.67	0.81	0.80	1.00	0.58	0.80
61	0.69	0.92	1.51	1.41	1.20	0.32	2.54	0.77	0.76	0.96	0.55	0.76
62	0.64	0.86	1.41	1.32	1.12	0.30	2.38	0.72	0.71	0.89	0.52	0.71
63	0.64	0.86	1.40	1.31	1.11	0.30	2.36	0.71	0.70	0.89	0.51	0.70
64	0.64	0.86	1.40	1.30	1.11	0.30	2.35	0.71	0.70	0.88	0.51	0.70
65	0.66	0.89	1.45	1.35	1.15	0.31	2.44	0.74	0.73	0.92	0.53	0.73
66	0.66	0.88	1.44	1.34	1.14	0.31	2.42	0.73	0.72	0.91	0.52	0.72
67	0.62	0.83	1.36	1.27	1.08	0.29	2.29	0.69	0.68	0.86	0.50	0.68
68	0.63	0.84	1.37	1.28	1.09	0.30	2.31	0.70	0.69	0.87	0.50	0.69
69	0.68	0.91	1.49	1.39	1.19	0.32	2.51	0.76	0.75	0.94	0.55	0.75
70	0.77	1.03	1.68	1.56	1.33	0.36	2.82	0.85	0.84	1.06	0.61	0.84
71	0.83	1.11	1.82	1.69	1.44	0.39	3.06	0.92	0.91	1.15	0.66	0.91
72	0.85	1.14	1.86	1.73	1.48	0.40	3.13	0.95	0.94	1.18	0.68	0.94
73	0.83	1.11	1.82	1.69	1.44	0.39	3.06	0.92	0.91	1.15	0.66	0.91
74	0.79	1.05	1.72	1.60	1.37	0.37	2.89	0.88	0.86	1.09	0.63	0.86
75	0.74	1.00	1.63	1.52	1.29	0.35	2.74	0.83	0.82	1.03	0.59	0.82
76	0.71	0.95	1.55	1.44	1.23	0.33	2.60	0.79	0.78	0.98	0.56	0.78
77	0.69	0.93	1.52	1.41	1.21	0.33	2.55	0.77	0.76	0.96	0.55	0.76
78	0.67	0.90	1.46	1.36	1.16	0.31	2.47	0.75	0.74	0.93	0.54	0.74
79	0.68	0.91	1.48	1.38	1.18	0.32	2.49	0.75	0.74	0.94	0.54	0.74
80	0.70	0.94	1.54	1.43	1.22	0.33	2.59	0.78	0.77	0.97	0.56	0.77
81	0.68	0.92	1.50	1.40	1.19	0.32	2.52	0.76	0.75	0.95	0.55	0.75
82	0.64	0.86	1.41	1.32	1.12	0.30	2.38	0.72	0.71	0.89	0.52	0.71
83	0.60	0.81	1.32	1.23	1.05	0.28	2.22	0.67	0.66	0.83	0.48	0.66
84	0.56	0.75	1.23	1.14	0.98	0.26	2.07	0.63	0.62	0.78	0.45	0.62
85	0.56	0.76	1.24	1.15	0.98	0.27	2.08	0.63	0.62	0.78	0.45	0.62
86	0.62	0.83	1.35	1.26	1.07	0.29	2.28	0.69	0.68	0.86	0.49	0.68

87	0.69	0.93	1.52	1.41	1.21	0.33	2.56	0.77	0.76	0.96	0.55	0.76
88	0.72	0.97	1.58	1.47	1.25	0.34	2.66	0.80	0.79	1.00	0.58	0.79
89	0.71	0.95	1.55	1.44	1.23	0.33	2.61	0.79	0.78	0.98	0.57	0.78
90	0.68	0.92	1.50	1.39	1.19	0.32	2.52	0.76	0.75	0.95	0.55	0.75
91	0.65	0.88	1.43	1.33	1.14	0.31	2.41	0.73	0.72	0.91	0.52	0.72
92	0.62	0.84	1.37	1.27	1.09	0.29	2.30	0.70	0.69	0.86	0.50	0.69
93	0.59	0.79	1.30	1.21	1.03	0.28	2.18	0.66	0.65	0.82	0.47	0.65
94	0.55	0.74	1.21	1.13	0.97	0.26	2.04	0.62	0.61	0.77	0.44	0.61
95	0.55	0.74	1.20	1.12	0.96	0.26	2.02	0.61	0.60	0.76	0.44	0.60
96	0.60	0.80	1.31	1.22	1.04	0.28	2.20	0.67	0.66	0.83	0.48	0.66
97	0.71	0.95	1.55	1.45	1.24	0.33	2.62	0.79	0.78	0.98	0.57	0.78
98	0.81	1.09	1.78	1.66	1.41	0.38	3.00	0.91	0.89	1.13	0.65	0.89
99	0.86	1.15	1.88	1.75	1.49	0.40	3.16	0.96	0.94	1.19	0.69	0.94
100	0.89	1.19	1.94	1.81	1.54	0.42	3.27	0.99	0.98	1.23	0.71	0.98
101	0.92	1.23	2.01	1.87	1.60	0.43	3.38	1.02	1.01	1.27	0.73	1.01
102	0.94	1.26	2.06	1.92	1.64	0.44	3.47	1.05	1.04	1.30	0.75	1.04
103	0.96	1.28	2.10	1.95	1.67	0.45	3.53	1.07	1.05	1.33	0.77	1.05
104	0.97	1.30	2.12	1.97	1.68	0.45	3.57	1.08	1.06	1.34	0.77	1.06
105	0.98	1.31	2.14	1.99	1.70	0.46	3.60	1.09	1.07	1.35	0.78	1.07
106	1.03	1.38	2.26	2.10	1.79	0.48	3.80	1.15	1.13	1.43	0.82	1.13
107	1.11	1.49	2.43	2.26	1.93	0.52	4.09	1.24	1.22	1.54	0.89	1.22
108	1.19	1.60	2.61	2.43	2.07	0.56	4.39	1.33	1.31	1.65	0.95	1.31
109	1.31	1.76	2.88	2.68	2.29	0.62	4.84	1.46	1.44	1.82	1.05	1.44
110	1.41	1.90	3.10	2.89	2.46	0.66	5.21	1.58	1.56	1.96	1.13	1.56
111	1.48	1.98	3.24	3.02	2.58	0.70	5.46	1.65	1.63	2.05	1.18	1.63
112	1.52	2.03	3.32	3.09	2.64	0.71	5.59	1.69	1.67	2.10	1.21	1.67
113	1.54	2.06	3.37	3.14	2.68	0.72	5.67	1.72	1.69	2.13	1.23	1.69
114	1.56	2.09	3.41	3.18	2.71	0.73	5.74	1.74	1.71	2.16	1.25	1.71
115	1.62	2.17	3.54	3.30	2.81	0.76	5.96	1.80	1.78	2.24	1.29	1.78
116	1.65	2.21	3.61	3.37	2.87	0.78	6.08	1.84	1.82	2.29	1.32	1.82
117	1.66	2.22	3.63	3.38	2.89	0.78	6.11	1.85	1.82	2.30	1.33	1.82
118	1.67	2.23	3.65	3.40	2.90	0.78	6.14	1.86	1.83	2.31	1.33	1.83
119	1.67	2.24	3.67	3.41	2.91	0.79	6.17	1.87	1.84	2.32	1.34	1.84
120	1.68	2.25	3.67	3.42	2.92	0.79	6.18	1.87	1.84	2.32	1.34	1.84
121	1.71	2.29	3.75	3.49	2.98	0.80	6.30	1.91	1.88	2.37	1.37	1.88
122	1.72	2.30	3.76	3.50	2.99	0.81	6.33	1.91	1.89	2.38	1.37	1.89
123	1.69	2.26	3.69	3.44	2.94	0.79	6.22	1.88	1.86	2.34	1.35	1.86
124	1.64	2.19	3.59	3.34	2.85	0.77	6.03	1.83	1.80	2.27	1.31	1.80
125	1.58	2.12	3.47	3.23	2.75	0.74	5.83	1.76	1.74	2.19	1.27	1.74
126	1.57	2.10	3.44	3.20	2.73	0.74	5.79	1.75	1.73	2.18	1.26	1.73
127	1.57	2.11	3.45	3.21	2.74	0.74	5.80	1.76	1.73	2.18	1.26	1.73
128	1.57	2.10	3.44	3.20	2.73	0.74	5.78	1.75	1.73	2.17	1.26	1.73
129	1.60	2.14	3.50	3.26	2.78	0.75	5.89	1.78	1.76	2.21	1.28	1.76
130	1.64	2.20	3.59	3.35	2.85	0.77	6.04	1.83	1.80	2.27	1.31	1.80
131	1.64	2.20	3.60	3.35	2.86	0.77	6.05	1.83	1.81	2.27	1.31	1.81
132	1.62	2.17	3.55	3.31	2.82	0.76	5.97	1.81	1.78	2.24	1.30	1.78
133	1.64	2.20	3.60	3.35	2.86	0.77	6.05	1.83	1.81	2.27	1.31	1.81
134	1.68	2.25	3.68	3.43	2.92	0.79	6.19	1.87	1.85	2.33	1.34	1.85

135	1.71	2.29	3.75	3.49	2.98	0.80	6.30	1.91	1.88	2.37	1.37	1.88
136	1.75	2.35	3.84	3.58	3.05	0.82	6.46	1.96	1.93	2.43	1.40	1.93
137	1.74	2.33	3.81	3.55	3.03	0.82	6.41	1.94	1.91	2.41	1.39	1.91
138	1.73	2.31	3.78	3.52	3.01	0.81	6.37	1.93	1.90	2.39	1.38	1.90
139	1.72	2.31	3.77	3.51	3.00	0.81	6.34	1.92	1.89	2.38	1.38	1.89
140	1.70	2.27	3.71	3.46	2.95	0.80	6.25	1.89	1.87	2.35	1.36	1.87
141	1.68	2.25	3.68	3.43	2.92	0.79	6.19	1.87	1.85	2.33	1.34	1.85
142	1.68	2.25	3.68	3.43	2.92	0.79	6.19	1.87	1.85	2.33	1.34	1.85
143	1.69	2.26	3.69	3.44	2.93	0.79	6.21	1.88	1.85	2.33	1.35	1.85
144	1.69	2.26	3.69	3.44	2.93	0.79	6.21	1.88	1.85	2.34	1.35	1.85
145	1.68	2.25	3.68	3.43	2.93	0.79	6.20	1.87	1.85	2.33	1.35	1.85
146	1.68	2.25	3.68	3.43	2.92	0.79	6.19	1.87	1.85	2.33	1.34	1.85
147	1.69	2.27	3.71	3.45	2.94	0.80	6.24	1.89	1.86	2.34	1.35	1.86
148	1.70	2.27	3.71	3.46	2.95	0.80	6.25	1.89	1.86	2.35	1.36	1.86
149	1.68	2.25	3.68	3.43	2.93	0.79	6.20	1.88	1.85	2.33	1.35	1.85
150	1.68	2.24	3.67	3.42	2.92	0.79	6.17	1.87	1.84	2.32	1.34	1.84
151	1.67	2.24	3.67	3.41	2.91	0.79	6.17	1.87	1.84	2.32	1.34	1.84
152	1.68	2.25	3.68	3.43	2.92	0.79	6.19	1.87	1.85	2.33	1.34	1.85
153	1.71	2.29	3.74	3.48	2.97	0.80	6.29	1.90	1.88	2.36	1.37	1.88
154	1.74	2.33	3.80	3.54	3.02	0.82	6.40	1.94	1.91	2.40	1.39	1.91
155	1.75	2.34	3.83	3.57	3.04	0.82	6.44	1.95	1.92	2.42	1.40	1.92
156	1.74	2.33	3.81	3.55	3.03	0.82	6.42	1.94	1.92	2.41	1.39	1.92
157	1.72	2.31	3.77	3.51	2.99	0.81	6.34	1.92	1.89	2.38	1.38	1.89
158	1.70	2.28	3.72	3.46	2.95	0.80	6.26	1.89	1.87	2.35	1.36	1.87
159	1.67	2.24	3.67	3.42	2.91	0.79	6.17	1.87	1.84	2.32	1.34	1.84
160	1.69	2.26	3.69	3.44	2.93	0.79	6.21	1.88	1.85	2.33	1.35	1.85
161	1.71	2.29	3.75	3.49	2.98	0.80	6.30	1.91	1.88	2.37	1.37	1.88
162	1.70	2.27	3.72	3.46	2.95	0.80	6.26	1.89	1.87	2.35	1.36	1.87
163	1.68	2.26	3.69	3.43	2.93	0.79	6.20	1.88	1.85	2.33	1.35	1.85
164	1.67	2.24	3.66	3.41	2.91	0.78	6.15	1.86	1.84	2.31	1.34	1.84
165	1.65	2.22	3.62	3.38	2.88	0.78	6.10	1.85	1.82	2.29	1.32	1.82
166	1.66	2.23	3.64	3.39	2.89	0.78	6.12	1.85	1.83	2.30	1.33	1.83
167	1.68	2.25	3.68	3.43	2.92	0.79	6.19	1.87	1.85	2.33	1.34	1.85
168	1.73	2.32	3.78	3.53	3.01	0.81	6.37	1.93	1.90	2.39	1.38	1.90
169	1.77	2.37	3.87	3.60	3.07	0.83	6.50	1.97	1.94	2.44	1.41	1.94
170	1.79	2.40	3.92	3.65	3.11	0.84	6.59	1.99	1.97	2.48	1.43	1.97
171	1.81	2.43	3.96	3.69	3.15	0.85	6.67	2.02	1.99	2.51	1.45	1.99
172	1.83	2.45	4.00	3.73	3.18	0.86	6.73	2.04	2.01	2.53	1.46	2.01
173	1.84	2.47	4.04	3.76	3.21	0.87	6.79	2.05	2.03	2.55	1.47	2.03
174	1.85	2.48	4.05	3.77	3.22	0.87	6.81	2.06	2.03	2.56	1.48	2.03
175	1.84	2.46	4.03	3.75	3.20	0.86	6.78	2.05	2.02	2.55	1.47	2.02
176	1.82	2.44	3.98	3.71	3.16	0.85	6.70	2.03	2.00	2.52	1.45	2.00
177	1.80	2.41	3.93	3.66	3.12	0.84	6.62	2.00	1.98	2.49	1.44	1.98
178	1.76	2.35	3.84	3.58	3.05	0.82	6.47	1.96	1.93	2.43	1.40	1.93
179	1.71	2.29	3.75	3.49	2.98	0.80	6.31	1.91	1.88	2.37	1.37	1.88
180	1.68	2.25	3.68	3.43	2.92	0.79	6.19	1.87	1.85	2.33	1.34	1.85
181	1.66	2.22	3.64	3.39	2.89	0.78	6.12	1.85	1.83	2.30	1.33	1.83
182	1.67	2.24	3.67	3.41	2.91	0.79	6.17	1.87	1.84	2.32	1.34	1.84

183	1.70	2.28	3.72	3.47	2.96	0.80	6.26	1.89	1.87	2.35	1.36	1.87
184	1.73	2.32	3.79	3.53	3.01	0.81	6.38	1.93	1.90	2.40	1.38	1.90
185	1.77	2.37	3.87	3.61	3.08	0.83	6.51	1.97	1.94	2.45	1.41	1.94
186	1.81	2.42	3.96	3.69	3.14	0.85	6.66	2.01	1.99	2.50	1.45	1.99
187	1.86	2.49	4.08	3.80	3.24	0.87	6.86	2.08	2.05	2.58	1.49	2.05
188	1.92	2.57	4.19	3.91	3.33	0.90	7.06	2.14	2.11	2.65	1.53	2.11
189	1.95	2.62	4.28	3.99	3.40	0.92	7.20	2.18	2.15	2.71	1.56	2.15
190	1.98	2.66	4.34	4.04	3.45	0.93	7.30	2.21	2.18	2.74	1.59	2.18
191	2.00	2.68	4.38	4.08	3.48	0.94	7.38	2.23	2.20	2.77	1.60	2.20
192	2.02	2.70	4.41	4.11	3.51	0.95	7.43	2.25	2.22	2.79	1.61	2.22
193	2.01	2.70	4.41	4.11	3.50	0.95	7.42	2.25	2.22	2.79	1.61	2.22
194	2.00	2.68	4.38	4.08	3.48	0.94	7.38	2.23	2.20	2.77	1.60	2.20
195	1.98	2.65	4.33	4.04	3.44	0.93	7.29	2.21	2.18	2.74	1.58	2.18
196	1.95	2.62	4.28	3.99	3.40	0.92	7.20	2.18	2.15	2.71	1.56	2.15
197	1.91	2.56	4.18	3.89	3.32	0.90	7.03	2.13	2.10	2.64	1.53	2.10
198	1.86	2.49	4.07	3.79	3.24	0.87	6.85	2.07	2.05	2.58	1.49	2.05
199	1.83	2.45	4.01	3.73	3.18	0.86	6.74	2.04	2.01	2.53	1.46	2.01
200	1.81	2.43	3.97	3.70	3.15	0.85	6.68	2.02	1.99	2.51	1.45	1.99
201	1.80	2.41	3.93	3.66	3.13	0.84	6.62	2.00	1.98	2.49	1.44	1.98
202	1.78	2.38	3.89	3.62	3.09	0.83	6.54	1.98	1.95	2.46	1.42	1.95
203	1.77	2.37	3.87	3.60	3.07	0.83	6.51	1.97	1.94	2.45	1.41	1.94
204	1.73	2.32	3.80	3.54	3.02	0.81	6.39	1.93	1.91	2.40	1.39	1.91
205	1.68	2.25	3.68	3.43	2.92	0.79	6.19	1.87	1.85	2.33	1.34	1.85
206	1.64	2.20	3.59	3.34	2.85	0.77	6.04	1.83	1.80	2.27	1.31	1.80
207	1.60	2.14	3.49	3.26	2.78	0.75	5.88	1.78	1.76	2.21	1.28	1.76
208	1.55	2.07	3.38	3.15	2.69	0.73	5.69	1.72	1.70	2.14	1.24	1.70
209	1.50	2.01	3.28	3.06	2.61	0.70	5.52	1.67	1.65	2.08	1.20	1.65
210	1.46	1.95	3.19	2.97	2.53	0.68	5.36	1.62	1.60	2.02	1.16	1.60
211	1.41	1.89	3.10	2.88	2.46	0.66	5.21	1.58	1.56	1.96	1.13	1.56
212	1.38	1.85	3.02	2.81	2.40	0.65	5.08	1.54	1.52	1.91	1.10	1.52
213	1.35	1.81	2.96	2.76	2.35	0.64	4.98	1.51	1.49	1.87	1.08	1.49
214	1.34	1.80	2.94	2.74	2.33	0.63	4.94	1.50	1.48	1.86	1.07	1.48
215	1.34	1.80	2.94	2.74	2.34	0.63	4.95	1.50	1.48	1.86	1.07	1.48
216	1.35	1.81	2.95	2.75	2.34	0.63	4.97	1.50	1.48	1.87	1.08	1.48
217	1.35	1.81	2.95	2.75	2.35	0.63	4.97	1.50	1.48	1.87	1.08	1.48
218	1.34	1.80	2.94	2.74	2.33	0.63	4.94	1.50	1.48	1.86	1.07	1.48
219	1.33	1.78	2.91	2.71	2.31	0.62	4.89	1.48	1.46	1.84	1.06	1.46
220	1.31	1.75	2.86	2.67	2.27	0.61	4.81	1.46	1.44	1.81	1.05	1.44
221	1.28	1.71	2.80	2.61	2.23	0.60	4.71	1.43	1.41	1.77	1.02	1.41
222	1.25	1.68	2.74	2.55	2.18	0.59	4.61	1.40	1.38	1.73	1.00	1.38
223	1.23	1.65	2.69	2.51	2.14	0.58	4.53	1.37	1.35	1.70	0.98	1.35
224	1.21	1.62	2.65	2.47	2.11	0.57	4.46	1.35	1.33	1.68	0.97	1.33
225	1.19	1.59	2.61	2.43	2.07	0.56	4.38	1.33	1.31	1.65	0.95	1.31
226	1.16	1.56	2.55	2.37	2.02	0.55	4.29	1.30	1.28	1.61	0.93	1.28
227	1.14	1.52	2.49	2.32	1.98	0.53	4.18	1.27	1.25	1.57	0.91	1.25
228	1.10	1.48	2.42	2.25	1.92	0.52	4.07	1.23	1.21	1.53	0.88	1.21
229	1.07	1.43	2.34	2.18	1.86	0.50	3.94	1.19	1.18	1.48	0.86	1.18
230	1.04	1.39	2.28	2.12	1.81	0.49	3.83	1.16	1.14	1.44	0.83	1.14

231	1.02	1.37	2.24	2.09	1.78	0.48	3.77	1.14	1.12	1.42	0.82	1.12
232	1.02	1.37	2.24	2.08	1.78	0.48	3.76	1.14	1.12	1.41	0.82	1.12
233	1.03	1.38	2.25	2.10	1.79	0.48	3.79	1.15	1.13	1.42	0.82	1.13
234	1.04	1.39	2.27	2.12	1.81	0.49	3.82	1.16	1.14	1.44	0.83	1.14
235	1.04	1.40	2.28	2.12	1.81	0.49	3.84	1.16	1.15	1.44	0.83	1.15
236	1.04	1.39	2.27	2.11	1.80	0.49	3.82	1.15	1.14	1.43	0.83	1.14
237	1.02	1.37	2.24	2.09	1.78	0.48	3.77	1.14	1.12	1.42	0.82	1.12
238	1.00	1.34	2.19	2.04	1.74	0.47	3.69	1.12	1.10	1.39	0.80	1.10
239	0.97	1.30	2.13	1.98	1.69	0.46	3.58	1.08	1.07	1.35	0.78	1.07
240	0.94	1.26	2.05	1.91	1.63	0.44	3.46	1.05	1.03	1.30	0.75	1.03
241	0.90	1.21	1.98	1.84	1.57	0.42	3.33	1.01	0.99	1.25	0.72	0.99
242	0.87	1.16	1.90	1.77	1.51	0.41	3.20	0.97	0.95	1.20	0.69	0.95
243	0.84	1.12	1.83	1.70	1.45	0.39	3.08	0.93	0.92	1.16	0.67	0.92
244	0.81	1.08	1.77	1.65	1.41	0.38	2.98	0.90	0.89	1.12	0.65	0.89
245	0.79	1.06	1.74	1.62	1.38	0.37	2.92	0.88	0.87	1.10	0.63	0.87
246	0.79	1.06	1.73	1.61	1.37	0.37	2.91	0.88	0.87	1.09	0.63	0.87
247	0.79	1.05	1.72	1.60	1.37	0.37	2.89	0.88	0.86	1.09	0.63	0.86
248	0.78	1.04	1.70	1.59	1.35	0.37	2.87	0.87	0.86	1.08	0.62	0.86
249	0.76	1.02	1.67	1.56	1.33	0.36	2.82	0.85	0.84	1.06	0.61	0.84
250	0.75	1.00	1.64	1.52	1.30	0.35	2.75	0.83	0.82	1.03	0.60	0.82
251	0.73	0.97	1.59	1.48	1.26	0.34	2.68	0.81	0.80	1.01	0.58	0.80
252	0.70	0.94	1.54	1.43	1.22	0.33	2.58	0.78	0.77	0.97	0.56	0.77
253	0.67	0.90	1.48	1.38	1.17	0.32	2.48	0.75	0.74	0.93	0.54	0.74
254	0.65	0.87	1.42	1.32	1.13	0.30	2.38	0.72	0.71	0.90	0.52	0.71
255	0.62	0.84	1.37	1.27	1.09	0.29	2.30	0.70	0.69	0.87	0.50	0.69
256	0.61	0.81	1.33	1.24	1.05	0.28	2.23	0.68	0.67	0.84	0.48	0.67
257	0.59	0.79	1.29	1.20	1.03	0.28	2.17	0.66	0.65	0.82	0.47	0.65
258	0.57	0.77	1.25	1.17	1.00	0.27	2.11	0.64	0.63	0.79	0.46	0.63
259	0.55	0.74	1.21	1.13	0.97	0.26	2.04	0.62	0.61	0.77	0.44	0.61
260	0.54	0.72	1.18	1.10	0.94	0.25	1.98	0.60	0.59	0.74	0.43	0.59
261	0.52	0.70	1.14	1.06	0.91	0.24	1.92	0.58	0.57	0.72	0.42	0.57
262	0.50	0.67	1.10	1.03	0.88	0.24	1.85	0.56	0.55	0.70	0.40	0.55
263	0.49	0.65	1.06	0.99	0.85	0.23	1.79	0.54	0.53	0.67	0.39	0.53
264	0.47	0.63	1.03	0.96	0.82	0.22	1.73	0.52	0.52	0.65	0.38	0.52

REFERENCES

CONTACT US

t 1300 363 400
+61 7 3833 5565
e enquiries@csiro.au
w www.csiro.au

YOUR CSIRO

Australia is founding its future on science and innovation. Its national science agency, CSIRO, is a powerhouse of ideas, technologies and skills for building prosperity, growth, health and sustainability. It serves governments, industries, business and communities across the nation.

FOR FURTHER INFORMATION

Land and Water/Water in the Resources Sector
Sreekanth Janardhanan
t +61 7 3833 5565
e Sreekanth.janardhanan@csiro.au
w http://www.csiro.au/Organisation-Structure/Flagships/Land-and-Water.aspx